

# Polimery w Medycynie

Polymers in Medicine

BIANNUAL ISSN: 0370-0747 e-ISSN: 2451-2699

[www.polimery.umed.wroc.pl](http://www.polimery.umed.wroc.pl)

2018, Vol. 48, No. 1 (January–June)

Ministry of Science and Higher Education – 9 pts.  
Index Copernicus (ICV) – 109.18 pts.



WROCLAW  
MEDICAL UNIVERSITY

# Polimery w Medycynie

## Polymers in Medicine

ISSN 0370-0747 (PRINT)

ISSN 2451-2699 (ONLINE)

[www.polimery.umed.wroc.pl](http://www.polimery.umed.wroc.pl)

**BIANNUAL**  
**2018, Vol. 48, No. 1**  
**(January–June)**

“Polymers in Medicine” is an independent, multidisciplinary forum to exchange scientific and clinical information, which publishes original papers (technical, analytical, experimental, clinical), preliminary reports and reviews regarding the use of polymers (natural and synthetic) and biomaterials in different specialties of medicine (biochemistry, clinical medicine, pharmacology, dentistry, implantology), biotechnology and veterinary science.

### Address of Editorial Office

Marcinkowskiego 2–6  
50-368 Wrocław, Poland  
Tel.: +48 71 784 11 33  
E-mail: [polimery@umed.wroc.pl](mailto:polimery@umed.wroc.pl)

### Publisher

Wrocław Medical University  
Wybrzeże L. Pasteura 1  
50-367 Wrocław, Poland

© Copyright by Wrocław Medical University,  
Wrocław 2019

Online edition is the original version of the journal

### Editor-in-Chief

Magdalena Krajewska  
Mariusz Kuształ

### Vice-Editor-in-Chief

Jerzy Gosk

### Editorial Board

Rajmund Adamiec  
Beata Dejak  
Bożena Karolewicz  
Witold Musiał

### Thematic Editors

Bożena Karolewicz  
(Multifunctional polymers in pharmaceutical technology and medical applications)  
Witold Musiał  
(Physicochemical evaluation of polymers used in pharmacy and medicine)  
Agnieszka Wojciechowska  
(Bioinorganic chemistry and coordination chemistry)  
Agnieszka Noszczyk-Nowak  
(Experimental research)

### International Advisory Board

Jenifer B. Dressman (Germany)  
Mirosława El Fray (Poland)  
Mukesh G. Gohel (India)  
Vipin B. Gupta (India)  
Anthony J. Hickey (USA)  
Jacek Kaczmarczyk (Poland)

### Secretary

Maciej Szymczak

Michał Nachajski  
Tadeusz Orłowski  
Lidia Usnarska-Zubkiewicz  
Włodzimierz Więckiewicz

### Technical Editorship

Adam Barg, Marek Misiak,  
Aleksandra Raczkowska

### Statistical Editors

Dorota Diakowska, Leszek Noga

### English Language Copy Editors

Jason Schock, Marcin Tereszewski,  
Sherill Howard Pocięcha

Agnieszka Noszczyk-Nowak (Poland)  
Paweł Reichert (Poland)  
Maciej Urban (Poland)  
Timothy S. Wiedmann (USA)  
Katarzyna Winnicka (Poland)  
Waldemar Wysokiński (USA)  
Samuel Yalkowsky (USA)

## Editorial Policy

During the review process, the Editorial Board conforms to the "Uniform Requirements for Manuscripts Submitted to Biomedical Journals: Writing and Editing for Biomedical Publication" approved by the International Committee of Medical Journal Editors (<http://www.icmje.org/>). Experimental studies must include a statement that the experimental protocol and informed consent procedure were in compliance with the Helsinki Convention and were approved by the ethics committee.

For more information visit the following page: <http://www.polimery.umed.wroc.pl>

Indexed in: OCLC, WorldCat, PBL, EBSCO, MEDLINE, Index Copernicus

This publication has been co-financed by the Ministry of Science and Higher Education

Typographic design: Monika Kołęda, Piotr Gil

Cover: Monika Kołęda

DTP: Wrocław Medical University Press

Printing and binding: EXDRUK

Circulation: 11 copies

## Contents

- 5 Mariusz Budaj, Andrzej Michalski, Bogdan Miškowiak, Katarzyna Filipecka, Sylwia Mandecka  
**Study of the structure of contact lenses using PALS, MIR and Raman spectroscopy in the regard of safety of persons exposed to ionizing radiation**
- 11 Katarzyna Filipecka, Mariusz Budaj, Bogdan Miškowiak, Sylwia Mandecka, Radosław Mandecki, Małgorzata Makowska-Janusik, Jacek Filipecki  
**A study of the effect of X-ray irradiation on the structure of Narafilcon A biopolymer soft contact lenses**
- 17 Jyotsana R. Madan, Akshaya R. Pawar, Rajesh B. Patil, Rajendra Awasthi, Kamal Dua  
**Preparation, characterization and in vitro evaluation of tablets containing microwave-assisted solid dispersions of apremilast**
- 25 Monika Sujka, Urszula Pankiewicz, Radosław Kowalski, Karolina Nowosad, Agnieszka Noszczyk-Nowak  
**Porous starch and its application in drug delivery systems**
- 31 Samvedna, Shammy Jindal, Gaurav Mishra, Jyotsana R. Madan, Gaurav Gupta, Rajendra Awasthi, Terezinha de Jesus Andreoli Pinto, Kamal Dua, Giriraj T. Kulkarni  
**Formulation and characterization of oral rapid disintegrating tablets of levocetirizine**
- 41 Michael Ayodele Odeniyi, Omobolanle A. Omotoso, Adewale O. Adepoju, Kolawole T. Jaiyeoba  
**Starch nanoparticles in drug delivery: A review**
- 47 Krystyna Grzebieluch-Reichert, Jarosław Marek, Marta Misiuk-Hoźło  
**Safety assessment of using collamer phakic implants in the correction of refractive errors**
- 53 Maciej Leciejewski, Aleksandra Królikowska, Paweł Reichert  
**Polyethylene terephthalate tape augmentation as a solution in recurrent quadriceps tendon ruptures**
- 57 Piotr Olczyk, Artur Małyszczak, Mariusz Kusztal  
**Dialysis membranes: A 2018 update**

# Badanie struktury soczewek kontaktowych z użyciem metod PALS, MIR, Ramana w aspekcie bezpieczeństwa osób przebywających w warunkach działania promieniowania jonizującego

## Study of the structure of contact lenses using PALS, MIR and Raman spectroscopy in the regard of safety of persons exposed to ionizing radiation

Mariusz Budaj<sup>1,A-D</sup>, Andrzej Michalski<sup>2,B-D</sup>, Bogdan Miśkowiak<sup>1,3,E-F</sup>, Katarzyna Filipecka<sup>4,A-D</sup>, Sylwia Mandecka<sup>5,B-C</sup>

<sup>1</sup> Zakład Optometrii, Katedra Chorób Oczu i Optometrii, Uniwersytet Medyczny im. Karola Marcinkowskiego w Poznaniu, Polska

<sup>2</sup> Klinika Chorób Oczu, Katedra Chorób Oczu i Optometrii, Uniwersytet Medyczny im. Karola Marcinkowskiego w Poznaniu, Polska

<sup>3</sup> Wyższa Szkoła Zdrowia, Urody i Edukacji w Poznaniu, Polska

<sup>4</sup> Zakład Badań Strukturalnych i Fizyki Medycznej, Instytut Fizyki, Wydział Matematyczno-Przyrodniczy, Akademia im. Jana Długosza w Częstochowie, Polska

<sup>5</sup> Zakład Radioterapii, Wojewódzki Szpital Specjalistyczny im. Najświętszej Maryi Panny w Częstochowie, Polska

A – research concept and design; B – collection and/or assembly of data; C – data analysis and interpretation;

D – writing the article; E – critical revision of the article; F – final approval of the article

Polymers in Medicine, ISSN 0370-0747 (print), ISSN 2451-2699 (online)

Polim Med. 2018;48(1):5–9

### Adres do korespondencji

Mariusz Budaj

E-mail: mariuszbudaj@neostrada.pl

### Źródła finansowania

Brak

### Konflikt interesów

Nie występuje

Praca wpłynęła do Redakcji: 17.05.2018 r.

Po recenzji: 6.09.2018 r.

Zaakceptowano do druku: 25.09.2018 r.

### Cytowanie

Budaj M, Michalski A, Miśkowiak B, Filipecka K, Mandecka S. Badanie struktury soczewek kontaktowych z użyciem metod PALS, MIR, Ramana w aspekcie bezpieczeństwa osób przebywających w warunkach działania promieniowania jonizującego. *Polim Med.* 2018;48(1):5–9. doi:10.17219/pim/96287

### DOI

10.17219/pim/96287

### Copyright

© 2018 by Wrocław Medical University

This is an article distributed under the terms of the

Creative Commons Attribution Non-Commercial License

(<http://creativecommons.org/licenses/by-nc-nd/4.0/>)

## Streszczenie

Wielu pacjentów i przedstawicieli personelu medycznego poddawanych działaniu promieniowania jonizującego podczas realizacji procedur diagnostycznych bądź terapeutycznych ma wady wzroku, które korygowane są m.in. miękkimi soczewkami kontaktowymi. Na bezpieczeństwo użytkowania tego typu korekcji mogą mieć wpływ zmiany w strukturze wewnętrznej soczewek, które mogą modyfikować ich uwodnienie lub transport tlenu do rogówki. Niezbędna jest zatem analiza wpływu czynników zewnętrznych, w tym promieniowania jonizującego wykorzystywanego w medycynie, na wybrane parametry soczewek kontaktowych, a szczególnie zbadanie i porównanie występowania swobodnych objętości w strukturze wewnętrznej polimerowych miękkich soczewek kontaktowych. Ewentualna zmiana rozmiarów i ich ilości w strukturze materiałów miękkich soczewek kontaktowych, która wynikałaby z oddziaływania promieniowania jonizującego, może wpływać niekorzystnie na przepuszczalność tlenu. Do przeprowadzenia wyżej wspomnianej analizy można użyć różnych metod, m.in. spektroskopii czasów życia anihilujących pozytonów (PALS), spektroskopii Ramana i MIR. Podczas użytkowania soczewek kontaktowych, ograniczających transport tlenu do rogówki zwiększa się ryzyko jej niedotlenienia, które stanowi jedno z możliwych powikłań. Badania skutków oddziaływania różnych typów promieniowania jonizującego (X, gamma czy beta) na materiały wykorzystywane do produkcji soczewek kontaktowych są ważne, w kontekście bezpieczeństwa użytkowników soczewek kontaktowych.

**Słowa kluczowe:** promieniowanie jonizujące, soczewki kontaktowe, wolne objętości, anihilacja pozytonów

## Abstract

Among patients and health professionals who are exposed to ionizing radiation during diagnostic and therapeutic procedures, refractive errors are common and soft contact lenses are widely used to correct them. Changes in the inner structure of contact lens may influence the safety of its usage through modification of its water content or oxygen accessibility to cornea. Therefore, analysis of impact of external factors, therein ionizing radiation used in medicine, on contact lenses parameters is necessary, particularly to compare the presence of free volume gaps in the structure of the polymer soft contact lenses. Possible change in dimensions or quantity of free volume gaps in the structure of the material caused by the exposure to ionizing radiation may have negative influence on oxygen permeability. To prevent such process, different means could be used, i.e., positron annihilation lifetime spectroscopy (PALS), Raman spectroscopy and mid-infrared spectroscopy (MIR). Use of contact lenses which reduce transport of oxygen to cornea increases the risk of corneal hypoxia – one of the possible complications of using contact lenses. Research on effects of different types of ionizing radiation (X-ray, gamma, beta) on materials used in production of contact lenses is vital because of the connection of this issue with the safety of contact lenses wearers. Such research can also shed light on the problem of safe use of contact lenses by persons exposed to ionizing radiation.

**Key words:** ionizing radiation, contact lenses, free volumes, positron annihilation

## Wstęp

Promieniowanie jonizujące stosowane jest w medycynie już od ponad 100 lat. Korzyści, jakie z tego wynikają, są nieocenione. W każdym przypadku wykorzystania promieniowania jonizującego w diagnostyce i leczeniu należy prawidłowo uzasadnić użycie danej procedury, przede wszystkim mając na uwadze bezpieczeństwo pacjenta. Na nadmierną ekspozycję na promieniowanie jonizujące podczas badań diagnostycznych, zabiegów czy terapii mogą być narażeni zarówno pacjenci, jak i personel medyczny. Powyższe zagadnienie omówiono w licznych badaniach, po przeprowadzeniu których postulowano stosowanie właściwych środków zapobiegających nadmiernemu narażeniu na skutki promieniowania. Wśród środków ochrony wymieniane są osłony ołowiane, gogle ze szkłem ołowiowym, zastosowanie kolimatorów wiązki promieniowania i zachowanie właściwego dystansu od źródeł promieniowania.<sup>1-2</sup> U pacjentów poddawanych działaniu promieniowania jonizującego, jak i wśród personelu medycznego często występują wady układu wzrokowego korygowane przez noszenie przez nich soczewek kontaktowych. W badaniu Mozolewskiej-Piotrowskiej et al. stwierdzono występowanie ametropii u 51% studentów kierunku lekarskiego i 47% dentystycznego. Najczęściej występującą wadą wzroku była krótkowzroczność.<sup>3</sup>

## Podstawowe parametry soczewek kontaktowych

Materiały stosowane do produkcji soczewek kontaktowych są biokompatybilne dla organizmu, co oznacza, że nie wywołują reakcji biologicznych ze strony tkanek oka (są dobrze tolerowane). Nie powodują nadmiernego parowania łez oraz osadzania się na nich złogów. Przykładowym biokompatybilnym materiałem używanym do produkcji soczewek kontaktowych może być fosforylocholina – składnik błony komórkowej erytrocytów.<sup>4</sup>

Soczewki kontaktowe są opisywane na podstawie różnych parametrów. Jedne z najistotniejszych to te, które są związane z możliwością transportu tlenu przez soczewkę kontaktową do rogówki. Warto wspomnieć, że początkowo soczewki wykonywane były z nieprzepuszczalnego dla gazów polimetakrylanu metylu (PMMA). Dopiero później do produkcji zostały wprowadzone materiały gazoprzepuszczalne miękkie (hydrożelowe i silikonowo-hydrożelowe) oraz sztywne. Prace nad wpływem dostępności tlenu do rogówki są prowadzone od kilkadziesiąt lat. Już podczas pierwszych z nich opisano negatywny wpływ środowiska anaerobowego na właściwości optyczne rogówki, a nowsze badania dostarczają coraz dokładniejszych danych o zjawiskach związanych z hipoksją rogówki.

W swoim opracowaniu Leung et al. przedstawili spójne ilościowe wyjaśnienie powstawania obrzęku rogówki w przypadku niewystarczającego dopływu tlenu – jego niedobór zwiększa wydzielanie mleczanów, których zwiększone stężenie powoduje wzrost osmolarności na styku śródbłonna i istoty właściwej rogówki w stosunku do warunków właściwego utlenowania i osłabienie działania aktywnej pompy elektrolitowej zależnej od osmolarności.<sup>5</sup>

Niewystarczające zaopatrzenie rogówki w tlen jest określane jako hipoksja. Stan ten może prowadzić do zmian w metabolizmie rogówki, obrzęku, przymglenia rogówki, zaburzeń w obrębie jej nabłonka i śródbłonna. Przedłużające się niewystarczające zaopatrzenie rogówki w tlen prowadzi do powstania mikrocyst, przekrwienia okołorąbkowego, neowaskularyzacji, a nawet przesunięcia refrakcji w stronę krótkowzroczności.<sup>6</sup>

W odniesieniu do soczewek kontaktowych używa się parametru  $Dk$  (tlenoprzepuszczalność), gdzie  $D$  oznacza współczynnik dyfuzji, a  $k$  rozpuszczalność tlenu w materiale soczewki kontaktowej. W ten sposób charakteryzuje się materiał soczewki o jednostkowej grubości. Aby uzyskać informację o soczewce o danej mocy, wprowadza się parametr  $Dk/t$ , czyli tlenotransmisyjność, gdzie  $t$  to grubość soczewki.<sup>7</sup> Wprowadzenie materiałów o wysokim  $Dk$  spowodowało znaczne zmniejszenie opisywanych powyżej negatywnych zjawisk związanych z ograniczeniem

dostępności tlenu do rogówki.<sup>8</sup> Oprócz powyższych parametrów stosowane są też inne, np. ekwiwalent procentowy tlenu, który ma określać stężenie tlenu pod soczewką kontaktową, i strumień przepływu tlenu określający rzeczywistą ilość tlenu dostępnego dla rogówki.<sup>4</sup>

Poza wskaźnikami związanymi z przepuszczalnością tlenu soczewki kontaktowe są też opisywane takimi parametrami, jak zwilżalność powierzchni, moduł sztywności, uwodnienie, jonowość, kształt krawędzi, system stabilizacji (w przypadku soczewki torycznej). Podkreślenia wymaga fakt, że w soczewkach hydrożelowych przepuszczalność tlenu zwiększa się wraz ze stopniem uwodnienia materiału, natomiast w soczewkach silikonowo-hydrożelowych parametry te nie są od siebie tak zależne – tlenoprzepuszczalność zależy głównie od rodzaju użytego silikonu.

Podczas profesjonalnego doboru soczewki kontaktowej niezbędne jest też określenie właściwej średnicy i krzywizny soczewki, aby umożliwić jej wygodne i bezpieczne użytkowanie. Ostatecznie bezpieczeństwo i komfort użytkowania soczewki zależy od jej interakcji w konkretnych warunkach biologiczno-medycznych, mechanicznych i środowisku zewnętrznym.

## Badanie wolnych objętości w soczewkach kontaktowych

Mając na uwadze negatywny wpływ promieniowania jonizującego, należy przyjąć hipotezę, że w soczewkach kontaktowych poddanych jego działaniu mogą zachodzić zmiany w obrębie ich wewnętrznej struktury, które mogą wpływać na uwodnienie i upośledzenie transportu tlenu do komórek rogówki.

W badaniach struktury i właściwości materiałów polimerowych wykorzystywanych do produkcji soczewek kontaktowych szerokie zastosowanie znalazły metody spektroskopowe, takie jak spektroskopia czasów życia anihilujących pozytonów (ang. *positron annihilation lifetime spectroscopy* – PALS), spektroskopia Ramana oraz spektroskopia w średniej podczerwieni (ang. *mid-infrared spectroscopy* – MIR).

Dotychczasowe badania z wykorzystaniem powyższych metod przeprowadzono na silikonowo-hydrożelowych i hydrożelowych soczewkach kontaktowych poddawanych działaniu promieniowania jonizującego w warunkach laboratoryjnych i użytkowaniu w czasie. Grupę kontrolną stanowiły soczewki kontaktowe fabrycznie nowe.

Spektroskopia PAL jest niezwykle czułą metodą umożliwiającą charakteryzowanie właściwości strukturalnych, takich jak defekty i swobodne objętości oraz pozwalającą na określenie ich korelacji ze współczynnikiem przepuszczalności tlenu.<sup>9–11</sup>

Technika PALS opiera się na zjawisku anihilacji pozytonów. Czas życia pozytonu jest uwarunkowany środowiskiem, w którym się znajduje. W próżni czas ten jest praktycznie nieskończony, natomiast w materii jest ograni-

czony momentem spotkania elektronu i zazwyczaj nie jest dłuższy od kilkudziesięciu nanosekund. W wyniku anihilacji pary pozyton–elektron masa tych cząstek jest zamieniana w równoważną energię promieniowania elektromagnetycznego. Z największym prawdopodobieństwem następuje emisja parzystej ( $2\gamma$ ) lub nieparzystej ( $3\gamma$ ) liczb kwantów gamma. Jak w każdym procesie fizycznym spełnione są prawa zachowania pędu, momentu pędu, energii, ładunku i parzystości. W związku z tym badanie fotonów powstałych w wyniku procesu anihilacji dostarcza informacji o stanie anihilującej pary pozyton–elektron. W przypadku materiałów amorficznych może dochodzić do tworzenia się stanu związanego elektronu i pozytonu, tzw. pozytu (Ps). Pozyt może występować w dwóch stanach spinowych – singletowym jako *para*-pozyt (*p*-Ps) z antyrównoległym ułożeniem spinów pozytonu i elektronu lub trypletowym jako *orto*-pozyt (*o*-Ps) z równoległą orientacją spinów. Prawdopodobieństwo powstania *o*-Ps trzykrotnie przewyższa prawdopodobieństwo powstania *p*-Ps. Pozyt jest układem nietrwałym. W próżni *p*-Ps anihiluje do 2 kwantów gamma po czasie ok. 0,125 ns, natomiast *o*-Ps do 3 kwantów gamma po czasie ok. 142 ns.<sup>12–13</sup> W ośrodkach materialnych czas życia *o*-Ps jest znacznie krótszy (kilka nanosekund) i zależny od upakowania struktury wewnętrznej. Skrócenie czasu życia *o*-Ps jest konsekwencją procesu gaszenia, tzw. *pick-off*, dzięki któremu anihilacja następuje do 2 kwantów gamma. Ze względu na krótki czas życia *p*-Ps proces *pick-off* dotyczy głównie *o*-Ps.<sup>13–16</sup>

Zależność pomiędzy czasem życia *o*-Ps a rozmiarem wolnej objętości jest określana na podstawie modelu Tao-Eldrupa:<sup>15–16</sup>

$$\tau_3 = 0.5 \left[ 1 + \frac{R}{R + \Delta R} + \frac{1}{2\pi} \sin \left( \frac{2\pi R}{R + \Delta R} \right) \right]^{-1}$$

gdzie:

$\tau_3$  – średni czas życia *o*-Ps [ns],

$R$  – średni promień objętości swobodnej [nm],

$\Delta R$  – empiryczna stała dopasowania.

Równanie to stanowi podstawę do obliczania średniego rozmiaru i koncentracji swobodnych objętości.<sup>13</sup>

Spektroskopia Ramana i MIR dostarczają informacji o budowie chemicznej związków poprzez identyfikację drgań charakteryzujących dane grupy funkcyjne oraz analizę widm w zakresie tzw. *fingerprint*. Metoda MIR wykorzystuje zjawisko absorpcji promieniowania przez molekuły badanego materiału w zakresie podczerwieni, dzięki czemu uzyskuje się widma z pasmami absorpcyjnymi przypisane odpowiednim grupom funkcyjnym, natomiast metoda Ramana opiera swoje działanie na zjawisku rozpraszania monochromatycznego promieniowania laserowego na atomach badanego materiału, przez co uzyskuje się widma zawierające pasma odpowiadające poziomom oscylacyjnym molekuł struktury materiału.<sup>17</sup>

Należy zaznaczyć, że w przypadku materiałów polimerowych wykorzystywanych do produkcji soczewek kontaktowych, będących mieszaninami różnych monomerów o nieznanym proporcjach (prawo patentowe), wiele pasm może się na siebie nakładać, znacznie utrudniając analizę i interpretację.

Badania za pomocą PALS wykazały, że rozmiary oraz ilości swobodnych objętości w badanych soczewkach kontaktowych znacznie różnią się między sobą. Największe rozmiary i ilości wolnych objętości obserwuje się w soczewkach silikonowo-hydrożelowych. Są one ściśle związane z przepuszczalnością tlenu – im większe rozmiary i ilości swobodnych objętości, tym większy współczynnik przepuszczalności tlenu.

W materiałach hydrożelowych w stanie uwodnionym wszystkie wolne przestrzenie wypełnione są wodą, tzw. wodą wolną.<sup>13,18</sup> Woda wolna jest odpowiedzialna za przenikanie tlenu,<sup>19,20</sup> a jej zawartość zależy od rozmiarów i ilości wolnych objętości. Wprowadzenie grup siloksanowych powoduje zwiększenie porowatości materiału. Wiązania Si–O charakteryzują się wysoką elastycznością i mobilnością.<sup>21,22</sup> Giętkość łańcucha siloksanowy zawdzięczają względnie długim wiązaniom Si–O (ok. 1,64 Å) i Si–C (ok. 1,88 Å) minimalizującym utrudnienie rotacji wokół wiązań łańcucha oraz przemiennemu rozmieszczeniu atomów Si oraz O.<sup>23</sup> Istnieje możliwość tworzenia kanałów – swobodnych objętości – umożliwiających transport gazów poprzez matrycę polimerową. Wysoki współczynnik przepuszczalności tlenu dla soczewek silikonowo-hydrożelowych można więc interpretować jako większe rozmiary wolnych objętości oraz ich ilości. Ilość silikonu w monomerach oraz proporcja samych monomerów w materiale odgrywają kluczową rolę.

Ewentualna zmiana rozmiarów i ilości wolnych objętości w strukturze materiału wynikająca z oddziaływania promieniowania jonizującego może wpłynąć na zmianę parametru przepuszczalności tlenu i bezpieczeństwo użytkowników soczewek kontaktowych.<sup>18</sup>

## Możliwe powikłania związane z użytkowaniem soczewek kontaktowych

Mimo zachowania należytej staranności podczas doboru soczewek kontaktowych i właściwego ich użytkowania może dojść do powikłań. Efekty uboczne mogą występować na powiekach, spojówkach i rogówce. Wśród objawów niepożądanych dotyczących powiek wymienić można niepełne mruganie, opadnięcie powieki, zapalenie brzegów powiek, niewydolność gruczołów Meiboma czy jęczmień. Powikłania dotyczące spojówek to np. przekrwienia czy też nadwrażliwość – olbrzymiobrodawkowe zapalenie spojówek. Na rogówce mogą wystąpić liczne stany związane z ubytkami komórek nabłonka określane w testach barwienia, m.in. barwienie na godzinie 3 i 9,

barwienie nabłonka łukowate górne czy dolne. Czasem w nabłonku rogówki można też zaobserwować cysty i wakuole oraz obrzęk. W przypadku istoty właściwej rogówki może pojawić się jej obrzęk, przymglenie lub neowaskularyzacja. Zmiany związane ze stosowaniem soczewek kontaktowych mogą prowadzić do zmiany kształtu i liczby komórek śródbłonka rogówki. Specjalnego podkreślenia wymaga fakt, że w przebiegu użytkowania soczewek kontaktowych może dojść do zapalenia rogówki (*keratitis*).<sup>24</sup>

*Keratitis* jest stanem, który może prowadzić do trwałego upośledzenia ostrości wzroku. Zapalenie rogówki może być jałowe (lepsze rokowanie) bądź związane z infekcją – bakteryjną, pełzakową lub grzybiczą. Przyjmuje się, że typowe dla stosowania soczewek kontaktowych jest infekcyjne pełzakowe zapalenie rogówki wywołane przez *Acanthamoeba*, które jest stanem bezpośrednio zagrażającym widzeniu. Jako istotny czynnik ryzyka rozwoju tego zapalenia wymienia się także brak stosowania się do zaleceń producentów poszczególnych rodzajów soczewek.<sup>24,25</sup>

## Podsumowanie

Jednym z możliwych powikłań związanych ze stosowaniem soczewek kontaktowych jest niedotlenienie rogówki. Ryzyko niedotlenienia rogówki wzrasta przy użytkowaniu soczewek kontaktowych znacznie ograniczających dostęp tlenu do rogówki (o niskim  $Dk/t$ ). Wrażliwość rogówek na niedotlenienie jest jednak bardzo zróżnicowana. Niedotlenienie rogówki powoduje, że zachodzą w niej zmiany metaboliczne zmniejszające skuteczność działania mechanizmów obronnych oka. Skutkiem tego może być zwiększona podatność na infekcję, w tym bakteryjne, grzybicze czy pierwotniakowe. Najbardziej zagrożoną niedotlenieniem częścią jest jej centrum.

Analiza wpływu czynników zewnętrznych, w tym promieniowania jonizującego, na zmianę parametru tlenu-przepuszczalności wydaje się ważna w kontekście bezpieczeństwa użytkowników soczewek.

Przedstawione powyżej dane wskazują, że istnieje konieczność wykonania niezależnych od producentów badań dotyczących struktury materiałów soczewek kontaktowych różnego typu w celu określenia ich tolerancji na działanie promieniowania jonizującego i tym samym zagwarantowania bezpieczeństwa ich użytkownikom narażonym na kontakt z promieniowaniem jonizującym (zarówno pacjentom, jak i personelowi medycznemu).

## Piśmiennictwo

1. Hubbe U, Sircar R, Scheiwe C, et al. Surgeon, staff, and patient radiation exposure in minimally invasive transforaminal lumbar interbody fusion: Impact of 3D fluoroscopy-based navigation partially replacing conventional fluoroscopy: Study protocol for a randomized controlled trial. *Trials*. 2015;16:142. doi: 10.1186/s13063-015-0690-5.
2. Klingler J, Sircar R, Scheiwe C, et al. Comparative study of C-arms for intraoperative 3-dimensional imaging and navigation in minimally invasive spine surgery. Part II – radiation exposure. *Clin Spine Surg*. 2017;30:669–676.



3. Mozolewska-Piotrowska K, Stepniewska J, Nawrocka J. Występowanie krótkowzroczności szkolnej u studentów medycyny. *Klin Oczna*. 2005;107:468–470.
4. Gasson A, Morris JA. *Soczewki kontaktowe – praktyczny przewodnik właściwego dopasowania*. Ścibior R, red. wyd. pol. Wrocław: Elsevier Urban & Partner; 2014.
5. Leung BK, Bonanno JA, Radke CJ. Oxygen-deficient metabolism and corneal edema. *Prog Retin Eye Res*. 2011;30(6):471–492.
6. Harvitt DM, Bonanno JA. Re-evaluation of the oxygen diffusion model for predicting minimum contact lens  $Dk/t$  values needed to avoid corneal anoxia. *Optom Vision Sci*. 1999;76:712–719.
7. Chhabra M, Prausnitz JM, Radke CJ. A single-lens polarographic measurement of oxygen permeability ( $Dk$ ) for hypertransmissible soft contact lenses. *Biomaterials*. 2007;28(30):4331–4342.
8. Fonn D, Sweeney DF, Holden BA, Cavanagh D. Corneal oxygen deficiency. *Eye Contact Lens*. 2005;31(1):23–27.
9. Filipecka K, Budaj M, Chamerski K, et al. PALS, MIR and UV-vis-NIR spectroscopy studies of pHEMA hydrogel, silicon- and fluoro-containing contact lens materials. *J Mol Struct*. 2017;1148:521–530.
10. Singh JJ, Eftekhari A, Upchurch BT, Burns KS. An investigation on microstructural characteristics of contact lens polymers. *NASA Technical Paper*. 1990:3034.
11. Sane P, Tumisto F, Holopainen JM. Void volume variations in contact lens polymers. *Cont Lens Anterior Eye*. 2011;34(1):2–6.
12. Dryzek J. *Wstęp do spektroskopii anihilacji pozytonów w ciele stałym*. Kraków: Wydawnictwo Uniwersytetu Jagiellońskiego; 1997.
13. Filipecki J, Kocela A, Korzekwa P, et al. Structural study of polymer hydrogel contact lenses by means of positron annihilation lifetime spectroscopy and UV-vis-NIR methods. *J Mater Sci Mater Med*. 2013;24:1837–1842.
14. Chamerski K. Analiza porównawcza struktury wewnętrznej implantów hydrofilowych oraz hydrofobowych stosowanych w chirurgii okulistycznej metodą spektroskopii czasów życia pozytonów. *Technical Issues*. 2015;3:3–10.
15. Liao KS, Chen H, Awad S, et al. Determination of free-volume properties in polymers without orthopositronium components in positron annihilation lifetime spectroscopy. *Macromolecules*. 2011;44:6818–6826.
16. Jean YC, Van Horn JD, Hung WS, Lee KR. Perspective of positron annihilation spectroscopy in polymers. *Macromolecules*. 2013; 46:7133–7145.
17. Kęcki Z. *Podstawy spektroskopii molekularnej*. Warszawa: Wydawnictwo Naukowe PWN; 2013.
18. Filipecki J, Korzekwa P, Filipecka K, et al. Badanie zmian wolnych objętości w strukturze polimerowych dwuogniskowych soczewek kontaktowych metodą anihilacji pozytonów. *Polim Med*. 2010;40(4):27–33.
19. Hoffman AS. Hydrogels for biomedical applications. *Adv Drug Deliv Rev*. 2012;64:18–23.
20. Tranoudis I, Efron N. Water properties of soft contact lens materials. *Cont Lens Anterior Eye*. 2004;27(4):193–208.
21. Reddy BSR, Senthilkumar U. Prospects of siloxane membrane technology for gas separation. *J Sci Ind Res*. 2003;62(7):666–677.
22. Zhao Z, Xie H, An S, Jiang Y. The Relationship between oxygen permeability and phase separation morphology of the multicomponent silicone hydrogels. *J Phys Chem B*. 2014;118(50):14640–14647.
23. Cypriak M, Delczyk B, Pospiech P, Strzelec K. Modyfikacje polimerów siloksanowych. *Polimery*. 2007;52:496–502.
24. Efron N. *Contact Lens Complications*. 3<sup>rd</sup> ed. Philadelphia: Saunders; 2012.
25. Ibrahim YW, Boase DL, Cree IA. How could contact lens wearers be at risk of *Acanthamoeba* infection? A Review. *Journal Optom*. 2009;2(2):60–66.



# A study of the effect of X-ray irradiation on the structure of Narafilcon A biopolymer soft contact lenses

Katarzyna Filipecka<sup>1,A–D</sup>, Mariusz Budaj<sup>2,A–D</sup>, Bogdan Miškowiak<sup>2,E,F</sup>, Sylwia Mandecka<sup>3,B,C</sup>, Radosław Mandecki<sup>3,B,C</sup>, Małgorzata Makowska-Janusik<sup>1,E,F</sup>, Jacek Filipecki<sup>1,E,F</sup>

<sup>1</sup> Institute of Physics, Faculty of Mathematics and Natural Sciences, Jan Długosz University in Częstochowa, Poland

<sup>2</sup> Department of Optometry and Biology of Visual System, Poznan University of Medical Sciences, Poland

<sup>3</sup> Department of Radiotherapy, Specialist District Hospital, Częstochowa, Poland

A – research concept and design; B – collection and/or assembly of data; C – data analysis and interpretation; D – writing the article; E – critical revision of the article; F – final approval of the article

Polymers in Medicine, ISSN 0370-0747 (print), ISSN 2451-2699 (online)

*Polim Med.* 2018;48(1):11–16

## Address for correspondence

Jacek Filipecki

E-mail: j.filipecki@ajd.czest.pl

## Funding sources

None declared

## Conflict of interest

None declared

Received on June 1, 2018

Reviewed on July 24, 2018

Accepted on September 25, 2018

## Abstract

**Background.** The effects of external factors such as X-ray irradiation on the structure and physical properties of contact lenses are very important for both the patients using contact lenses and medical personnel.

**Objectives.** The aim of the study was to investigate the effect of X-rays on the structure of Narafilcon A silicone-hydrogel contact lenses.

**Material and methods.** In order to study the structural changes caused by X-rays in Narafilcon A polymer contact lenses, the following spectroscopy methods were used: positron annihilation lifetime spectroscopy (PALS), Fourier transform middle infrared spectroscopy (FTIR) and Raman spectroscopy (RS). Irradiation of the investigated sample was carried out using an Elekta Synergy accelerator. The contact lenses were irradiated with the following total doses of X-rays: 0.05 Gy, 0.5 Gy, 0.8 Gy, and 1.0 Gy.

**Results.** The PALS measurements showed that X-ray irradiation caused slight changes in the size of the free volume and the fractional free volume in the structure of the polymer contact lenses examined. However, the FTIR and RS measurements showed that X-rays did not break the monomer bonds in the polymeric structure of the sample.

**Conclusions.** The changes revealed by the PALS method may be related to possible displacement of monomer chains, resulting in changes in the dimensions and numbers of free volumes. The finding that X-ray radiation does not affect or damage polymer bonds can in the future contribute to the use of X-ray and gamma radiation to sterilize contact lenses.

**Key words:** positron annihilation lifetime spectroscopy, Fourier transform middle infrared spectroscopy, Raman spectroscopy, contact lens, radiation

## Cite as

Filipecka K, Budaj M, Miškowiak B, et al. A study of the effect of X-ray irradiation on the structure of Narafilcon A biopolymer soft contact lenses. *Polim Med.* 2018;48(1):11–16. doi:10.17219/pim/96288

## DOI

10.17219/pim/96288

## Copyright

© 2018 by Wrocław Medical University

This is an article distributed under the terms of the Creative Commons Attribution Non-Commercial License (<http://creativecommons.org/licenses/by-nc-nd/4.0/>)



## Materials and methods

The study was carried out on originally packed Narafilcon A soft contact lenses, which belong to the silicone-hydrogel family. Detailed parameters obtained from the manufacturer (Cooper Vision, Phoenix, USA) of the contact lenses are shown in Table 1.

**Table 1.** Detailed parameters obtained from the manufacturer of the contact lenses

Sample	Material	Water content [%]	Oxygen permeability: Dk ( $\times 10^{-11}$ )
Soft contact lens (silicone-hydrogel)	Narafilcon A	46	100*

\* taking into account the edge effect and the border effect.

Irradiation of the samples was carried out using an Elekta Synergy accelerator MLCi 80 (Elekta Instrument AB, Stockholm, Sweden).<sup>17</sup> The Elekta Synergy accelerator emits photon and electron radiation of nominal energy (photons – 4, 6, 15 MeV and electrons – 6, 9, 12, 15 MeV) with a multi-leaf collimator (MLCi 80). The maximum dimension of the field adjusted by the jaws and MLCi is 40 cm  $\times$  40 cm. The samples were irradiated in a water phantom in reference conditions (field size: 10 cm  $\times$  10 cm; source to surface distance (SSD): 90 cm; depth: 10 cm; energy: 6 MeV). The apparatus was calibrated to 1-to-1 relations, i.e., 1 monitor unit was equivalent to a dose of 1 Gy. The contact lenses were irradiated with the following total doses of X-rays: 0.05 Gy, 0.5 Gy, 0.8 Gy, and 1.0 Gy, which are equivalent to doses that patients wearing contact lenses may be exposed to during medical X-ray examinations, or the medical personnel during their professional work with X-ray radiation. Irradiation of the samples in a water phantom was dictated by the fact that devices for measuring doses are calibrated in water. Moreover, doses given in water are more uniform and the electron equilibrium is maintained, which makes it easier to define the dose. As a result, we can precisely calculate the dose absorbed by contact lenses. According to the International Atomic Energy Agency (IAEA) TRS398 dosimetric standards, measurements should be performed in water. The previous IAEA dosimetric report (TRS277) allowed measurements in the air, but such measurements are extremely complex and it is difficult to define the dose.<sup>18</sup>

The PALS measurements were performed at room temperature using an ORTEC spectrometer (ORTEC, Oak Ridge, USA), based on a “start-stop” method.<sup>19,20</sup> A spectrometer with a lifetime resolution – the full width at half maximum (FWHM) of 250 ps, monitored with a Cobalt-60 (<sup>60</sup>Co) source, was used to record all the PALS spectra. Each sample consisted of 6 layers of contact lenses with a diameter of 10 mm and a thickness of 1 mm. All the samples were of the same diameter and thickness. A sample, along with the source of positrons, which was the <sup>22</sup>Na isotope of an  $4 \times 10^5$  Bq activity, formed the so-called “sandwich system”.

The FTIR studies were carried out on a DigiLab Excalibur series spectrometer (Digilab Inc., Hopkinton, USA) equipped with a Pike MIRacle™ attenuated total reflection (ATR) attachment (PIKE Technologies Inc., Madison, USA).<sup>21</sup> A total of 128 scans were accumulated in the range of 550–4000  $\text{cm}^{-1}$  and the resolution was set at 4  $\text{cm}^{-1}$ .

The RS spectra were recorded using an alpha300 confocal Raman microscope (WITec Wissenschaftliche Instrumente und Technologie GmbH, Ulm, Germany) equipped with an air-cooled solid state laser, operating at 488 nm, and a charge-coupled device (CCD) detector, cooled to  $-82^\circ\text{C}$ . A dry Olympus MPLAN (1006/0.90NA) objective lens (Olympus Corp., Tokyo, Japan) was used. The power of the laser at the sample position was between 14.4 mW and 14.6 mW for each measurement. A minimum of 120 scans with integration times of 0.3–0.5 s and a resolution of 3  $\text{cm}^{-1}$  were collected and averaged.<sup>21</sup>

## Results and discussion

Positron lifetime spectra were analyzed using LT software (LT Software Solutions, Portsmouth, USA).<sup>22</sup> The obtained positron lifetime values revealed the existence of 3 components –  $\tau_1$ ,  $\tau_2$  and  $\tau_3$  in the positron lifetime spectrum. The component  $\tau_1$  represents the annihilation of *p*-Ps, which in this paper fits a value of 0.125 ns, while the component  $\tau_2$  is typical for positron trapping.<sup>23,24</sup> As in our previous papers on the subject, attention was paid to the analysis of the longest-lived component of the positron lifetime –  $\tau_3$  (the “pick-off” process).<sup>7–9</sup> The positron lifetime values of  $\tau_3$  *o*-Ps and their intensity  $I_3$ , hole radius  $R$ , the sizes of the free volumes  $V_f$  and the fractional free volumes  $f_v$  for all the samples before and after irradiation are given in Table 2. The main parameters of annihilation converted to means  $\pm$  measurement error were calculated using LT software.

The relationship between the sizes of the free volumes  $V_f$  and the fractional free volumes  $f_v$  as a function of X-ray irradiation is shown in Fig. 2.

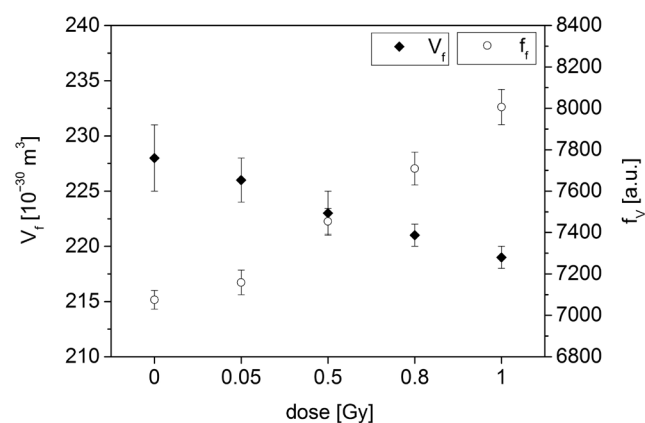


**Fig. 2.** The relationship between the sizes of the free volumes  $V_f$  and the fractional free volumes  $f_v$  as a function of X-ray irradiation

**Table 2.** Calculated mean values of positron lifetime  $\tau_3$  and their intensity  $I_3$ , hole radius  $R$ , the size of the free volume  $V_f$ , and the fractional volume  $f_v$ 

Sample	$\tau_3$ [ns]	$I_3$ [%]	$R$ [nm]	$V_f$ [ $10^{-30}$ m <sup>3</sup> ]	$f_v$ [au]
Nar A	3.167 ± 0.052	17.24 ± 0.28	0.379 ± 0.002	228 ± 3	7075 ± 26
Nar A – 0.05 Gy	3.147 ± 0.048	17.60 ± 0.31	0.378 ± 0.002	226 ± 2	7159 ± 28
Nar A – 0.5 Gy	3.133 ± 0.042	18.57 ± 0.33	0.376 ± 0.001	223 ± 2	7454 ± 29
Nar A – 0.8 Gy	3.121 ± 0.036	19.38 ± 0.35	3.375 ± 0.001	221 ± 1	7709 ± 29
Nar A – 1 Gy	3.098 ± 0.032	20.31 ± 0.37	0.374 ± 0.001	219 ± 1	8006 ± 31

Nar A – Narafilcon A; data presented as mean ± standard deviation (SD).

It is evident from the results presented in Table 2 and Fig. 2 that as the dose of X-ray irradiation of the sample increases, there is a tendency towards decreases in the sizes of the free volumes  $V_f$ . However, there is a significant increase in the intensity  $I_3$  of the *o*-Ps lifetime component and in the fractional free volumes  $f_v$ . It can be concluded that X-ray radiation doses from 0.05 Gy to 1 Gy result simultaneously in a slight decrease in the free volume dimensions and an increase in the number of free volumes in the irradiated sample.

In order to check whether the doses of X-ray irradiation affect the bond structure of the samples, measurements were made using RS and FTIR. The results are shown in Fig. 3–5. A close analysis of the obtained spectra indicated that irradiation of the samples did not cause any changes in their structure. Therefore, it is possible to conclude that in spite of active irradiation, no bonds disappeared nor did any additional bonds appear.

The study found no other significant changes in the structure of the samples examined or in the angles of the existing bonds. To sum up, the FTIR and RS studies showed that the applied radiation did not result in any significant changes in the structure of Narafilcon A lenses, or that the changes were so small that they could not be noticed in the corresponding spectra.

Ionizing radiation of different types, e.g., electron or gamma beams, has long been recognized as a suitable tool

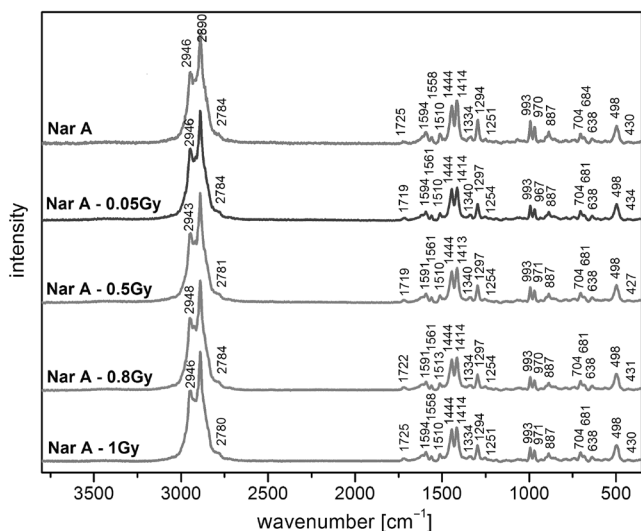


Fig. 3. Raman (RS) spectra of Narafilcon A contact lenses before and after X-ray radiation

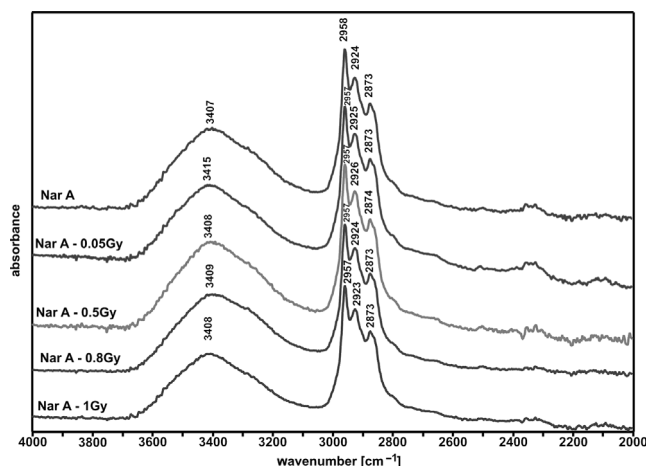


Fig. 4. Fourier transform middle infrared (FTIR) spectra of Narafilcon A contact lenses before and after X-ray radiation (in the 2000–4000 cm<sup>-1</sup> range)

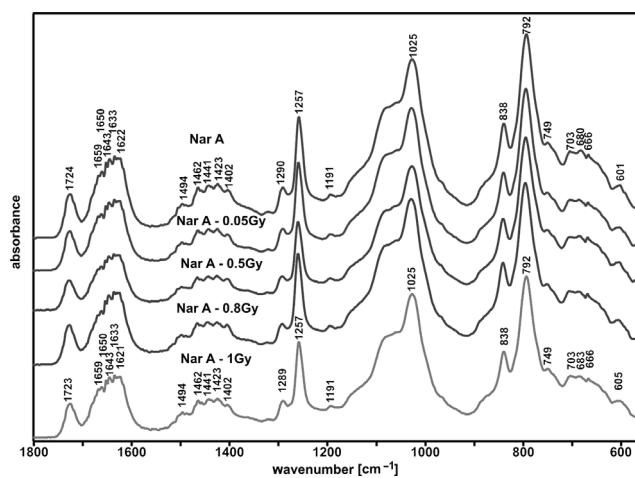


Fig. 5. Fourier transform middle infrared (FTIR) spectra of Narafilcon A contact lenses before and after X-ray radiation (in the 550–1800 cm<sup>-1</sup> range)

for the synthesis and modification of the structure and properties of polymeric materials. The exposure of polymers to ionizing radiation causes modifications such as radiation cross-linking, radiation-induced polymerization (graft polymerization and curing) and degradation of polymers.<sup>25</sup> However, it should be pointed out that the effects of ionizing radiation on the properties and performance of polymers depend greatly on the chemical structure of a polymer.

One of the components of contact lenses is water. There are 3 main types of water found in polymers: non-freezable bound water (tightly bound), freezable bound water

(loosely bound) and free water (bulk). Tightly bound water is generally attributed to water molecules directly linked by hydrogen bonding with the polar groups of the polymer matrix or strongly interacting with the ionic residues of the polymer matrix. Loosely bound water is usually related to water molecules loosely associated with the polar groups through hydrogen bonding in water-swollen polymers.<sup>26–28</sup> Free (bulk) water refers to water molecules that do not interact with the polymer matrix, having hydrogen bonding typical of pure water. The amount of bound water can vary according to the polymer microstructure. Changes in the polymer structure caused by ionizing radiation can affect the water dynamics within the material.<sup>26</sup>

The dose of radiation necessary to produce similar significant effects in 2 different materials can vary significantly between them. From the results of this study, it can be deduced that X-ray irradiation causes only microstructural changes to the polymer network of Narafilcon A contact lenses.

## Conclusions

The aim of this project was to study the effect of external X-ray radiation in total doses of 0.05 Gy, 0.5 Gy, 0.8 Gy, and 1.0 Gy on changes in the soft structure of Narafilcon A contact lenses. The PALS method, which is extremely sensitive to detecting changes in the structure of materials, showed minor changes in the dimensions and number of free volumes in the lenses. At the same time, the FTIR and RS studies indicated that the applied radiation did not result in any significant changes in the bond structure of the examined material, or that the changes were so insignificant that they were impossible to trace in the corresponding spectra. We can speculate that the applied X-ray radiation was very hard and did not break the bonds, nor did it result in changing the bond angles of the monomers in the molecular structure of the Narafilcon A contact lenses. The changes revealed by the PALS method can be related to possible displacement of monomer chains, which results in changes in the dimensions and numbers of the occurring free volumes. The finding that X-ray radiation does not affect or damage polymer bonds can in the future contribute to the use of X-ray and gamma radiation to sterilize contact lenses. This may become clearer as a result of further studies on the effect of electron-type radiation (beta radiation) on Narafilcon A samples, with the same total doses of irradiation as in this study, which will be carried out by the authors of this paper in the near future.

## References

- Tranoudis I, Efron N. In-eye performance of soft contact lenses made from different materials. *Cont Lens Anterior Eye*. 2004;27(3):133–148.
- Wolffsohn JS, Hunt OA, Basra AK. Simplified recording of soft contact lens fit. *Cont Lens Anterior Eye*. 2009;32(1):37–42.
- Morgan PB, Chamberlain P, Moody K, Maldonado-Codina C. Ocular physiology and comfort in neophyte subjects fitted with daily disposable silicone hydrogel contact lenses. *Cont Lens Anterior Eye*. 2013;36(3):118–125.
- Jean YC. Characterizing free volumes and holes in polymers by positron annihilation spectroscopy. In: *Advances with Positron Spectroscopy of Solids and Surfaces*. NATO Advanced Research Workshop. 1993:563–580.
- Eldrup M, Lighbody D, Sherwood JN. The temperature dependence of positron lifetimes in solid pivalic acid. *Chem Phys*. 1981;63:51–62.
- Brandt W, Berko S, Walker WW. Positronium decay in molecular substances. *Phys Rev*. 1960;120(4):1289–1295.
- Kocela A, Filipecki J, Korzekwa P, Golis E. Investigation of the free volume changes in one day hydrogel and one day silicone hydrogel contact lenses by means of positron annihilation lifetime spectroscopy. *Polim Med*. 2012;42(1):61–68.
- Filipecki J, Kocela A, Korzekwa W. Study of free volumes of polymer hydrogel and silicone-hydrogel contact lenses by means of the positron annihilation lifetime spectroscopy method. *Polim Med*. 2014;44(4):255–260.
- Filipecka K, Budaj M, Miškowiak B, Makowska-Janusik M, Filipecki J. Comparison of occurrence of free volumes for rigid gas permeable and soft contact lenses. *Polim Med*. 2015;45(1):31–35.
- Tao SJ. Positronium annihilation in molecular substances. *J Chem Phys*. 1972;56(11):5499–5510.
- Liao KS, Chen H, Awad S, et al. Determination of free-volume properties in polymers without orthopositronium components in positron annihilation lifetime spectroscopy. *Macromolecules*. 2011;44(17):6818–6826.
- Filipecki J, Kocela A, Korzekwa P, et al. Structural study of polymer hydrogel contact lenses by means of positron annihilation lifetime spectroscopy and UV-vis-NIR methods. *J Mater Sci Mater Med*. 2013;24(8):1837–1842.
- Pathrick RA. Positron annihilation: A probe for nanoscale voids and free volume. *Prog Polymer Sci*. 1997;22(1):1–47.
- Noda I. Two-dimensional infrared (2D IR) spectroscopy: Theory and applications. *Appl Spectrosc*. 1990;44(4):550–561.
- Koenig JL. *Spectroscopy of Polymers*. 2<sup>nd</sup> ed. New York, NY: Elsevier Science Inc.; 1999.
- Ramanathan T, Fisher FT, Ruoff RS, Brinson LC. Amino-functionalized carbon nanotubes for binding to polymers and biological systems. *Chem Mater*. 2005;17(6):1290–1295.
- Mandecki R, Filipecki J. Teleradiotherapy and brachytherapy [in Polish]. *Prace Naukowe AJD w Częstochowie FIZYKA IX*. 2014;9:95–116.
- Andreo P, Burns DT, Hohlfield K, et al. Absorbed Dose Determination in External Beam Radiotherapy: An International Code of Practice for Dosimetry based on Standards of Absorbed Dose to Water. Vienna, Austria: International Atomic Energy Agency (IAEA); 2006.
- Filipecki J, Golis E, Reben M, Filipecka K, Kocela A, Wasylak J. Positron lifetime spectroscopy as a method to study of the defect degree materials with disordered structure. *Optoelectron Adv Mat*. 2013;7(11–12):1029–1031.
- Reben M, Golis E, Filipecki J, et al. Voids in mixed-cation silicate glasses: Studies by positron annihilation lifetime and Fourier transform infrared spectroscopies. *Spectrochim Acta A Mol Biomol Spectrosc*. 2014;129:643–648.
- Filipecki J, Sitarz M, Kocela A, et al. Studying functional properties of hydrogel and silicone-hydrogel contact lenses with PALS, MIR and Raman spectroscopy. *Spectrochim Acta A Mol Biomol Spectrosc*. 2014;131:686–690.
- Kansy J. Microcomputer program for analysis of positron annihilation lifetime spectra. *Nucl Instrum Methods Phys Res Section A*. 1996;374(2):235–244.
- Krause-Rehberg R, Leipner HS. *Positron Annihilation in Semiconductors. Defect Studies*. Berlin-Heidelberg-New York: Springer-Verlag; 1999.
- Jean YC, David Van Horn J, Wei-Song H, Kuier-Rarn L. Perspective of positron annihilation spectroscopy in polymers. *Macromolecules*. 2013;46(18):7133–7145.

25. Rosiak JM, Olejniczak J. Medical applications of radiation formed hydrogel. *Radiat Phys Chem.* 1993;42(4):903–906.
26. Tranoudis I, Efron N. Water properties of soft contact lens materials. *Cont Lens Anterior Eye* 2004;27:193–208.
27. Krysztofiak K, Szczyzewski A. Study of dehydration and water states in new and worn soft contact lens materials. *Optica Applicata.* 2014;44(2):237–249.
28. Mullarney MP, Seery TAP, Weiss RA. Drug diffusion in hydrophobically modified *N,N*-dimethylacrylamide hydrogels. *Polymer.* 2006;47(11):3845–3855.



# Preparation, characterization and in vitro evaluation of tablets containing microwave-assisted solid dispersions of apremilast

Jyotsana R. Madan<sup>1,A–F</sup>, Akshaya R. Pawar<sup>1,B–E</sup>, Rajesh B. Patil<sup>1,B–D,F</sup>, Rajendra Awasthi<sup>2,C–F</sup>, Kamal Dua<sup>3,C–F</sup>

<sup>1</sup> Department of Pharmaceutics, Smt. Kashibai Navale College of Pharmacy, Savitribai Phule Pune University, India

<sup>2</sup> Amity Institute of Pharmacy, Amity University, Noida, India

<sup>3</sup> Discipline of Pharmacy, Graduate School of Health, University of Technology, Sydney, Australia

A – research concept and design; B – collection and/or assembly of data; C – data analysis and interpretation;

D – writing the article; E – critical revision of the article; F – final approval of the article

Polymers in Medicine, ISSN 0370-0747 (print), ISSN 2451-2699 (online)

*Polim Med.* 2018;48(1):17–24

## Address for correspondence

Jyotsana R. Madan

E-mail: jyotsna.madan@sinhgad.edu

## Funding sources

None declared

## Conflict of interest

None declared

Received on July 21, 2018

Reviewed on September 15, 2018

Accepted on November 15, 2018

## Cite as

Madan JR, Pawar AR, Patil RB, Awasthi R, Dua K. Preparation, characterization and in vitro evaluation of tablets containing microwave-assisted solid dispersions of apremilast.

*Polim Med.* 2018;48(1):17–24. doi:10.17219/pim/99801

## DOI

10.17219/pim/99801

## Copyright

© 2018 by Wrocław Medical University

This is an article distributed under the terms of the

Creative Commons Attribution Non-Commercial License

(<http://creativecommons.org/licenses/by-nc-nd/4.0/>)

## Abstract

**Background.** Solid dispersions are among the techniques successfully employed to enhance the dissolution of poorly water-soluble drugs. Microwave (MW)-assisted evaporative crystallization has been used to prepare solid dispersions of drugs and polymers.

**Objectives.** The aim of the study was to investigate the solubility of apremilast (APM) in water by exploring the effect of MW-assisted solid dispersion technology.

**Material and methods.** In the present study, solid dispersions of APM, a poorly water-soluble drug, were prepared. The solid dispersions were prepared using the conventional method (CM) and the MW-based solvent evaporation technique. Microwave energy was used to enhance the solubility and dissolution rate of APM. The physical mixture and solid dispersions were characterized using Fourier-transform infrared spectroscopy (FTIR), X-ray powder diffraction (XRPD), differential scanning calorimetry (DSC), and scanning electron microscopy (SEM). Apremilast tablets containing MW-assisted solid dispersions were prepared by the direct compression technique and compared with the marketed formulation (Aprezo tablets).

**Results.** The results obtained confirmed the conversion of crystalline APM to an amorphous form. The XRPD pattern of the MW-assisted formulation at a 2:1 ratio suggests the amorphous structure of APM within the formulation. Based on solubility studies results, Syloid<sup>®</sup> 244FP was selected as the best carrier. The dissolution study results suggested that the APM tablet prepared using MW-assisted solid dispersions at a 2:1 carrier/drug ratio improved the APM dissolution rate compared to the marketed formulation.

**Conclusions.** Based on the results, it can be concluded that the MW-assisted solid dispersion technique may be an effective approach to enhancing the dissolution profile of other poorly water-soluble drugs.

**Key words:** microwave, solubility, apremilast, solid dispersions

## Introduction

A drug being developed into an oral formulation requires sufficient solubility in the dissolution medium in order to obtain optimal dissolution rates. The Biopharmaceutics Classification System (BCS) recognizes the importance of the rate of dissolution and aqueous solubility as key factors in the determination of the oral absorption of drugs.

Solid dispersions are among the techniques successfully employed to enhance the dissolution of poorly water-soluble drugs.<sup>1–9</sup> Traditionally, solid dispersions are prepared by the melting, melting-solvent or solvent methods. Newer methods for the manufacture of solid dispersions include hot spin mixing,<sup>10</sup> supercritical fluid technology and hot-melt extrusion (HME).<sup>11,12</sup> Researchers are also investigating the potential of microwaves (MWs) to enhance solubility and bioavailability of poorly soluble drugs using the formation of solid dispersions and nanocomposite materials. In a recent study, MW-assisted evaporative crystallization was used to prepare solid dispersions of drugs and polymers.<sup>13</sup>

Microwaves are part of the electromagnetic spectrum, the frequency range of which is 0.3–300 GHz. The migration of MW within materials causes molecular oscillation, which leads to the generation of heat.<sup>14,15</sup> The MW approach to heating is different from conventional heating, in which heat transfer takes place from the surface to the inner core. In the MW approach, heat is generated in the material and then passes to the entire volume, with a constant heating rate leading to uniform and deep heating of materials.<sup>14,16</sup> Microwave technology is rapid, cost-effective, energy-saving, and environmentally safe. The crystalline drug is generally converted into an amorphous form, which means the approach can be used for the improvement of the dissolution profiles of BCS class II and IV drugs.<sup>14,17</sup>

Apremilast (APM) is a novel, orally available small molecule inhibitor of type 4 cyclic nucleotide phosphodiesterase (PDE4). It is indicated in the treatment of active psoriatic arthritis in adults and moderate to severe plaque psoriasis.<sup>18–21</sup> It is practically insoluble in aqueous buffers, irrespective of pH range; it is soluble in acetone, acetonitrile, methyl ethyl ketone, methylene chloride, and tetrahydrofuran. The BCS classifies APM as having low solubility and low permeability (i.e., BCS class 4). Very poor solubility of APM in water influences the dissolution of the drug in aqueous media. Its oral bioavailability has been reported to be 20–33%.<sup>22,23</sup> In order to achieve an acceptable dissolution profile, crystal forms of APM or reduction of the APM particle size have been studied to improve its dissolution.<sup>24,25</sup>

Considering the various attempts at improving solubility of APM with different approaches, the objective of present study was to increase the solubility of APM in water by exploring the effect of MW-assisted solid dispersion technology.

## Material and methods

Apremilast was provided for the study by Glenmark Pharmaceuticals Ltd. (Nashik, India); APM tablets (Aprezo, the reference tablet) were purchased from the same company. Syloid<sup>®</sup> 244FP and Syloid<sup>®</sup> XDP 3150 were purchased from Grace GmbH & Co. KG (Worms, Germany). Polyethylene glycol (PEG) 6000, polyvinylpyrrolidone (PVP),  $\beta$ -cyclodextrin, lactose monohydrate, ethyl cellulose, and magnesium stearate were obtained from Research Lab Fine Chem Industries (Mumbai, India). Idacol Erythrosine Food Red-4 coloring agent was obtained from Roha Dyechem Pvt. Ltd. (Mumbai, India). All other reagents were of analytical grade.

### Determination of apremilast solubility in various buffers

Saturation solubility studies of APM in water, pH 1.2 acidic buffer, pH 2, pH 4, pH 6.8, and pH 7.4 phosphate buffers, as well as pH 6.8 phosphate buffer with 0.15% sodium lauryl sulfate (SLS) were conducted, using a magnetic stirrer (REMI Instruments Ltd., Mumbai, India). All media were prepared in individual flasks, and an excess amount of APM ( $\approx$ 50 mg) was weighed and transferred into the flasks. The flasks were placed on a magnetic stirrer at a speed of 200 rpm for 24 h at 37°C. After 24 h, the solution was centrifuged at 2000 rpm for 15 min. The supernatants were diluted with the respective media. Absorbance was measured at 230 nm using a Shimadzu V-630UV Visible Spectrophotometer (Shimadzu Corp., Kyoto, Japan) and solubility was calculated.<sup>6,26</sup>

### Preparation of physical mixtures of carriers and apremilast

Apremilast and carriers (Syloid<sup>®</sup> 244FP (S244), Syloid<sup>®</sup> XDP 3150 (S3150), PEG 6000, PVP, and  $\beta$ -cyclodextrin) were each passed through a No. 100 sieve and physical mixtures (PMs) were prepared by mixing pre-weighed amounts of APM with each carrier at a 1:1 ratio.

### Preliminary trials for the preparation of solid dispersions by the conventional method

We prepared solid dispersions of APM with the 5 selected carriers – S244, S3150, PEG 6000, PVP, and  $\beta$ -cyclodextrin – at a carrier/drug ratio of 1:1. The solid dispersions of APM with S244, S3150 and  $\beta$ -cyclodextrin were prepared using the solvent evaporation method: APM (250 mg) was dissolved in 3 mL of ethanol; after complete dissolution, the solution was transferred into a round-bottom flask with a polymer carrier. The solvent was evaporated at 45°C and dried in a Hei-VAP Value HB/G5 rotary evaporator (Heidolph Instruments GmbH & CO. KG, Schwabach, Germany) for 2 h, and the residues were passed through a No. 85 sieve.

To prepare solid dispersions of APM in PEG 6000 and PVP, APM (250 mg) was dissolved in 3 mL of ethanol; after complete dissolution, the solutions were transferred to beakers holding the polymeric carriers PEG 6000 and PVP. The solvent was evaporated at 45°C and the resulting residues were dried in a hot air oven for 1 h and stored in a desiccator. Subsequently, the residues were ground in a mortar and passed through a No. 85 sieve.

On the basis of solubility studies, solid dispersions of APM with S244 at ratios of 2:1 and 3:1 were also prepared. All the solid dispersions were stored in vials at room temperature until further use. These batches were identified with the symbol CM.<sup>27,28</sup>

## The preparation of solid dispersions by the microwave-assisted solvent evaporation method

For the microwaving process, we used a CATA 2R MW oven (Catalyst Systems, Pune, India), containing an in-built mode stirrer to ensure even MW distribution. Accurately weighed 0.5 g amounts of physically mixed S244 with APM at ratios of 1:1, 2:1 and 3:1 were dissolved in 3 mL of ethanol. After complete dissolution, the solutions were transferred to silica crucibles. The crucibles were kept in a MW oven at 560 W for 3 min, until the solvent completely evaporated.<sup>13,29,30</sup> The prepared solid dispersions were passed through a No. 85 sieve and stored in vials at room temperature until further use. These formulations were identified with the symbol MW.

## Characterization of the solid dispersions

### Drug content

The drug content of all the prepared solid dispersions was calculated. For each solid dispersion, an accurately weighed amount of solid dispersion containing 30 mg of APM was transferred to a 100 mL volumetric flask, diluted to 100 mL with methanol and sonicated for 30 min for complete solubilization of the drug. The mixture was filtered using Whatman grade 41 filter paper and the absorbance was measured at 230 nm. The drug content was calculated using a Shimadzu V-1800 UV spectrophotometer (Shimadzu Corp., Kyoto, Japan).<sup>14,25</sup>

### Phase solubility studies

The phase solubility studies were performed according to the method described by Higuchi and Connors.<sup>31</sup> Physical mixtures and solid dispersions containing different carrier/APM ratios were prepared and added to glass vials containing 10 mL each of different media. Each vial was shaken in a mechanical shaker for 12 h to obtain equilibrium solubility, and the solution was allowed to equilibrate for 24 h. Each solution was further

centrifuged at 2000 rpm for 10 min in an ultra-centrifuge and filtered through Whatman grade 41 filter paper. An aliquot was suitably diluted with distilled water and analyzed using the Shimadzu V-1800 UV spectrophotometer at 230 nm.<sup>32</sup>

### Fourier-transform infrared study

The Fourier-transform infrared spectra (FTIR) of APM, the PM of APM with S244 and solid dispersion (Batch 7, MW 2:1) were recorded over a range of 4000–400 cm<sup>-1</sup> to study the principal peaks with an Affinity-1 FTIR spectrophotometer (Shimadzu Corp.) using the potassiumbromide (KBr) disc method.

### X-ray powder diffraction analysis of apremilast

The X-ray powder diffraction (XRPD) spectra of APM, S244, the PM of APM with S244 and all the solid dispersions were recorded using a Smart Lab high power powder X-ray diffractometer (Rigaku Corp., Tokyo, Japan) with Cu as a target filter, a voltage/current of 40 kV/40 mA and a scan speed of 4°/min. The samples were analyzed at a 2θ angle range from 10° to 89°. The step time was 0.5 s and the acquisition time was 1 h.<sup>33,34</sup>

### Differential scanning calorimetry analysis

Thermograms of APM, S244, the PM of APM with S244 and all the solid dispersions were recorded by using a Shimadzu DSC-60 differential scanning calorimeter (Shimadzu Corp.). An empty aluminum pan was used as a reference. The differential scanning calorimetry (DSC) measurements were performed at a heating rate of 10°C/min from 30°C to 300°C.<sup>29,35</sup>

### Surface morphology

The surface morphology of APM, the PM of APM with S244 and solid dispersion (Batch 7, MW 2:1) was studied using a Supra 5 scanning electron microscope (SEM) (Carl Zeiss AG, Oberkochen, Germany) with an accelerating voltage of 10 kV.

## Preparation of apremilast tablets using the direct compression technique

All the ingredients as shown in Table 1 were individually passed through a No. 60 sieve. A solid dispersion containing 30 mg of APM and microcrystalline cellulose were mixed to obtain a uniform mixture. The other ingredients were weighed, mixed and tablets were pressed using an 11 mm concave round punch on a Rimek compression machine (Karnavati Engineering Ltd., Ahmedabad, India). The post-compression parameters of the uncoated tablets were evaluated before they were coated.<sup>36</sup>

**Table 1.** Composition of apremilast (APM) tablets prepared by direct compression method

Ingredients	mg/Tablet
S244 + APM MW (2:1)	90.00
Lactose monohydrate	140.00
Croscarmellose sodium	16.30
Microcrystalline cellulose	41.50
Magnesium stearate	2.20
Total weight	290.00

### Preparation of coating solution for film coating

Ethyl cellulose (1% w/w) was weighed accurately and added to approx. 5 mL of acetone in a beaker with continuous stirring using the handshake method. Idacol Erythrosine Food Red-4 coloring agent (Roha Dyechem Pvt. Ltd., Mumbai, India) was then added. The stirring was continued for 15 min.

### Film coating of tablets

The compressed tablets were coated in a conventional coating pan (Avon Engineering Work, Mumbai, India) with an inlet air temperature of 50–55°C, a tablet bed temperature of 35–40°C and exhaust air temperature of 35–42°C. The pan speed, spray air pressure and solution spray rate were 25–30 rpm, 3 kg/cm<sup>2</sup> and 20 mL/min, respectively. The tablets were dried for 15 min at 45°C. The coating increased weight of the core tablets by 4%.

### Dissolution studies

The dissolution rates of the APM tablets and Aprezo (the reference tablet) were studied using a USP XXIII Dissolution Test Apparatus (Labindia Instruments, Mumbai, India) at 50 rpm in 900 mL of phosphate buffer (pH 6.8) with 0.15% SLS. The temperature of the dissolution medium was maintained at 37 ± 0.5°C. Aliquots (5 mL) were withdrawn at 5-, 10-, 20-, 30-, 40-, 50-, and 60-minute intervals and filtered. The absorbance of the filtered sample solution was measured using the Shimadzu V-1800 UV spectrophotometer at 230 nm, and concentration of APM was determined from the standard calibration curve.

## Results and discussion

### Solubility studies

Our study showed that APM has poor solubility in all buffers. The highest solubility (24.74 ± 0.857 µg/mL) was observed in phosphate buffer (pH 6.8) with 0.15% SLS (Table 2). The FDA has also suggested phosphate buffer (pH 6.8) with 0.15% SLS as a dissolution medium for APM tablets.<sup>37</sup>

**Table 2.** Results of solubility study of apremilast (APM) in different media

Dissolution media	Solubility [µg/mL]
Water	5.4 ± 0.298
pH 1.2, acidic buffer	5.2 ± 0.118
pH 2, phosphate buffer	9.96 ± 0.827
pH 4, phosphate buffer	14.96 ± 1.065
pH 6.8, phosphate buffer	16.22 ± 0.640
pH 6.8, phosphate buffer with 0.15% SLS	24.74 ± 0.857
pH 7.4, phosphate buffer	22.84 ± 0.331

Data presents mean ± standard deviation (SD), n = 3.

All the carriers used in the preliminary trials showed an increase in the solubility of APM in both PMs and solid dispersions (Tables 3 and 4). Several studies on solid dispersions have been published, confirming the advantageous properties of solid dispersions in increasing the solubility and dissolution rate of poorly water-soluble drugs. Solid dispersions tend to reduce particle size, possibly to a molecular level, and change the crystalline state of drugs, thereby promoting their solubility.<sup>38,39</sup> The results of phase solubility studies indicate that the solubility of APM was maximally enhanced when S244 was used as the carrier for preparing solid dispersions utilizing the conventional method (CM). This is because the increase in surface area, along with the potential existence of the drug in pores in an amorphous (rather than crystalline) form, can aid in enhancing solubility. When MW heating is used for solvent evaporation, a 3 mL solution completely evaporates within 3 min. Thus, the time consumed by MW-assisted solvent evaporation was significantly shorter than in the conventional method.

Further, when a solid dispersion is prepared using the MW-assisted solvent evaporation method, it is possible that APM molecules are transported into the pores by capillary action and stored in the pores in a partially crystalline and partially amorphous form. Earlier findings suggest that particle size decreased to the submicron range when using the MW-assisted technique, thus improving dissolution rate.<sup>13</sup> However, at a low carrier/drug ratio (1:1), surface adsorption of APM was noted. These results were also supported by the DSC thermogram. When the carrier/drug ratio is increased to 2:1, APM is more confined to the pores and can exist in an amorphous or a semi-crystalline state.

**Table 3.** Results of phase solubility studies of physical mixtures (PMs)

Physical mixtures	Solubility [µg/mL]
S244 + APM (1:1)	28 ± 0.221
Syloid XDP 3150 + APM (1:1)	22 ± 0.123
PVP + APM (1:1)	18 ± 0.344
PEG 6000 + APM (1:1)	19 ± 0.243
β-cyclodextrin + APM (1:1)	20 ± 0.354

Data presents mean ± standard deviation (SD), n = 3.

**Table 4.** Results of drug content and solubility studies of solid dispersion

Batch code	Solid dispersion	Drug content [%]	Solubility [ $\mu\text{g/mL}$ ]
APM 1	S244 + APM (CM 1:1)	97.24 $\pm$ 3.24	28 $\pm$ 0.154
APM 2	Syloid XDP 3150 + APM (CM 1:1)	96.88 $\pm$ 2.84	23 $\pm$ 0.231
APM 3	PVP+ APM (CM 1:1)	99.12 $\pm$ 5.31	24 $\pm$ 0.269
APM 4	PEG 6000 + APM (CM 1:1)	97.37 $\pm$ 2.57	23 $\pm$ 0.347
APM 5	$\beta$ -cyclodextrin + APM (CM 1:1)	96.56 $\pm$ 3.62	21 $\pm$ 0.215
APM 6	S244 + APM (MW 1:1)	98.23 $\pm$ 3.64	30 $\pm$ 0.364
APM 7	S244 + APM (MW 2:1)	100.32 $\pm$ 2.81	33 $\pm$ 0.385
APM 8	S244 + APM (MW 3:1)	98.41 $\pm$ 4.11	33 $\pm$ 0.316

Data presents mean  $\pm$  standard deviation (SD),  $n = 3$

A similar reduction in crystallinity was observed as the carrier/drug ratio is increased to 3:1.

On the basis of our solubility studies, S244 was selected as the best carrier for the further studies.

### Fourier-transform infrared study

The FTIR spectrum of APM (Fig. 1) shows the characteristic strong N–H stretching peak for APM at  $3364\text{ cm}^{-1}$ . The FTIR spectrum of APM also shows the characteristic peak at  $1764\text{ cm}^{-1}$  due to amide carbonyl (C=O), along with the peaks between  $2837\text{ cm}^{-1}$  and  $3081\text{ cm}^{-1}$  for aliphatic and aromatic benzene ring C–H stretching. The peak for amide N–H bending was observed at  $1597\text{ cm}^{-1}$  and the peak for C–O stretching was observed at  $1164\text{ cm}^{-1}$ . The FTIR spectrum of S244 showed a stronger intensity band from  $900\text{ cm}^{-1}$  to  $1300\text{ cm}^{-1}$  due to Si–O stretching of the silanol group. The FTIR spectra for the PM of APM with S244 and for solid dispersion (Batch 7, MW 2:1) show the combined individual characteristic peaks for APM and S244. The individual peaks for APM are more intense in the PM as compared to the solid dispersion. This suggests that in the PM, the physical interaction of APM with S244

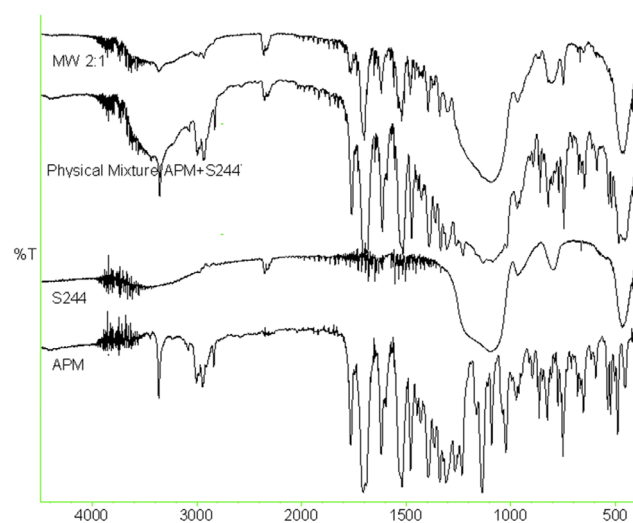


**Fig. 1.** Fourier transform infrared (FTIR) spectra of solid dispersion (MW 2:1), the physical mixture (PM) of S244 and apremilast (APM), S244 alone and APM alone

is weak; possibly APM is only physically interacting with the outer surface of the silica particles. In the solid dispersion, the individual peaks for APM are weak, which suggests that MW irradiation results in pronounced physical interaction between APM at the deeper sites of the S244 pores. The FTIR spectrum also clearly suggests that in both the PM and the solid dispersion, APM was physically adsorbed rather than undergoing any chemical interaction on the surface of the porous silica particles of S244.

### Differential scanning calorimetry and X-ray diffraction

Differential scanning calorimetry and XRPD were employed to investigate the crystal lattice of pure APM and APM solid dispersions with S244. Figure 2 depicts the DSC thermograms for S244, a PM of APM and S244, solid dispersions of S244 and APM obtained using the CM and the MW-assisted solvent evaporation method. Apremilast was characterized by a single sharp melting endothermic peak at  $157.56^\circ\text{C}$ . The peak onset temperature and heat of fusion ( $\Delta\text{H}_f$ ) were  $155.01^\circ\text{C}$  and  $111.0595\text{ Jg}^{-1}$ , respectively. This characteristic peak appeared in the PMs and in the CM batches at carrier/drug ratios of both 1:1 and 2:1, with slight variations in terms of the melting peak depression and broadening, indicating the transition from

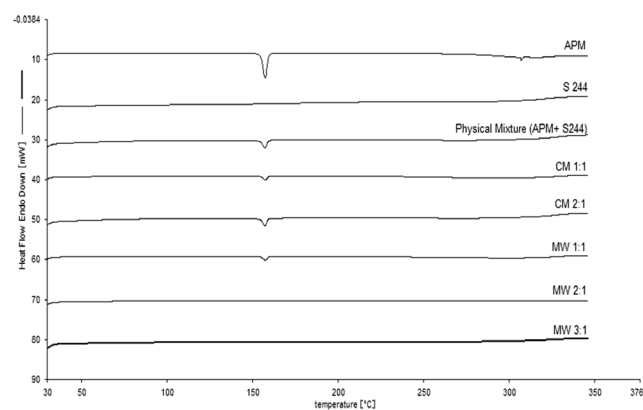


**Fig. 2.** Differential scanning calorimetry (DSC) thermograms of apremilast (APM), S244, the physical mixture (PM) of S244 and APM, solid dispersion (CM 1:1, CM 2:1), solid dispersion (MW 1:1, MW 2:1, and MW 3:1)

a crystalline to a semi-crystalline state. In the MW solid dispersion of APM with S244 at a carrier/drug ratio of 1:1, a melting peak of less intensity was detected. At this ratio, the pore volume of S244 was insufficient for hosting extra APM molecules, and the residual APM instead remained on the external surface of S244. However, the melting peak was completely absent in the 2:1 and 3:1 MW solid dispersions, confirming the amorphous state of APM within these formulations.

Figure 3 displays the XRPD patterns of APM, S244 and the MW solid dispersions with ratios of 1:1 and 2:1. The characteristic diffraction peaks observed at 10.09°, 11.87°, 13.53°, 16.34°, 26.09°, and 26.92° correspond to the powder diffraction pattern for pure APM, while the absence of diffraction peaks in the solid dispersions confirms their amorphous structure. The crystalline state of APM in the physical mixture of S244 and APM is evident from the characteristic diffraction peaks. The less intense diffraction peaks in the MW solid dispersion at a ratio of 1:1 indicates the partially crystalline state of APM deposited between the pore walls as a result of the blockage of pores with viscous molten APM. However, the XRPD pattern in the MW solid dispersion at a ratio of 2:1 suggests the amorphous structure of APM within the formulation.

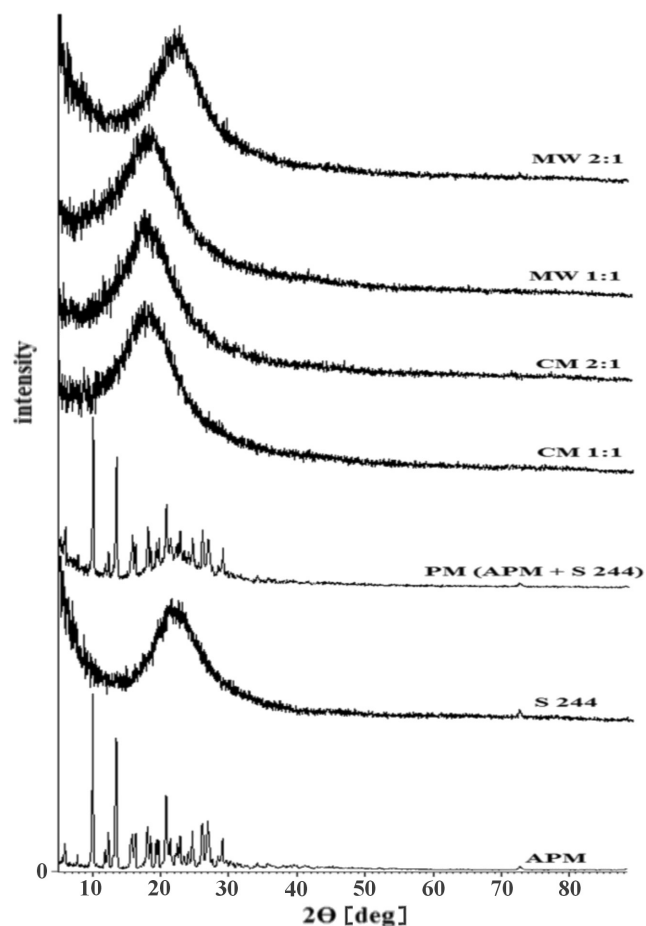


Fig. 3. X-ray powder diffraction (XRPD) patterns of solid dispersion (MW 2:1, MW 1:1), solid dispersion (CM 1:1), the physical mixture (PM) of S244 and apremilast (APM), S244, and APM

It also confirms that the APM was confined within the pores of S244. These XRPD results are compatible with the DSC observations discussed above. S244 is a non-ordered porous silicon dioxide with a neutral pH and has randomly oriented pores with an average pore diameter of 19 nm.<sup>40</sup> The single-crystal structure of APM has been reported for its ethanol hemisolvate solvomorph.<sup>24</sup> This single-crystal structure is most stable experimentally determined conformation of APM, and this conformation was therefore used to measure the size and shape of APM. Another reason for using the single-crystal structure is that very small changes in the conformation of a molecule or changes in the hydrogen bonds around the molecule can have major effects on its size, shape, surface area and volume.

As shown in Fig. 4, the most widely spaced atoms in APM are 14.7 Å apart. The unit cell dimensions required to fit the conformer of APM are 1.29 × 1.29 × 1.47 nm, calculated using Discovery Studio (Biovia, San Diego, USA) with the PyMOL interface (Schrödinger LLC, New York, USA). This suggests that the size of APM is below 1.9 nm, whereas the pore size of S244 is in the range of 19–20 nm. Therefore, the restricted pore size of S244 may have inhibited the crystallization of APM inside the pores. In summary, the transformation of APM from crystalline to amorphous form is highly dependent on the selection of an optimum carrier/drug ratio and on the formulation method.

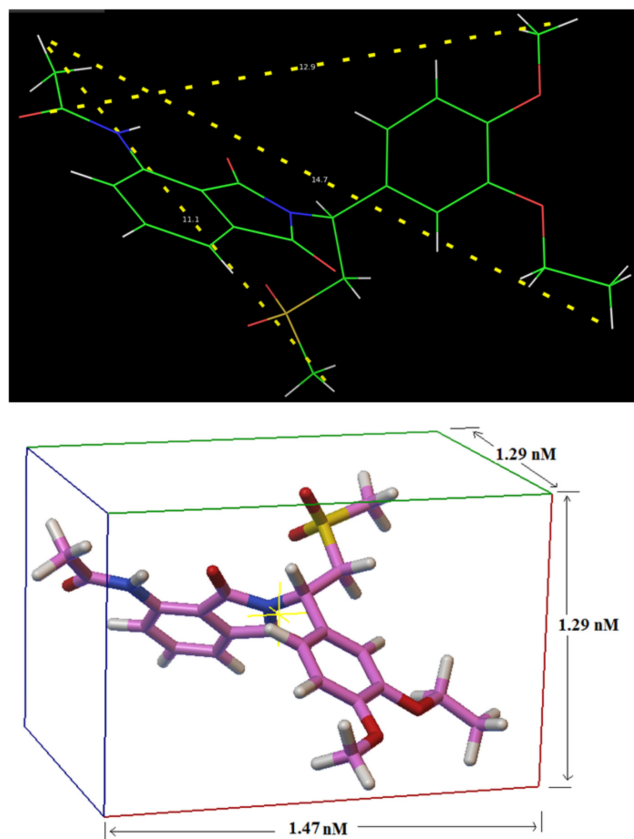


Fig. 4. Representation of a 3-dimensional apremilast (APM) molecule with inter-atomic distances shown

## Surface morphology

Scanning electron microscopy images of APM, the physical mixture of APM and S244 and the MW solid dispersion of S244 and APM (2:1) are presented in Fig. 5. The SEM images of pure APM showed irregularly shaped crystals of the drug with large particles, showing its existence in the crystalline form. When APM was converted into solid dispersions, the morphology changed to an amorphous state with a fine particle size.

## Preparation of apremilast tablets

Based on the results of our solubility studies, DSC thermograms and X-ray powder diffraction patterns, the best solid dispersion was found to be Batch 7 (MW 2:1). This was used to prepare tablets. The post-compression parameters of the uncoated tablets are presented in Table 5.

## Dissolution studies

From the dissolution profiles, it is evident that the APM tablets prepared with the MW-assisted solid dispersion at a 2:1 ratio had a significantly better APM dissolution rate as compared to the marketed formulation (Aprezo tablets) (Fig. 6). Factors such as the lack of a crystalline form, the increased surface area of the drug, and the hydrophilic surface of S244 helped improve the dissolution of APM. When this formulation comes into contact with the dissolution media, a rapid release of APM in the form of fine particles occurs, possibly because of desorption of APM by the influx of the dissolution media inside the pores of S244.<sup>28</sup> These results are in agreement with the findings of earlier researchers,<sup>39</sup> who used MW-induced solid dispersions to improve the solubility of APM.

## Conclusions

In summary, solid dispersions of APM, a poorly water-soluble drug, with Syloid 244FP as a carrier were prepared by CM and MW-assisted method. The latter was found to be a suitable and less time-consuming method. The prepared solid dispersions were evaluated for physicochemical parameters. The study shows that the dissolution rate of APM can be improved using Syloid 244FP as a carrier. The transformation of APM from crystalline to amorphous form is highly dependent on the selection of an optimum carrier/drug ratio and formulation method. The tablet formulation of solid dispersion (Batch 7, MW 2:1) (S244 with APM, MW 2:1) showed a higher dissolution rate when compared with the reference tablets.

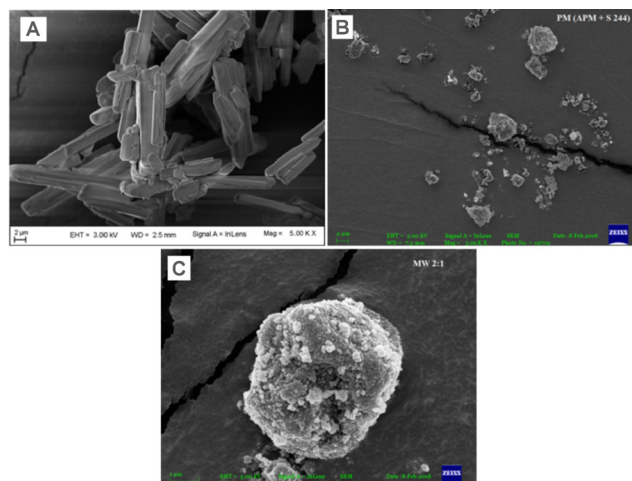


Fig. 5. A – scanning electron micrographs of pure apremilast (APM); B – the physical mixture (PM) of S244 and APM; C – solid dispersion (batch 7, MW 2:1). Scales are given on the individual micrographs

Table 5. Results of uncoated Apremilast (APM) tablet

Average weight [mg]	Friability [%]	Disintegration time [s]	Hardness [kg/cm <sup>2</sup> ]
290	0.63 ± 0.05	66 ± 1.52	7.5 ± 0.5

Data are presented as mean ± standard deviation (SD), n = 3.

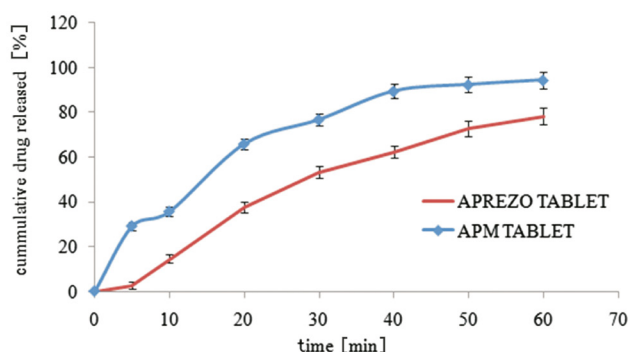


Fig. 6. Comparative dissolution profiles of prepared apremilast (APM) tablets and the marketed formulation (Aprezo tablets). Data are presented as means ± standard deviation (SD), n = 3

## References

- Serajuddin A. Solid dispersion of poorly water-soluble drugs: Early promises, subsequent problems, and recent breakthroughs. *J Pharm Sci.* 1999;88(10):1058–1066.
- Chiou WL, Riegelman S. Pharmaceutical applications of solid dispersion systems. *J Pharm Sci.* 1971;60(9):1281–1302.
- Dua K, Pabreja K, Ramana MV, Bukhari NI. Preparation, characterization, and in vitro evaluation of aceclofenac PVP-solid dispersions. *J Disper Sci Technol.* 2011;32(8):1151–1157.
- Schver GCRM, Lee PI. Combined effects of supersaturation rates and doses on the kinetic-solubility profiles of amorphous solid dispersions based on water-insoluble poly (2-hydroxyethyl methacrylate) hydrogels. *Mol Pharm.* 2018;15(5):2017–2026. doi:10.1021/acs.molpharmaceut.8b00162
- Muhammad RS, Bashir S, Mahmood A, et al. Application of various polymers and polymers based techniques used to improve solubility of poorly water soluble drugs: A review. *Acta Poloniae Pharmaceutica.* 2017;74(2):347–356.

6. Madan JR, Pawar KT, Dua K. Solubility enhancement studies on lurasidone hydrochloride using mixed hydrotropy. *Int J Pharm Investig.* 2015;5(2):114–120.
7. Dua K, Pabreja K, Ramana MV, Lather V. Dissolution behavior of  $\beta$ -cyclodextrin molecular inclusion complexes of aceclofenac. *J Pharm Bioallied Sci.* 2011;3(3):417–425.
8. Dua K, Ramana MV, Sara UV, et al. Investigation of enhancement of solubility of norfloxacin beta-cyclodextrin in presence of acidic solubilizing additives. *Curr Drug Deliv.* 2007;4(1):21–25.
9. Dua K, Pabreja K, Gorajana A. Dissolution behaviour of aceclofenac-PVP coprecipitates. *Ars Pharm.* 2012;53(3):7–12.
10. Dittgen M, Fricke S, Gerecke H, Osterwald H. Hot spin mixing: A new technology to manufacture solid dispersions. I: Testosterone. *Pharmazie.* 1995;50(3):225–226.
11. Van Nijlen T, Brennan K, Van der Mooter G, Bleton N, Kinget R, Augustijns P. Improvement of the dissolution rate of artemisinin by means of supercritical fluid technology and solid dispersion. *Int J Pharm.* 2003;254(2):173–181.
12. Ghaderi R, Artursson P, Carlfors J. Preparation of biodegradable microparticles using solution enhanced dispersion by supercritical fluids (SEDS). *J Pharm Res.* 1999;16(5):676–681.
13. Radacsi N, Stefanidis G, Szabo-Revesz P, Ambrus R. Analysis of niflumic acid prepared by rapid microwave-assisted evaporation. *J Pharm Biomed Anal.* 2014;98:16–21.
14. Alshehri S, Shakeel F, Ibrahim M, et al. Influence of the microwave technology on solid dispersions of mefenamic acid and flufenamic acid. *PLOS ONE.* 2017;12(7):e0182011.
15. Wang W, Zhao C, Sun J, et al. Quantitative measurement of energy utilization efficiency and study of influence factors in typical microwave heating process. *Energy.* 2015;87:678–685.
16. Xiqiang Z, Wenlong W, Hongzhen L, Yampeng M, Chunyuan M, Zhanlong S. Temperature rise and weight loss characteristics of wheat straw under microwave heating. *J Anal Appl Pyrol.* 2014;107:59–66.
17. Moneghini M, Bellich B, Baxa P, Princivalle F. Microwave generated solid dispersion containing ibuprofen. *Int J Pharm.* 2008;361(1–2):125–130.
18. Martin BC, Thomas LW, Dann FJ. Apremilast for the treatment of psoriatic arthritis. *Dermatol Online J.* 2017;23(2):1–12.
19. Manhart R, Rich PC. Nail psoriasis. *Clin Exp Rheumatol.* 2015;33(5 Suppl 93):S7–S13.
20. Papp K, Cather JC, Rosoph L, et al. Efficacy of apremilast in the treatment of moderate to severe psoriasis: A randomized controlled trial. *Lancet.* 2012;380(9843):738–746.
21. Oram Y, Akkaya AD. Treatment of nail psoriasis: Common concepts and new trends. *Dermatol Res Pract.* 2013;2013:180496. doi:10.1155/2013/180496
22. EMA (2014). Full prescribing information available at: [http://www.ema.europa.eu/docs/enGB/documentlibrary/EPAR\\_Public\\_assessment-report/human/003746/WC500182629.pdf](http://www.ema.europa.eu/docs/enGB/documentlibrary/EPAR_Public_assessment-report/human/003746/WC500182629.pdf). Accessed January 21, 2018.
23. FDA (2014a). Full prescribing information available at: [http://www.accessdata.fda.gov/drugsatfda\\_docs/nda/2014/205437Orig1s000ChemR.pdf](http://www.accessdata.fda.gov/drugsatfda_docs/nda/2014/205437Orig1s000ChemR.pdf). Accessed November 11, 2017.
24. Wu YD, Zhang XL, Liu XH, et al. The preparation, characterization, structure and dissolution analysis of apremilast solvatomorphs. *Acta Crystallogr C: Struct Chem.* 2017;73(Pt 4):305–313.
25. Tang M, Hu P, Huang S, Zheng Q, Yu H, He Y. Development of an extended-release formulation for apremilast and a level A in vitro–in vivo correlation study in beagle dogs. *Chem Pharm Bull.* 2016;64(11):1607–1615.
26. Madan JR, Pawar KT, Dua K. Solubility enhancement studies on lurasidone hydrochloride using mixed hydrotropy. *Int J Pharm Investig.* 2015;5(2):114–120.
27. Madan JR, Kamate VJ, Dua K, Awasthi R. Improving the solubility of nevirapine using a hydrotropy and mixed hydrotropy based solid dispersion approach. *Polim Med.* 2017;47(2):83–90.
28. Lai J, Lin W, Scholes P, Li M. Investigating the effects of loading factors on the in vitro pharmaceutical performance of mesoporous material as drug carrier ibuprofen. *Materials (Basel).* 2017;10(2):E150. doi:103390/ma10020150
29. Gorajana A, Rajendra A, Yew LM, Dua K. Preparation and characterization of cefuroxime axetil solid dispersion using hydrophilic carriers. *Int J Pharm Investig.* 2015;5(3):171.
30. Talib H. *The application of microwave formulation and isothermal titration calorimetry for pharmaceutical compounds* [PhD thesis]. University of Huddersfield; 2014.
31. Higuchi TK, Connors KA. Phase solubility techniques. *Adv Anal Chem Instrum.* 1965;4:117–212.
32. Maheshwari RK, Indurkha A. Formulation and evaluation of aceclofenac injection made by mixed hydrotropic solubilization technique. *Iran J Pharm Res.* 2010;9(3):233–242.
33. Bhole PG, Patil VR. Enhancement of water solubility of felodipine by preparing solid dispersion using poly-ethylene glycol 6000 and polyvinyl alcohol. *Asian J Pharm.* 2014;28(3):240–244.
34. Gorajana A, Kit WW, Dua K. Characterization and solubility study of norfloxacin-polyethylene glycol, polyvinylpyrrolidone and carbopol 974P solid dispersions. *Recent Pat Drug Deliv Formul.* 2015;9(2):167–182.
35. Lyn LY, Sze HW, Rajendran A, Adinarayana G, Dua K, Garg S. Crystal modifications and dissolution rate of piroxicam. *Acta Pharm.* 2011;61(4):391–402.
36. Madan JR, Kamate VJ, Awasthi R, Dua K. Formulation, characterization and in-vitro evaluation of fast dissolving tablets containing gli-clazide hydrotropic solid dispersions. *Recent Pat Drug Deliv Formul.* 2017;11(2):147–154.
37. FDA (2014b), Full prescribing information available at: [https://www.accessdata.fda.gov/scripts/cder/dissolution/dsp\\_getIIData.cfm](https://www.accessdata.fda.gov/scripts/cder/dissolution/dsp_getIIData.cfm). Accessed July 24, 2017.
38. Vasconcelos T, Costa P. Development of a rapid dissolving ibuprofen solid dispersion. *Pharm Res.* 2007;16:676–681.
39. Maurya D, Belgamwar V, Tekade A. Microwave induced solubility enhancement of poorly water soluble atorvastatin calcium. *J Pharm Pharmacol.* 2010;62(11):1599–1606.
40. Lai J, Lin W, Scholes P, Li M. Investigating the effects of loading factors on the in vitro pharmaceutical performance of mesoporous materials as drug carriers for ibuprofen. *Materials.* 2017;10(2):150. doi:10.3390/ma10020150



# Porous starch and its application in drug delivery systems

Monika Sujka<sup>1,A,D</sup>, Urszula Pankiewicz<sup>1,C,F</sup>, Radosław Kowalski<sup>1,E</sup>, Karolina Nowosad<sup>1,B</sup>, Agnieszka Noszczyk-Nowak<sup>2,E,F</sup>

<sup>1</sup> Department of Analysis and Evaluation of Food Quality, University of Life Sciences in Lublin, Poland

<sup>2</sup> Department of Internal Medicine and Clinic of Diseases of Horses, Dogs and Cats, Wrocław University of Environmental and Life Sciences, Poland

A – research concept and design; B – collection and/or assembly of data; C – data analysis and interpretation;

D – writing the article; E – critical revision of the article; F – final approval of the article

Polymers in Medicine, ISSN 0370-0747 (print), ISSN 2451-2699 (online)

*Polim Med.* 2018;48(1):25–29

## Address for correspondence

Monika Sujka

E-mail: monika.sujka@up.lublin.pl

## Funding sources

None declared

## Conflict of interest

None declared

Received on August 10, 2018

Reviewed on October 17, 2018

Accepted on November 15, 2018

## Abstract

In recent years, starch has become a new potential biomaterial for pharmaceutical applications. This biopolymer has unique physicochemical and functional characteristics, as well as various advantages such as low price, relative ease of isolation in pure form from the plant source, non-toxicity, biodegradability, good biocompatibility, and interaction with living cells. Starch is currently used in pharmacy as a binder, disintegrating agent, film-forming material, raw material for production of microspheres and nanoparticles, and a component of drug delivery systems. Porous starch, which can be obtained with physical, chemical and enzymatic methods of modification, has a large specific surface area thanks to the presence of pores and channels. It has excellent adsorption capacity and can be used to enhance the dissolution rate of poorly soluble drugs or as shell material to improve the stability and water-solubility of compounds. As a component of drug delivery systems, porous starch has another advantage: it is biodegradable, so there is no need to remove it from the body after the release of the active agent.

**Key words:** starch, porosity, drug delivery systems

## Cite as

Sujka M, Pankiewicz U, Kowalski R, Nowosad K, Noszczyk-Nowak A. Porous starch and its application in drug delivery systems. *Polim Med.* 2018;48(1):25–29. doi:10.17219/pim/99799

## DOI

10.17219/pim/99799

## Copyright

© 2018 by Wrocław Medical University

This is an article distributed under the terms of the Creative Commons Attribution Non-Commercial License (<http://creativecommons.org/licenses/by-nc-nd/4.0/>)

## Starch and its properties

Starch is a natural storage polysaccharide in higher plants and the most common carbohydrate in human and animal diets. It is found in leaves, stems, seeds, fruits, roots, and tubers. The main sources of starch for industrial applications are maize (82%), wheat (8%), potatoes (5%), and cassava (5%).<sup>1</sup> Structurally, starch is composed of linear amylose and highly branched amylopectin, both made up of D-glucose units joined together via glycosidic linkages:  $\alpha$  (1 $\rightarrow$ 4) and  $\alpha$  (1 $\rightarrow$ 6) (only in branch points). It is laid down in the form of semi-crystalline granules of different sizes (from 1  $\mu$ m to over 100  $\mu$ m in diameter) and shapes.<sup>2</sup> The shape of a granule can vary from oval/round to polyhedral, and can be characteristic of a genus and species.

One of the most characteristic properties of starch is its ability to gelatinize and form thick pastes. This process takes place when starch is heated in excess water and results in irreversible disruption of the molecular order within a granule. Gelatinization is associated with diffusion of water into granules and their radial swelling, loss of starch crystallinity and amylose leaching into the solution. Granule swelling and disruption produce a viscous paste consisting of a continuous phase of solubilized amylose and/or amylopectin, and a discontinuous phase of granule fragments. On cooling, amylose and linear segments of amylopectin reassociate and form an ordered gel network. The formation of the junction zones of a gel can be considered to be the first stage of starch molecule crystallization. As starch pastes are cooled and stored, the starch becomes progressively less soluble. This process is called retrogradation.<sup>3</sup> In the food industry, starch retrogradation is a highly undesirable phenomenon, especially when a product requires freeze–thaw stability, but on the other hand retrograded starch is classified as one of the types of resistant starch considered a dietary fiber.<sup>4</sup>

Starch – in particular the linear component amylose – is able to form inclusion complexes with small molecules (e.g., lipids, alcohols, lactones, or iodine) and act as an encapsulating agent. The amylose wraps itself around the guest molecule and forms a single left-handed helix structure (so-called V amylose).<sup>5</sup> The number of glucose units in each turn of the helical coil (6, 7 or 8) is dependent on the size of the guest molecule, and the host molecule is able to expand or contract around the guest. These inclusion complexes can be used in the food and pharmaceutical industries for the controlled and targeted delivery of nutraceuticals and/or drugs to the lower gastrointestinal tract.<sup>5,6</sup>

## Porous starch

The definition of porosity states that it is the ratio of pore volume to the volume of the solid phase. Solid materials can contain closed pores, as well as a network of both one- or two-side opened pores, combined with

each other or not. The classification of pores based on the size of their diameter is as follows: macropores (diameter >50 nm), mesopores (diameter between 2 nm and 50 nm) and micropores (diameter <2 nm).<sup>7</sup> The occurrence of pores on the granule surface of sorghum, maize, millet, wheat, rye, and barley (along the equatorial groove of large granules) has been confirmed by microscopic observations. Granules of tapioca, rice, oat, canna, and arrowroot appear to be smooth, but there is no consensus among researchers about the presence of pores on the surface of potato starch granules.<sup>8,9</sup> Fannon et al. revealed that, apart from surface pores, there are also specific channels and cavities in maize starch granules.<sup>10</sup> The researchers suggested that surface pores are openings to serpentine channels penetrating the granule interior.<sup>10</sup> According to Huber and BeMiller, most channels penetrate granules from the external surface towards a cavity at the hilum, but the depth of penetration can vary.<sup>11</sup> Channels appeared to be open, whereas cavities tended to be closed. Huber and BeMiller reported the presence of such cavities in maize, waxy maize and sorghum starch granules.<sup>11</sup> It has been proven that the porosity of starch granules significantly influences its chemical reactivity. The presence of pores, channels and cavities increases the size of the surface area that can potentially be available for chemical or enzymatic reactions.<sup>11</sup> Pore size is an important factor in determining the loading capacity of starch granules for water and oil.<sup>12</sup> Porous starch can also be a good carrier for bacteria, enzymes, flavors, or bioactive compounds such as drugs.<sup>13,14</sup>

The applicability of starch in a native form is limited because of its sensitivity to processing conditions such as extreme temperature, low pH, high shear rate, and freeze–thaw variation. In the pharmaceutical industry, native starch has traditionally been used for the production of granules, capsules and tablets. Builders and Arhewoh recently published an excellent review of pharmaceutical applications of unmodified starch.<sup>15</sup> For many purposes, however, a modification of starch by chemical, physical or enzymatic methods, or combinations of these methods, is required. Among them, chemical methods are the most commonly used. The 3 available hydroxyl groups at position C2, C3 and C6 can be modified through esterification, etherification and oxidation.<sup>16</sup> The starch preparations obtained as a result of modification have different properties depending on the reagent used and the reaction.<sup>17</sup> As a result of starch modification, the following properties may be changed: granularity, water binding capacity and solubility, paste viscosity, gelatinization temperature, the rheological stability of pastes, paste transparency, retrogradation, adhesion, emulsifiability, texturizing properties, thickening, film formation, and/or chemical reactivity.<sup>18</sup>

Porous starch, which has received significant attention in recent years, can be obtained by physical, chemical or enzymatic methods, but ultrasonic and enzyme treatments have

been most frequently reported.<sup>19–23</sup> Other proposed methods are the solvent exchange technique,<sup>24</sup> extrusion,<sup>25,26</sup> microwave foaming,<sup>27</sup> grinding,<sup>28</sup> or enzymatic hydrolysis followed by oven-, spray- or vacuum freeze-drying.<sup>29</sup> Table 1 presents an overview of the methods applied for obtaining porous starch, as well as the specific surface area and average pore size of the products. Porous starch can be used for dissolution enhancement of poorly soluble drugs, has excellent adsorption capability because of its large specific surface area, or can be used as shell material to improve the stability and water-solubility of compounds.<sup>30</sup>

## Porous starch in drug delivery systems

Drug delivery systems usually include particulate carriers (composed primarily of lipids and/or polymers) and associated therapeutics. They are designed to alter the pharmacokinetics and biodistribution of the associated drugs, or to function as drug reservoirs, or both.<sup>31</sup> The ideal drug delivery system should be comfortable for the patient, inert, biocompatible, bioadhesive, and capable of high drug loading. Porous starch meets all these conditions. Starch is officially accepted by all major regulatory agencies for use in various oral drug delivery systems.<sup>32</sup> Starch polymer chains are hydrolyzed into smaller biologically acceptable compounds, so there is no need to remove the drug delivery system from the body after the release of the active agent.

The formation of inclusion complexes, micro- or nanoparticles, is one method of improving the oral delivery of poorly water-soluble drugs and drug stability. It has been found that biodegradable porous starch foam (BPSF) with a nanoporous structure, low density, and high specific surface area and pore volume has better characteristics than an inorganic carrier.<sup>33</sup> In *in vitro* and *in vivo* drug release studies, Wu et al. showed that the use of BPSF enhanced the release and oral bioavailabil-

ity of lovastatin in comparison with crude lovastatin and commercial capsules.<sup>34</sup> The drug absorbed by the BPSF was partially present as microcrystals, partially in amorphous form distributed in the pores of the BPSF and partially in crystalline form distributed on the surface of the BPSF.<sup>30</sup> Starch macrocellular foam (SMF) has been used to improve the dissolution rate and oral bioavailability of nitrendipine (NDP); the results demonstrated that SMF can be a promising carrier for the oral delivery of poorly water-soluble drugs.<sup>35</sup> The use of porous starch as a carrier for carbamazepine also enhanced its solubility.<sup>13</sup> García-González et al. reported that starch aerogel microspheres can be used as carriers for ketoprofen, as they showed high loading capacities.<sup>36</sup> The researchers produced aerogel microspheres from starch and loaded them with poorly water-soluble drugs, ketoprofen and benzoic acid via supercritical CO<sub>2</sub>-assisted adsorption. The starch aerogel microspheres presented a higher specific loading capacity for ketoprofen than for benzoic acid, but they released the latter drug faster than the former one.<sup>31</sup> Starch-based microparticles have been used for the entrapment and release of 3 corticosteroids: dexamethasone (DEX), 16 $\alpha$ -methylprednisolone (MP) and 16 $\alpha$ -methylprednisolone acetate (MPA).<sup>37</sup> The loading efficiencies of DEX and MPA were 82% and 84%, respectively, followed by MP (51%). The study showed that these starch-based systems were capable of sustained release of the entrapped steroids for up to 30 days.<sup>37</sup>

Jadhav and Vavia obtained supercritical processed starch nanosponge (SSNS) and used it as a carrier for poorly water-soluble fenofibrate. They reported significant dissolution enhancement of the SSNS formulation as compared to the plain drug, while an *in vivo* pharmacodynamic study showed that the SNSS-based formulation significantly improved the bioavailability of the drug.<sup>38</sup> In a study by Pawar et al., porous starch was used to improve the dissolution and oral bioavailability of itraconazole; the results showed a significant increase in the release and oral bioavailability of the drug compared to the marketed product.<sup>39</sup>

**Table 1.** Overview of the methods used to obtain porous starch, its specific surface area and mean pore size

Starch source	Method of modification	Specific surface area [m <sup>2</sup> /g]	Mean pore size [nm]	Reference
NDA	solvent exchange method	109.73	~200	13
Corn	hydrolysis with glucoamylase at 50°C for 1–8 h	0.76–1.86	200–1,150	19
Rice, corn, wheat, potato	ultrasounds (20 kHz, 170 W, 30 min, in water or ethanol)	0.16–1.27	6.38–10.16	22
NDA	solvent exchange method	127.75	20–80	34
Corn	emulsion–gelation method followed by supercritical drying	127	NDA	44
Potato, corn	hydrolysis with $\alpha$ -amylase at 50°C for 60 min	0.40–1.09	11.63–23.85	45
Wheat, rice	hydrolysis with $\alpha$ -amylase at 50°C for 60 min	0.83–1.66	8.06–17.87	46
NDA	cross-linking followed by drying and milling	39.80–49.80	NDA	47
Waxy rice	enzymatic hydrolysis ( $\alpha$ -amylase, amyloglucosidase and their mixture)	1.15–2.34	1.29–7.23	48
Maize	sol–gel method and effective supercritical drying technique	185.75	20–150	38

\*NDA – no data available.

Balmayor et al. applied an emulsion solvent extraction/evaporation technique to develop starch poly- $\epsilon$ -caprolactone (SPCL) microparticles (size between 5  $\mu\text{m}$  and 900  $\mu\text{m}$ ) for use in drug delivery and tissue engineering (TE) applications. The experiments with dexamethasone (DEX) as the model drug showed that up to 93% of DEX was entrapped in SPCL microparticles, depending on the polymer concentration and the drug-to-polymer ratio. The authors suggested that the DEX release was initially governed mainly by diffusion, and then by degradation of the polymeric matrix.<sup>40</sup> Ali et al. demonstrated that the use of porous starch as a carrier for carbamazepine (CBZ) enhanced the solubility of the drug, showing an improved in vivo performance compared to neat CBZ.<sup>13</sup>

Porous starch as a wall material can enhance the adsorbability and adhesive properties of microcapsules. Wan et al. used a spray-drying method of encapsulating lutein by using gelatin mixed with porous starch as wall materials. They obtained a high yield of product (92.6  $\pm$  1.7%) and good encapsulation efficiency (94.4  $\pm$  0.4%). The solubility and stability of the microcapsules were much higher than in the case of free lutein.<sup>41</sup> Malafaya et al. produced starch-based porous material by the microwave baking method and used it as a carrier for a non-steroid anti-inflammatory agent.<sup>42</sup> A porous starch-based self-assembled nanodelivery system was developed by Zhang et al. to improve the oral absorption of insoluble probucol. The study showed that the oral bioavailability of the drug from the nanocarrier was improved about 10-fold compared to that of a free drug suspension.<sup>43</sup>

All the published results of experiments indicate that porous starch is a very promising material for pharmacological applications. However, more attention should be focused on investigating the relationship between pore size and the properties of a carrier (e.g., loading capacity and drug release behavior). Other significant problems are how to scale up the production and application of porous starch, and how to obtain a carrier with strictly defined parameters. It should also be noted that although starch is generally regarded as safe, its derivatives, especially in form of nano- and microparticles, may pose some safety challenges as components of drug delivery systems.

## References

1. Le Corre D, Bras J, Dufresne A. Starch nanoparticles: A review. *Biomacromolecules*. 2010;11(5):1139–1153.
2. Tester RF, Karkalas J, Qi X. Starch-composition, fine structure and architecture. *J Cereal Sci*. 2004;39(2):151–165.
3. Copeland L, Blazek J, Salman H, Chiming Tang M. Form and functionality of starch. *Food Hydrocoll*. 2009;23(6):1527–1534.
4. Fuentes-Zaragoza E, Riquelme-Navarrete MJ, Sánchez-Zapata E, Pérez-Álvarez JA. Resistant starch as functional ingredient: A review. *Food Res Int*. 2010;43(4):931–942.
5. Putseys JA, Lamberts L, Delcour JA. Amylose-inclusion complexes: Formation, identity and physico-chemical properties. *J Cereal Sci*. 2010;51:238–247.
6. Cohen R, Orlova Y, Kovalev M, Ungar Y, Shimoni E. Structural and functional properties of amylose complexes with genistein. *J Agricultural Food Chem*. 2008;56(11):4212–4218.
7. Sing KS. Reporting physisorption data for gas/solid systems with special reference to the determination of surface area and porosity. *Pure Appl Chem*. 1985;57(4):603–619.
8. Fannon JE, Hauber RJ, BeMiller JN. Surface pores of starch granules. *Cereal Chem*. 1992;69(3):284–288.
9. Sujka M, Jamroz J. Characteristics of pores in native and hydrolyzed starch granules. *Starch/Stärke*. 2010;62(5):229–235.
10. Fannon JE, Shull JM, BeMiller JN. Interior channels of starch granules. *Cereal Chem*. 1993;70(5):611–613.
11. Huber KC, BeMiller JN. Channels of maize and sorghum starch granules. *Carbohydr Polym*. 2000;41(3):269–276.
12. Jung Y, Lee B-H, Yoo S-H. Physical structure and absorption properties of tailor-made porous starch granules produced by selected amyolytic enzymes. *PLoS ONE*. 2017;12(7):e0181372.
13. Ali MT, Fule R, Sav A, Amin P. Porous starch: A novel carrier for solubility enhancement of carbamazepine. *AAPS PharmSciTech*. 2013;14(3):919–926.
14. Zhu F. Encapsulation and delivery of food ingredients using starch based systems. *Food Chem*. 2017;229:542–552.
15. Builders PF, Arhewoh MI. Pharmaceutical applications of native starch in conventional drug delivery. *Starch/Stärke*. 2016;68(9–10):864–873.
16. Khan F, Ahmad SR. Polysaccharides and their derivatives for versatile tissue engineering application. *Macromol Biosci*. 2013;13(4):395–421.
17. Tomasik P, Zaranyika MF. Nonconventional methods of modification of starch. *Adv Carbohydr Chem Biochem*. 1995;51:243–318.
18. Singh J, Kaur L, McCarthy OJ. Factors influencing the physico-chemical, morphological, thermal and rheological properties of some chemically modified starches for food applications: A review. *Food Hydrocoll*. 2007;21(1):1–22.
19. Chen G, Zhang B. Hydrolysis of granular corn starch with controlled pore size. *J Cereal Sci*. 2012;56(2):316–320.
20. Majzoobi M, Hedayati S, Farahnaky A. Functional properties of microporous wheat starch produced by  $\alpha$ -amylase and sonication. *Food Biosci*. 2015;11(1):79–84.
21. Benavent-Gil Y, Rosell CM. Comparison of porous starches obtained from different enzyme types and levels. *Carbohydr Polym*. 2017;157:533–540.
22. Sujka M. Ultrasonic modification of starch: Impact on granules porosity. *Ultrason Sonochem*. 2017;37:424–429.
23. Zhang B, Cui D, Liu M, Gong H, Huang Y, Han F. Corn porous starch: Preparation, characterization and adsorption property. *Int J Biol Macromol*. 2012;50(1):250–256.
24. Chang PR, Yu J, Ma X. Preparation of porous starch and its use as a structure-directing agent for production of porous zinc oxide. *Carbohydr Polym*. 2011;83(2):1016–1019.
25. Guan JJ, Hanna MA. Extruding foams from corn starch acetate and native corn starch. *Biomacromolecules*. 2004;5(6):2329–2339.
26. Włodarczyk-Stasiak M, Mazurek A, Pankiewicz U, Sujka M, Jamroz J. Porosity of starch-proteins extrudates determined from nitrogen adsorption data. *Food Hydrocoll*. 2014;36:308–315.
27. Sjöqvist M, Gatenholm P. Effect of water content in potato amylopectin starch on microwave foaming process. *J Polym Environ*. 2007;15:43–50.
28. Nagata K, Okamoto H, Danjo K. Naproxen particle design using porous starch. *Drug Dev Ind Pharm*. 2001;27(4):287–296.
29. Gao F, Li D, Bi C-H, Mao Z-H, Adhikari B. Application of various drying methods to produce enzymatically hydrolyzed porous starch granules. *Drying Technology*. 2013;31(13–14):1627–1634.
30. Zhou M, Shen L, Hong Y, Feng Y. Design and pharmaceutical applications of porous particles. *RSC Adv*. 2017;7:39490–39501.
31. Allen TM, Cullis PR. Drug delivery systems: Entering the mainstream. *Science*. 2004;303(5665):1818–1822.
32. Rowe RC, Shesky PJ, Quinn ME. *Handbook of Pharmaceutical Excipients*. 6<sup>th</sup> ed. London, UK: Pharmaceutical Press; 2009:685–690.
33. Marques AP, Reis RI, Hunt JA. The biocompatibility of novel starch-based polymers and composites: In vitro studies. *Biomaterials*. 2002;23:1471–1478.
34. Wu C, Wang Z, Zhi Z, Jiang T, Zhang J, Wang S. Development of biodegradable porous starch foam for improving oral delivery of poorly water soluble drugs. *Int J Pharm*. 2011;403(1–2):162–169.
35. Zhao Y, Wu C, Zhao Z, et al. Preparation of starch macrocellular foam for increasing the dissolution rate of poorly water-soluble drugs. *Pharm Dev Technol*. 2015;21(6):749–754.

36. García-González CA, Uy JJ, Alnaief M, Smirnova I. Preparation of tailor-made starch-based aerogel microspheres by the emulsion-gelation method. *Carbohydr Polym.* 2012;88(4):1378–1386.
37. Silva GA, Costa FJ, Neves NM, Coutinho OP, Dias ACP, Reis RL. Entrapment ability and release profile of corticosteroids from starch-based microparticles. *J Biomed Mater Res A.* 2005;73A(2):234–243.
38. Jadhav NV, Vavia PR. Supercritical processed starch nanosponge as a carrier for enhancement of dissolution and pharmacological efficacy of fenofibrate. *Int J Biol Macromol.* 2017;99:713–720.
39. Pawar J, Ali MT, Fule R, et al. Biodegradable porous starch spheres as a novel carrier for enhancement of dissolution rate and oral bioavailability of itraconazole. *Curr Drug Deliv.* 2017;14(7):944–954.
40. Balmayor ER, Tuzlakoglu K, Azevedo HS, Reis RL. Preparation and characterization of starch-poly- $\epsilon$ -caprolactone microparticles incorporating bioactive agents for drug delivery and tissue engineering applications. *Acta Biomater.* 2009;5(4):1035–1045.
41. Wang Y, Ye H, Zhou C, Lv F, Bie X, Lu Z. Study on the spray-drying encapsulation of lutein in the porous starch and gelatin mixture. *Eur Food Res Technol.* 2012;234(1):157–163.
42. Malafaya PB, Elvira C, Gallardo A, San Román J, Reis RL. Porous starch-based drug delivery systems processed by a microwave route. *J Biomater Sci Polym Ed.* 2001;12(11):1227–1241.
43. Zhang Z, Huang J, Jiang S, et al. Porous starch based self-assembled nano-delivery system improves the oral absorption of lipophilic drug. *Int J Pharm.* 2013;444(1–2):162–168.
44. García-González CA, Jin M, Gerth J, Alvarez-Lorenzo C, Smirnova I. Polysaccharide-based aerogel microspheres for oral drug delivery. *Carbohydr Polym.* 2015;117:797–806.
45. Sujka M, Jamroz J.  $\alpha$ -Amylolysis of native potato and corn starches – SEM, AFM, nitrogen and iodine sorption investigations. *LWT-Food Sci Technol.* 2009;42(7):1219–1224.
46. Sujka M, Jamroz J, Kwiatkowski R. Influence of  $\alpha$ -amylolysis on the formation of electron density inhomogeneities on the surface of starch granules. *Starch/Stärke* 2011;63(1):17–23.
47. Meer TA, Moravkar K, Pawar J, Amin P. Cross-linked porous starch particles – a promising carrier. *Polim Med.* 2015;45(1):11–19.
48. Lacerda LD, Leite DC, Soares RMD, da Silveira NP. Effects of  $\alpha$ -amylase, amyloglucosidase, and their mixture on hierarchical porosity of rice starch. *Starch/Stärke.* 2018;70(11–12):1–7.



# Formulation and characterization of oral rapid disintegrating tablets of levocetirizine

Samvedna<sup>1,A-D,F</sup>, Shammy Jindal<sup>1,A,B,F</sup>, Gaurav Mishra<sup>2,C-F</sup>, Jyotsana R. Madan<sup>3,C-F</sup>, Gaurav Gupta<sup>4,C-F</sup>, Rajendra Awasthi<sup>5,A-F</sup>, Terezinha de Jesus Andreoli Pinto<sup>6,C-F</sup>, Kamal Dua<sup>7,C-F</sup>, Giriraj T. Kulkarni<sup>5,A,C-F</sup>

<sup>1</sup> Laureate Institute of Pharmacy, Jawalamukhi, India

<sup>2</sup> Drug Delivery and Nanotechnology Laboratory, Bhagyoday Teerth Pharmacy College, Sagar, India

<sup>3</sup> Department of Pharmaceutics, Smt. Kashibai Navale College of Pharmacy, Savitribai Phule Pune University, India

<sup>4</sup> School of Pharmaceutical Sciences, Jaipur National University, Jagatpura, India

<sup>5</sup> Amity Institute of Pharmacy, Amity University, Noida, India

<sup>6</sup> Department of Pharmacy, Faculty of Pharmaceutical Sciences, University of São Paulo, Brazil

<sup>7</sup> Discipline of Pharmacy, Graduate School of Health, University of Technology, Sydney, Australia

A – research concept and design; B – collection and/or assembly of data; C – data analysis and interpretation; D – writing the article; E – critical revision of the article; F – final approval of the article

Polymers in Medicine, ISSN 0370-0747 (print), ISSN 2451-2699 (online)

*Polim Med.* 2018;48(1):31–40

## Address for correspondence

Rajendra Awasthi

E-mail: awasthi02@gmail.com

## Funding sources

None declared

## Conflict of interest

None declared

Received on June 15, 2018

Reviewed on June 29, 2018

Accepted on November 23, 2018

## Cite as

Samvedna, Jindal S, Mishra G, Madan JR, Gupta G, Awasthi R, de Jesus Andreoli Pinto T, Dua K, Kulkarni GT. Formulation and characterization of oral rapid disintegrating tablets of levocetirizine. *Polim Med.* 2018;48(1):31–40. doi:10.17219/pim/99951

## DOI

10.17219/pim/99951

## Copyright

© 2018 by Wrocław Medical University

This is an article distributed under the terms of the Creative Commons Attribution Non-Commercial License (<http://creativecommons.org/licenses/by-nc-nd/4.0/>)

## Abstract

**Background.** Levocetirizine, active R (–) enantiomer of cetirizine, is an orally active and selective H1 receptor antagonist used medically as an anti-allergic. Allergic rhinitis is a symptomatic disorder of the nose induced by inflammation mediated by immunoglobulin E (IgE) in the membrane lining the nose after allergen exposure.

**Objectives.** The purpose of the present study was to prepare rapidly disintegrating tablets of levocetirizine after its complexation with  $\beta$ -cyclodextrin ( $\beta$ -CD).

**Material and methods.** Levocetirizine– $\beta$ -CD complex tablets were prepared by direct compression technique using 3 synthetic superdisintegrants in different proportions. Development of the formulation in the present study was mainly based on the concentration of superdisintegrants and the properties of the drug. Nine batches of tablets were formulated and evaluated for various parameters: drug content, weight variation, water absorption ratio, wetting time, in vitro disintegration, hardness, friability, thickness uniformity, and in vitro dissolution.

**Results.** A Fourier-transform infrared spectroscopy (FTIR) study showed that there were no significant interactions between the drug and the excipients. The prepared tablets were good in appearance and showed acceptable results for hardness and friability. The in vitro disintegrating time of the formulated tablet batches was found to be 15–35 s percentage and the drug content of tablets in all formulations was found to be between 90–102%, which complied with the limits established in the United States Pharmacopeia.

**Conclusions.** Complexation of levocetirizine with  $\beta$ -CD significantly improves the solubility of the drug. The disintegration time of the tablets was decreased with an increase in superdisintegrant amount. The tablets (batch CPX5) had a minimum disintegration time of 20 s and 99.99% of the drug was released within 10 min.

**Key words:** direct compression, superdisintegrants,  $\beta$ -cyclodextrin complex, rapidly disintegrating tablets

## Introduction

Tablets are the most widely accepted dosage forms.<sup>1,2</sup> Rapidly disintegrating tablets (RDTs) are gaining more popularity as they can be administered without the need to be swallowed with water, and they are dissolved or easily disintegrated in the mouth within a few seconds. The drug is released immediately when the tablet is placed on the tongue. The RDTs are in ever-increasing demand compared to liquid dosage forms due to the ease of handling, accurate dose and good stability during storage. They improve the oral bioavailability of drugs as compared to conventional tablets. The released drug will be absorbed from the whole gastrointestinal tract and thus the oral bioavailability will improve.<sup>3</sup> The disintegration time for orally rapid disintegrating tablets is generally considered to be less than 60 s.<sup>4,5</sup> Various RDTs have been reported to improve patient compliance and bioavailability, such as dispersible tablets, rapidly disintegrating tablets, orally disintegrating tablets, quick disintegrating tablets, rapid dissolving tablets, porous tablets, quick melt tablets, etc.<sup>6</sup>

Rapidly disintegrating drug delivery systems (RDDS) offer several benefits such as easy administration to children and elderly patients having difficulties swallowing (dysphagia) and in the case of tremors or mental retardation condition.<sup>7</sup> The RDDS are also useful for local action such as a local anesthetic for toothaches, oral ulcers, cold sores, or teething.<sup>8</sup> The RDTs can be prepared using conventional methods like direct compression, wet granulation, moulding, spray drying, freeze-drying, and sublimation. Proper choice of superdisintegrants and consistency in its performance are of critical importance to the formulation development of RDTs.<sup>9</sup> Examples of some widely used superdisintegrants are modified starch (sodium starch glycolate), modified cellulose (croscarmellose) and cross-linked polyvinylpyrrolidone (crospovidone).<sup>10</sup>

Basic considerations in formulating RDTs are palatability, aqueous solubility, hygroscopicity, and mechanical strength.<sup>11</sup> These systems are made to disintegrate or dissolve in the oral cavity, which may lead to the sensation of taste. Thus, taste masking of the bitter drugs becomes critical to patient compliance. Water solubility is another critical parameter that needs to be examined carefully during the manufacturing of RDTs. The formation of a eutectic mixture of most of the BCS (biopharmaceutical classification system) class I and III drugs leads to a depression in freezing point. This results in the formation of a glassy solid mass which can be easily sublimated with drying. Drying of the formed glassy solid mass may cause it to collapse due to the loss of supporting structures.<sup>12</sup> Normal storage conditions may affect the physical integrity of RDTs, hence specialized packaging is needed to protect them from environmental conditions such as temperature and humidity. For rapid disintegration, RDTs are manufactured at low compression force. This may lead to the formation of a friable or brittle tablet. The

handling of such products might be difficult and requires peel-off blister packing. The objective of compressed-tablet manufactures is to deliver the orally correct amount of the drug in proper time and to the desired location while subsequently maintaining its chemical integrity to that point. The aim of the present study was to prepare RDTs of levocetirizine to improve the drug stability and its therapeutic benefits.

## Material

The levocetirizine was a generous gift from Cipla Ltd., Ahmedabad, India.  $\beta$ -cyclodextrin ( $\beta$ -CD) was purchased from Central Drug House (P) Ltd., New Delhi, India. Sodium starch glycolate (SSG), croscarmellose sodium (CMS), microcrystalline cellulose (MCC), crospovidone (CP), magnesium stearate, aerosol, and mannitol were purchased from S.D. Fine Chem Ltd., Mumbai, India. All the chemicals used were of analytical grade.

## Methods

### Preparation of levocetirizine- $\beta$ -CD complex

Levocetirizine- $\beta$ -CD complex (1:1 molar ratio) was prepared using the kneading method. Briefly, an accurately weighed amount of the pure drug and  $\beta$ -CD was triturated in a clean and dry mortar with a small volume of the water-methanol solvent system to make a thick slurry. The mass was uniformly mixed and dried at 40°C. The dried mass was grained and sifted through a mesh (100).<sup>12-15</sup>

### Characterization of levocetirizine- $\beta$ -CD complex

#### UV spectroscopic study

The confirmation of complexation between the levocetirizine- $\beta$ -CD was carried out by ultraviolet-visible spectrophotometrically (UV-visible spectrophotometer, 3000+, LabIndia, Mumbai, India). Pure levocetirizine (10 mg) was dissolved in methanol (100 mL), filtered and analyzed at 231 nm after suitable dilution. Similarly, the same spectrum was taken for the levocetirizine- $\beta$ -CD complex (containing 10 mg levocetirizine) at 233 nm. The change in absorbance of the drug in levocetirizine- $\beta$ -CD complex was recorded.

#### Fourier-transform infrared spectroscopy

A Fourier-transform infrared (FTIR) spectroscopy of pure levocetirizine,  $\beta$ -CD and levocetirizine- $\beta$ -CD complex (1:1) was carried out by the FTIR peak match-



ing method (IR-affinity-1; Shimadzu, Kyoto, Japan). Briefly, the samples were mixed with dried potassium bromide (KBr) and compressed into a pellet using KBr press at 10 t. The pellets were scanned from 4000–400  $\text{cm}^{-1}$  at 4  $\text{cm}^{-1}$  resolution. The complex formation was evaluated by comparing the FTIR spectra of the drug- $\beta$ -CD complex and that of the pure drug.<sup>16,17</sup>

### X-ray diffraction studies

An X-ray diffraction study of pure levocetirizine and the drug- $\beta$ -CD complex (1:1) was done by X-ray powder diffractometer (PW 3040/60 Xpert PRO; PANalytical, Almelo, the Netherlands) using Cu  $K\alpha$  radiations ( $\lambda = 1.5405980 \text{ \AA}$ ), 40 mA current and 40 kV voltage. The samples were analyzed over 0–80  $2\theta$  range with a scan step size of  $2^\circ/\text{min}$ .<sup>18</sup>

## Powder characterization

### Determination of angle of repose

The angle of repose was determined to know the flow properties of granules using the funnel method. Briefly, the powder mix was allowed to pour from a funnel that can be raised vertically until a maximum cone height was obtained. The angle of repose ( $\theta$ ) was determined by measuring the height (h) and radius (r) of the cone using the following formula<sup>19</sup>:

$$\tan \theta = \frac{h}{r}$$

The mean result of triplicate measurements and the standard deviation (SD) were reported.

### Determination of loose density

Loose bulk density (LBD) is the ratio of powder weight in grams to the loose bulk volume [ $\text{cm}^3$ ]. A sample (5 g) was carefully introduced in a 10 mL graduated measuring cylinder and LBD was determined using the following formula<sup>19</sup>:

$$\text{loose bulk density} = \frac{\text{weight of powder [g]}}{\text{bulk volume [cm}^3\text{]}}$$

The mean result of triplicate measurements and the SD were reported.

### Determination of tapped density

For the determination of tapped density, a powder sample (5 g) was introduced in a 10 mL graduated measuring cylinder. The cylinder was dropped onto a flat surface 50 times

from 2.5 cm height. Tapped bulk density was determined by applying the following formula<sup>19</sup>:

$$\text{tapped density} = \frac{\text{weight of powder}}{\text{tapped volume of powder}}$$

The mean result of triplicate measurements and the SD were reported.

### Determination of the Hausner ratio

Hausner ratio (HR) is an indirect index of ease of powder flow. Lower HR ( $<1.25$ ) indicates better flow properties. It was determined by applying the following formula<sup>19</sup>:

$$\text{Hausner ratio} = \frac{\text{tapped density}}{\text{bulk density}}$$

The mean result of triplicate measurements and the SD were reported.

### Determination of void volume

The volume of the space between particles was determined by applying the following formula:

$$\text{void volume} = \text{bulk volume} - \text{tapped volume}$$

The mean result of triplicate measurements and the SD were reported.

### Determination of Carr's compressibility index

Carr's compressibility index is determined using density measurements. A particle bed having more compressibility is less flowable and vice versa. Carr's compressibility index [%] was determined by the following formula<sup>19</sup>:

$$\text{Carr's index} = \frac{\text{tapped density} - \text{bulk density}}{\text{tapped density}} \times 100$$

The mean result of triplicate measurements and the SD were reported.

### Determination of percentage porosity

The percent porosity of the granules of each prepared batch was determined using the following formula:

$$\text{porosity [\%]} = 1 - \frac{V_p}{V_b} \times 100$$

Where  $V_b$  is the bulk volume, and  $V_p$  is the particle volume. The mean result of triplicate measurements and the SD were reported.

## Preparation and evaluation of rapidly disintegrating tablets

Rapidly disintegrating tablets of levocetirizine were prepared by direct compression method. Croscarmellose sodium (CCS), sodium starch glycolate (SSG) and crospovidone (CP) were used as superdisintegrants. The  $\beta$ -CD was used as a complexing agent to improve the dissolution of the drug. Microcrystalline cellulose (MCC) was used as a binder (Table 1). Drug- $\beta$ -CD complex equivalent to 5 mg of the levocetirizine and all the excipients except magnesium stearate and aerosil were taken in a mortar and mixed. The powder mix was passed through a 80 sieve. Lubrication was done using magnesium stearate and aerosil. The final blend was compressed into caplets using a 10-station compression machine (Mini-press-1, Karnavati, Ahmedabad, India) to produce 120 mg tablets using 4 mm diameter die and punches.<sup>20</sup>

The prepared tablets were evaluated for both non-official and official tests. Tablets from each batch were subjected to the following tests.

### General appearance

The general appearance of a tablet, its visual identity and overall elegance is essential for patient's acceptance. The tablet's shape, size, color, presence or absence of an odor, and legibility of any identifying marking were studied as the general appearance characteristics.

### Test for weight uniformity

The United States Pharmacopeia (USP) procedure for the determination of uniformity of tablet weight was followed. Twenty tablets from each batch were taken and weighed individually and collectively on a digital weighing balance (MAB 182; Wensar, Mumbai, India). The average weight of 20 tablets was calculated. The weight variation was calculated for USP limits, i.e., for an average weight of 80 mg or less, 80–250 mg and more than 250 mg;

the maximum percentage differences allowed are 10%, 7.5% and 5%, respectively. The mean result of triplicate measurements and the SD were reported.<sup>21</sup>

### Determination of tablet thickness

The thickness of tablets was determined using vernier callipers. Twenty tablets from each batch were randomly selected for thickness measurements. The mean result of triplicate measurements and the SD were reported.

### Determination of tablet hardness

The resistance of tablets to chipping, abrasion or breakage under the conditions of storage, transformation and handling depends on its hardness. The tablet hardness was determined by diametral compression using a dial-type Monsanto tablet hardness tester. A tablet hardness of about 4–5 kg/cm<sup>2</sup> is considered adequate for mechanical stability. The sampling was carried out in triplicate for each batch.

### In vitro disintegration, dispersion and wetting test

One tablet was placed in each tube of a USP tablet disintegration test apparatus (ED-2 SAPO; Electrolab, Mumbai, India) and the basket rack was positioned in a 1 L beaker containing freshly prepared and cooled distilled water at 37  $\pm$ 0.5°C. The time required for a complete disintegration of the tablet with no palpable mass remaining in the apparatus was measured. Dispersion time of the tablet was recorded by placing 1 tablet from each batch in a Petri dish containing phosphate buffer (pH 6.8). For the determination of the wetting time of the tablet, a circular piece of tissue paper (12  $\times$  10.75 cm) folded twice was placed in a small Petri dish (internal diameter 6.5 cm) containing 10 mL of phosphate buffer (pH 6.8). A tablet was placed on the paper, and the time for complete wetting was measured. The sampling was carried out in triplicate for each batch.<sup>22</sup>

Table 1. Composition of various rapidly disintegrating tablets (RDTs) of levocetirizine (formulation CPX<sub>1</sub>–CPX<sub>9</sub>)

Ingredients	Formulation code								
	CPX <sub>1</sub> [mg]	CPX <sub>2</sub> [mg]	CPX <sub>3</sub> [mg]	CPX <sub>4</sub> [mg]	CPX <sub>5</sub> [mg]	CPX <sub>6</sub> [mg]	CPX <sub>7</sub> [mg]	CPX <sub>8</sub> [mg]	CPX <sub>9</sub> [mg]
Levocetirizine- $\beta$ -CD complex*	14.5	14.5	14.5	14.5	14.5	14.5	14.5	14.5	14.5
SSG	–	–	10	11	12	–	–	10	–
CMS	11	–	–	–	–	10	11	–	–
CP	–	10	–	–	–	–	–	–	10
Mg stearate	3	2	3	2	2	3	1	2	1
Aerosil	2	2	2	2	2	2	2	2	2
Mannitol	21.5	18.5	18.5	20	14.5	14.5	22	16.5	12.5
MCC	68	73	72	70	75	76	74	75	80

\* Complex equivalent to 5 mg of levocetirizine;  $\beta$ -CD –  $\beta$ -cyclodextrin; SSG – sodium starch glycolate; CMS – croscarmellose sodium; CP – crospovidone; MCC – microcrystalline cellulose.

### Determination of water absorption ratio

For the determination of water absorption ratio, a small piece of tissue paper (folded twice) was placed in a Petri dish containing distilled water (6 mL). The tablet was placed on the wet paper and the weight of the wet tablet was recorded. The water absorption ratio (R) was calculated using the following formulation<sup>22</sup>:

$$R = \frac{W_a - W_b}{W_b} \times 100$$

where  $W_b$  and  $W_a$  are the weight of the tablet before and after water absorption, respectively. The mean result of triplicate measurements and the SD were reported.

### Determination of percentage friability

A USP tablet friabilator (EF-2; Electrolab, Mumbai, India) was employed for the determination of tablet friability. Pre-weighted tablets (20 tablets) were placed in the friabilator. The friabilator was rotated for 4 min at 25 rpm. At the end of the test, the tablets were dusted and re-weighed. The loss in tablet weight was measured and the friability was calculated using the following formula:

$$\text{friability [\%]} = \frac{\text{weight after 100 counts}}{\text{initial weight}} \times 100$$

### Determination of drug content

Ten tablets of levocetirizine from each batch were crushed and the mass equivalent to 1 tablet was taken and transferred to a 100 mL volumetric flask. Final volume was adjusted with phosphate buffer (pH 6.8). The mixture was shaken for 30 min in a water bath shaker incubator. The mixture was filtered and the filtrate was analyzed at 233.00 nm after suitable dilutions using an ultraviolet-visible spectrophotometer (3000<sup>+</sup>; Labindia, Mumbai, India). The mean result of triplicate measurements and the SD were reported.<sup>23</sup>

### X-ray diffraction study

X-ray diffraction study of the prepared tablet (formulation CPX5) was carried out similarly as for the pure drug and complex.

### In vitro dissolution studies

An in vitro dissolution study was carried out using USP tablet dissolution test apparatus II (DS 8000; Labindia, Mumbai, India) at 50 rpm in 900 mL of phosphate buffer (pH 6.8). The temperature was maintained at  $37 \pm 0.5^\circ\text{C}$ . The samples were withdrawn at predetermined time in-

tervals of 0 min, 2 min, 4 min, 6 min, and 10 min. Aliquots (5 mL) were withdrawn, filtered and analyzed spectrophotometrically using a UV spectrophotometer (3000<sup>+</sup>) at 233 nm. Complete sink condition was maintained by adding an equal amount of fresh dissolution medium ( $37 \pm 0.5^\circ\text{C}$ ) after each sampling. The sampling study was carried out in triplicate for each batch. The kinetic study of drug release data was done by zero order (cumulative percentage drug released vs time) and first order (percentage drug retained vs time) plots.

## Results and discussion

### Characterization of levocetirizine- $\beta$ -CD complex

#### UV spectroscopic study

The results showed no shift in the  $\lambda_{\text{max}}$  of levocetirizine in the presence of  $\beta$ -CD complex (Fig. 1). The slight change in absorbance could be explained due to the changes in the solvent microenvironment and the transfer of the guest molecule of water in the  $\beta$ -CD cavity during complex formation.

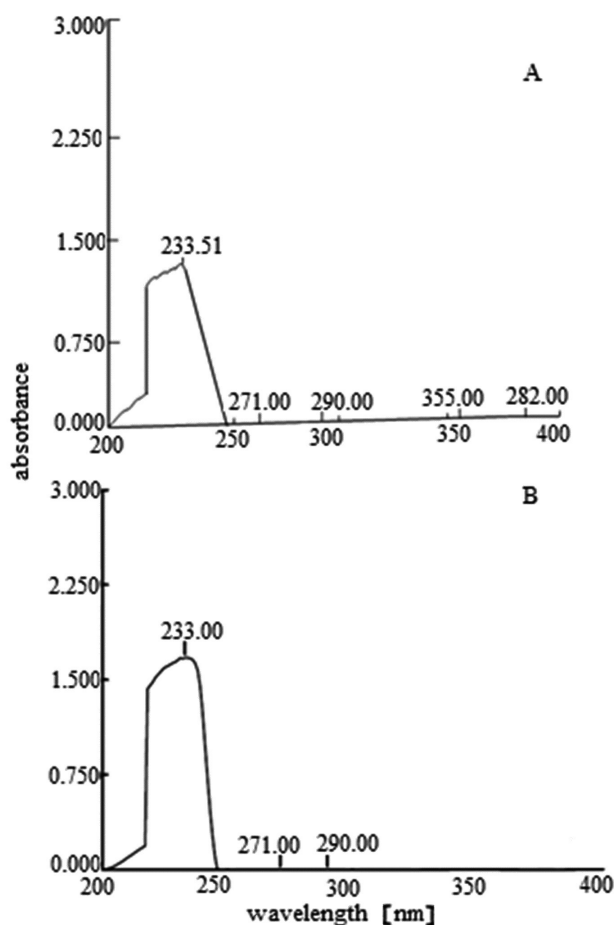


Fig. 1. UV scan spectrum of the levocetirizine- $\beta$ -cyclodextrin ( $\beta$ -CD) complex (A) and pure levocetirizine (B)

### Fourier-transform infrared spectroscopy

A FTIR spectroscopy was carried out to investigate the possible interaction between levocetirizine and  $\beta$ -CD, if any. The FTIR spectrum of levocetirizine,  $\beta$ -CD and physical mixture of levocetirizine- $\beta$ -CD complex are illustrated in Fig. 2. The chemical interaction between the levocetirizine- $\beta$ -CD leads to identifiable changes in the infrared profile of dispersion. In the present study, the FTIR spectrum of levocetirizine showed characteristic peaks at  $3641\text{ cm}^{-1}$  (OH stretching),  $2785\text{ cm}^{-1}$  ( $\text{CH}_2$  stretching),  $1718\text{ cm}^{-1}$  (stretching of ester carbonyl and  $-\text{COOH}$  groups),  $1602\text{ cm}^{-1}$  ( $\text{C}=\text{C}$ ),  $1479\text{ cm}^{-1}$  (ether group),  $1319\text{ cm}^{-1}$  ( $\text{C}-\text{N}$  stretching),  $1085\text{ cm}^{-1}$  ( $\text{C}=\text{O}$  stretching), and  $721\text{ cm}^{-1}$  ( $\text{C}-\text{Cl}$  stretching). In the case of  $\beta$ -CD, stretching (broad) of the O-H group was observed near  $3227\text{ cm}^{-1}$ .  $\beta$ -CD showed characteristic peaks near  $2928\text{ cm}^{-1}$  (antisymmetric and symmetric stretching of  $-\text{CH}_2$  group),  $1642\text{ cm}^{-1}$  (O-C (2-bands)  $\text{C}=\text{O}$  (amide I band)),  $1410\text{ cm}^{-1}$  (in plane bending) of OH, bending of  $\alpha\text{-CH}_2$  and deformation of  $\text{CH}_2$ ),  $1332\text{ cm}^{-1}$  (in plane bending of OH),  $1152\text{ cm}^{-1}$  (bending of  $\text{C}-\text{C}-\text{C}$ ),  $1077\text{ cm}^{-1}$

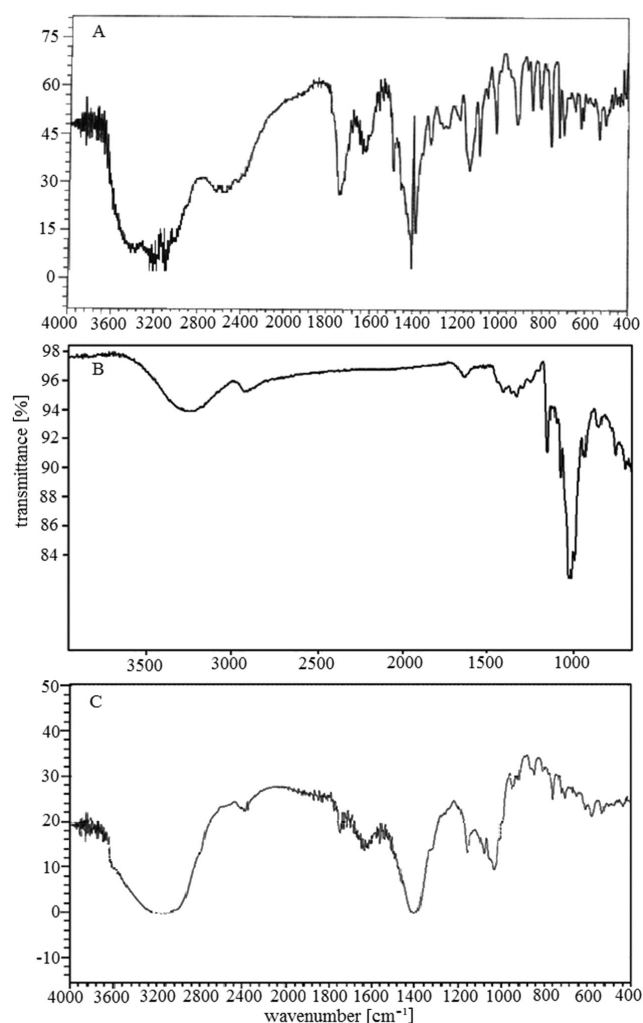


Fig. 2. Fourier-transform infrared spectroscopy (FTIR) spectrum of levocetirizine (A),  $\beta$ -cyclodextrin ( $\beta$ -CD) (B) and physical mixture of levocetirizine- $\beta$ -cyclodextrin ( $\beta$ -CD) complex (C)

and  $1022\text{ cm}^{-1}$  (O-H (H-bonded), usually broad C-O),  $937\text{ cm}^{-1}$ ,  $860\text{ cm}^{-1}$  and  $753\text{ cm}^{-1}$  (stretching of  $=\text{C}-\text{H}$  and  $=\text{CH}_2$ , bending and ring puckering of  $\text{C}-\text{H}$ ) and  $703\text{ cm}^{-1}$  (*cis*- $\text{RCH}=\text{CHR}$ ). The ester carbonyl stretching bend of levocetirizine shifted from  $1718\text{ cm}^{-1}$  down to  $1675\text{ cm}^{-1}$ . This may be due to the intermolecular hydrogen bonding between levocetirizine and  $\beta$ -CD. The peak due to the stretching vibration of the N-H bond near  $3317\text{ cm}^{-1}$  in the dihydropyridine ring was broadened, nearly disappeared in complex spectra. A broad peak near  $3227\text{ cm}^{-1}$  ( $-\text{OH}$  band of pure  $\beta$ -CD) was observed in the spectrum of the complex, indicating complex formation and inclusion of levocetirizine in the cavity of  $\beta$ -CD. The increment in intensity is due to the insertion of a benzene ring into the electron-rich cavity of  $\beta$ -CD, which increases electron density and leads to the increase in frequency. Thus, the FTIR spectrum proves the formation of the levocetirizine- $\beta$ -CD complex.

### X-ray diffraction

An X-ray diffraction study was used to evaluate the physical state of pure levocetirizine and the drug within the levocetirizine- $\beta$ -CD complex (1:1). The X-ray diffractograms of pure levocetirizine and levocetirizine- $\beta$ -CD complex are presented in Fig. 3. Levocetirizine has shown characteristic intense peaks at  $2\theta$  of 5.50, 6.50, 7.50, 8.32, 10.58, 12.42, 13.54, 14.51, 15.21, 16.03, 16.94, 17.87, 18.98, 19.20, 20.81, 21.54, 22.64, 23.84, 24.58, 25.24, 25.64, 26.23, 27.64, 29.00, 29.94, 30.32, 31.11, 31.75, 33.34, 35.51, 35.85, 36.35, 37.94, and 39.21 because of its crystalline state. In the levocetirizine- $\beta$ -CD complex, the drug peaks are visible at  $2\theta$  of 4.78, 6.54, 7.33, 7.68, 8.27, 9.27, 9.98, 10.93,

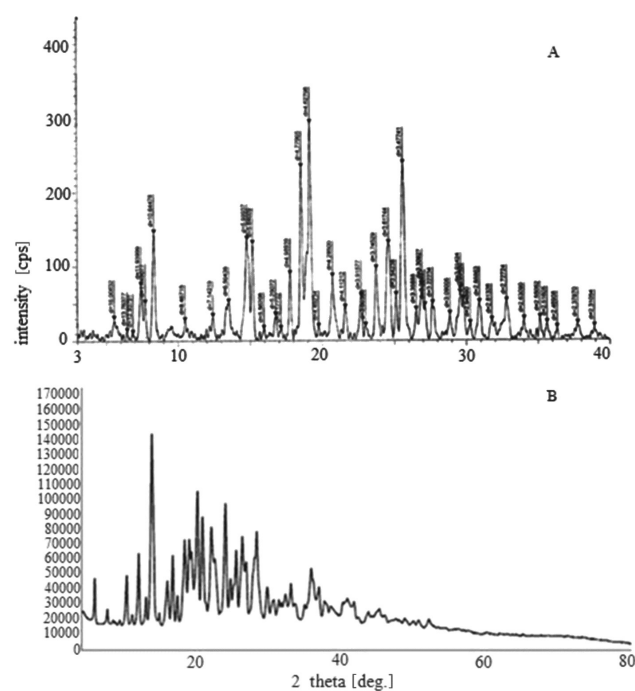


Fig. 3. X-ray diffraction patterns of pure levocetirizine (A) and levocetirizine- $\beta$ -cyclodextrin ( $\beta$ -CD) complex (1:1) (B)

12.742, 13.06, 14.90, 15.67, 16.32, 17.34, 18.30, 19.12, 19.80, 21.03, 23.10, 24.57, 25.38, 26.85, 27.36, 29.71, 30.47, 31.40, 32.18, 34.03, 35.03, 36.12, 37.69, 40.02, 41.03, and 44.53, indicating the crystalline form of the drug within the complex. The drug is not in amorphous form, otherwise the drug peaks would have disappeared completely in the complex. However, the crystallinity of the drug has been decreased in the case of the levocetirizine- $\beta$ -CD complex as some of the peaks disappeared.

## Evaluation of powder

### Angle of repose

The angle of repose ( $\theta$ ) was calculated to know the flow properties of granules. Based on the particle size, powders are broadly classified as very fine, fine, moderately fine, moderately coarse, and coarse. The particles having size <100  $\mu$ m tend to be more cohesive and less free-flowing. Larger particles have good flow properties. The cohesivity of powder decreases with the increase in particle size. The USP defined the range of angle of repose as: 25–30 for excellent flow, 31–35 for good, 36–40 for fair, 41–45 for passable, 46–55 for poor flow, 56–65 for very poor flow, and >66 for considerably poor flow.<sup>24</sup> In the present study, the value of angle of repose for all the batches ranged between 23.93  $\pm$ 0.22 to 30.04  $\pm$ 0.23 (Table 2), indicating excellent flow potential of the blend. The powdered mass of the different formulations was found to be non-aggregating. The results are acceptable for tablet manufacturing purposes.

### Bulk density

The results of bulk density are represented in Table 2. The bulk densities of all the batches were observed between

0.45  $\pm$ 0.27 g/cm<sup>3</sup> and 0.56  $\pm$ 0.38 g/cm<sup>3</sup>. The bulk density of batches CPX<sub>1</sub> and CPX<sub>6</sub> was found to be almost similar, indicating similar bulk volume and packing arrangements.

### Tapped density

The results of tapped density are represented in Table 2. The tapped density was observed between 0.54  $\pm$ 0.32 g/mL and 0.69  $\pm$ 0.28 g/mL. The difference in the values of bulk density and tapped density indicates very little or no change in powder volume even after 50 tappings.

### Hausner ratio

The HR is an indication of flow properties of the powder blend. A HR <1.25 indicates good flow properties, 1.25–1.50 indicates poor but improvable, and >1.50 indicates poor flowability of the powder.<sup>24</sup> The results show that the HR of all the formulations was in the range from 1.03  $\pm$ 0.02 to 1.32  $\pm$ 0.22 (Table 2), which indicates good flow properties of powder blends.

### Void volume

The void volume was found in the range from 0.3  $\pm$ 0.18 to 2.4  $\pm$ 0.39 (Table 2), indicating that the powder blend had good flow properties.

## Evaluation of rapidly disintegrating tablets

### General appearance

All the tablets were white to off-white in color, round and flat in shape with a score line through the center, and had a smooth surface.

Table 2. Micrometric properties of powder blend

Micrometric property	Formulation code								
	CPX <sub>1</sub>	CPX <sub>2</sub>	CPX <sub>3</sub>	CPX <sub>4</sub>	CPX <sub>5</sub>	CPX <sub>6</sub>	CPX <sub>7</sub>	CPX <sub>8</sub>	CPX <sub>9</sub>
Angle of repose [ $\theta$ ]	23.93 $\pm$ 0.22	30.04 $\pm$ 0.23	26.68 $\pm$ 0.16	24.93 $\pm$ 0.2	25.63 $\pm$ 0.56	28.93 $\pm$ 0.12	25.40 $\pm$ 0.17	27.00 $\pm$ 0.16	29.83 $\pm$ 0.18
Bulk density [g/mL]	0.56 $\pm$ 0.38	0.53 $\pm$ 0.34	0.47 $\pm$ 0.65	0.49 $\pm$ 0.12	0.54 $\pm$ 0.21	0.52 $\pm$ 0.3	0.53 $\pm$ 0.2	0.45 $\pm$ 0.27	0.47 $\pm$ 0.22
Tapped density [g/mL]	0.58 $\pm$ 0.23	0.59 $\pm$ 0.37	0.66 $\pm$ 0.30	0.63 $\pm$ 0.18	0.62 $\pm$ 0.18	0.69 $\pm$ 0.28	0.61 $\pm$ 0.50	0.59 $\pm$ 0.41	0.54 $\pm$ 0.32
Void volume	0.30 $\pm$ 0.18	1.10 $\pm$ 0.28	2.90 $\pm$ 0.39	2.20 $\pm$ 0.43	1.10 $\pm$ 0.19	2.40 $\pm$ 0.31	1.20 $\pm$ 0.22	2.40 $\pm$ 0.31	1.50 $\pm$ 0.25
Hausner ratio	1.03 $\pm$ 0.02	1.13 $\pm$ 0.17	1.30 $\pm$ 0.78	1.22 $\pm$ 0.18	1.12 $\pm$ 0.18	1.32 $\pm$ 0.22	1.13 $\pm$ 0.29	1.21 $\pm$ 0.50	1.18 $\pm$ 0.28
Porosity [%]	3.37 $\pm$ 0.05	11.50 $\pm$ 0.28	27.60 $\pm$ 0.42	21.70 $\pm$ 0.29	11.90 $\pm$ 0.42	25.00 $\pm$ 0.12	12.70 $\pm$ 0.08	22.00 $\pm$ 0.12	14.00 $\pm$ 0.16
Carr's compressibility index [%]	13.44 $\pm$ 0.29	12.60 $\pm$ 0.39	21.69 $\pm$ 0.27	22.22 $\pm$ 0.19	12.47 $\pm$ 0.19	24.63 $\pm$ 0.17	12.80 $\pm$ 0.52	22.24 $\pm$ 0.25	14.80 $\pm$ 0.21
Drug content [%]	90.63 $\pm$ 0.17	90.01 $\pm$ 0.34	97.07 $\pm$ 0.75	99.76 $\pm$ 0.87	102.09 $\pm$ 0.67	90.06 $\pm$ 0.16	90.78 $\pm$ 0.32	97.57 $\pm$ 0.43	90.76 $\pm$ 0.35

Data presented as mean  $\pm$  standard deviation (SD); n = 3.

### Uniformity of weight

Twenty tablets were randomly selected from each batch for weight variation testing. The tablets were weighed individually and the average weight of 20 tablets was calculated. The results were within the range from 198.40 ± 0.01 mg to 200.41 ± 0.12 mg (Table 3). The results were within the acceptable limit given in the USP.<sup>24</sup>

### Thickness

The thickness of the prepared tablets was found in the range from 2.0 ± 0.56 mm to 2.99 ± 0.05 mm (Table 3).

### Hardness

Tablet strength and disintegrating time depend on its hardness. It had been observed that the RDTs are less hard than conventional tablets because less compression force is applied. The hardness of the prepared tablets was in the range from 2.30 ± 0.40 kg/cm<sup>2</sup> to 3.90 ± 0.06 kg/cm<sup>2</sup>, which is sufficient to maintain the tablet integrity during storage and handling and also within the range ensuring rapid disintegration (Table 3).

### In vitro disintegrating and wetting time

The in vitro tablet disintegration time is the time taken to undergo complete disintegration of the tablet in USP tablet disintegration apparatus under specified conditions. Disintegrating time is related to the nature and concentration of superdisintegrants and hardness of the tablet. It allows breaking the tablet into small fragments upon contact with dissolution media. The in vitro disintegrating time of the prepared tablets was found to be between 15 s and 35 s. Formulations CPX<sub>4</sub> and CPX<sub>5</sub> had better disintegrating time, i.e., 19 s and 15 s, respectively. This might be due to the swelling and wicking mechanism (drawing water through capillary action) of water penetration in tablets containing SSG.<sup>25</sup>

Wetting time is closely related to the inner core density and hardness of the tablet. The wetting time of the prepared tablets was found to be between 12 s and 32 s. The wetting time of formulations CPX<sub>5</sub> and CPX<sub>4</sub> was 12 s and 19 s, respectively. It has been found that with an increase in the concentration of superdisintegrants, the wetting time is rapidly decreased. Figure 4 presents the relationship between disintegration time and wetting time of different RDTs. The relationship between wetting time and water absorption ratio of different RDTs is presented in Fig. 5.

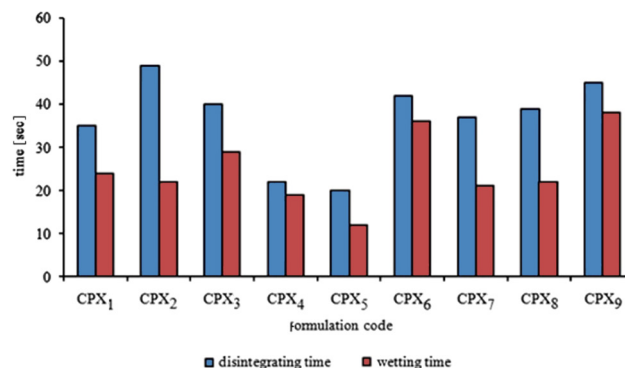


Fig. 4. Relationship between wetting time and disintegration time of different rapidly disintegrating tablets (RDTs) (formulation CPX<sub>1</sub>–CPX<sub>9</sub>)

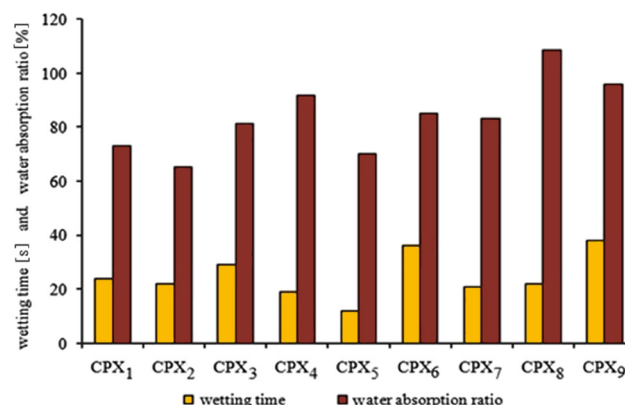


Fig. 5. Relationship between wetting time and water absorption ratio of different rapidly disintegrating tablets (RDTs) (formulation CPX<sub>1</sub>–CPX<sub>9</sub>)

Table 3. Post-compression parameter of prepared rapidly disintegrating tablets (RDTs)

Formulation code	Uniformity of weight [mg/tablet]	Thickness [mm] ±SD	Hardness [kg/cm <sup>2</sup> ]	Water absorption ratio [%]	Friability [%]
CPX <sub>1</sub>	198.51 ± 0.04	2.69 ± 0.23	3.40 ± 0.32	73.00 ± 0.17	0.36 ± 0.40
CPX <sub>2</sub>	200.41 ± 0.12	2.00 ± 0.56	3.90 ± 0.06	65.33 ± 0.45	0.26 ± 0.21
CPX <sub>3</sub>	199.01 ± 0.22	2.34 ± 0.04	2.90 ± 0.03	81.16 ± 0.62	0.30 ± 0.33
CPX <sub>4</sub>	200.03 ± 0.30	2.43 ± 0.08	3.80 ± 0.02	91.66 ± 0.98	0.34 ± 0.26
CPX <sub>5</sub>	200.01 ± 0.16	2.83 ± 0.04	3.16 ± 0.08	70.08 ± 0.72	0.25 ± 0.11
CPX <sub>6</sub>	198.40 ± 0.01	2.16 ± 0.07	2.90 ± 0.04	85.00 ± 0.09	0.26 ± 0.18
CPX <sub>7</sub>	199.03 ± 0.21	2.29 ± 0.02	3.12 ± 0.02	83.06 ± 0.05	0.29 ± 0.38
CPX <sub>8</sub>	200.04 ± 0.12	2.99 ± 0.05	3.20 ± 0.12	108.33 ± 0.68	0.34 ± 0.26
CPX <sub>9</sub>	200.23 ± 0.62	2.63 ± 0.61	2.30 ± 0.40	95.83 ± 0.91	0.37 ± 0.33

Data presented as mean ± standard deviation (SD); n = 3.

## Water absorption ratio

The water absorption ratio is used to determine the amount of water absorbed by the tablet. The water absorption ratio of the RDTs was observed in the range from  $65 \pm 0.45\%$  to  $108.33 \pm 0.68\%$ . Formulated batches of tablets CPX<sub>4</sub>, CPX<sub>8</sub> and CPX<sub>9</sub> absorbed more than 90% of the water, while the other batches had less capacity to absorb water (Table 3). The results indicated that SSG and CP had higher water absorption ratios when compared to the CMS.

## Friability

The friability of the prepared tablets was found to be between  $0.26 \pm 0.21\%$  and  $0.86 \pm 0.40\%$ , which is within the acceptable limit of less than 1% (Table 3). The formulated tablets had good mechanical strength and can be handled without excessive care.

## X-ray diffraction

The tablets developed using the drug- $\beta$ -CD complex did not show many characteristic peaks of the pure drug, indicating a molecular dispersion of the drug within the polymer matrix in amorphous form (Fig. 6).

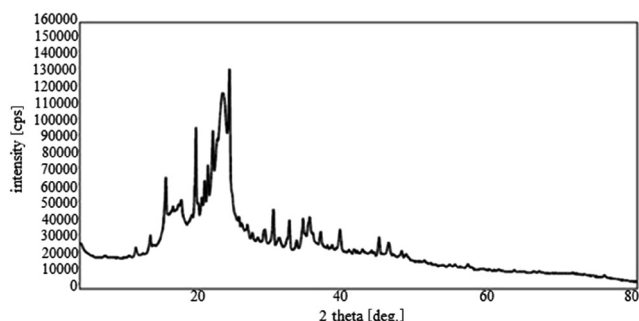


Fig. 6. X-ray diffraction patterns of best selected rapidly disintegrating tablet (RDT) (formulation CPX<sub>5</sub>)

## In vitro dissolution studies

Dissolution studies were conducted for all the formulations given in the USP dissolution apparatus II using phosphate buffer (pH 6.8). It had been observed from the drug release profile that >90% of the drug was released within 10 min; drug release profiles are shown in Fig. 7. As the concentration of superdisintegrants increases, the release of the drug also increases. The dissolution study results suggested that sodium starch glycolate acted as the best superdisintegrant among the investigated superdisintegrants.

From Table 4, it is evident that the drug release from the developed RDTs followed first order release kinetics.

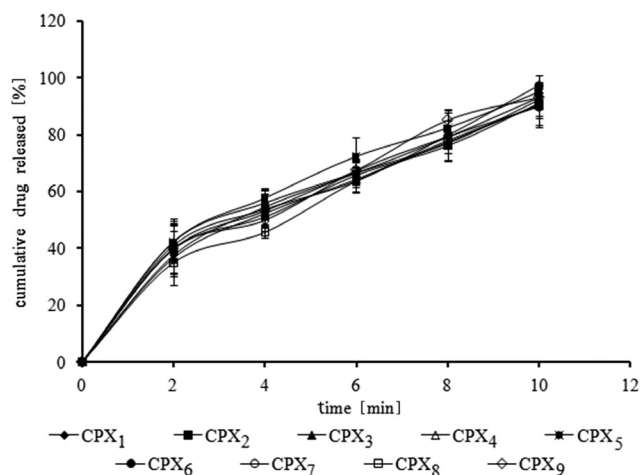


Fig. 7. In vitro release rate profile of levocetirizine from rapidly disintegrating tablets (RDTs) (formulation CPX<sub>1</sub>–CPX<sub>9</sub>) in phosphate buffer solution (pH 6.8) at  $37 \pm 0.2^\circ\text{C}$  (mean  $\pm$  standard deviation (SD),  $n = 3$ )

Table 4. Release kinetic data of formulation CPX<sub>1</sub>–CPX<sub>9</sub>

Formulation code	Zero order $r^2$	First order $r^2$
CPX <sub>1</sub>	0.923	0.926
CPX <sub>2</sub>	0.934	0.939
CPX <sub>3</sub>	0.944	0.960
CPX <sub>4</sub>	0.913	0.927
CPX <sub>5</sub>	0.919	0.935
CPX <sub>6</sub>	0.839	0.912
CPX <sub>7</sub>	0.933	0.971
CPX <sub>8</sub>	0.940	0.951
CPX <sub>9</sub>	0.939	0.958

## Conclusions

The prepared RDTs had ideal physical properties such as uniform weight, satisfactory hardness, better friability strength, less disintegration time, and rapid release profiles to be used as a RDDS for the anti-allergic drug. In vitro release of levocetirizine followed first order kinetics. The prepared tablets can be used in dysphagia conditions.

## References

- Comoglu T, Unal B. Preparation and evaluation of an orally fast disintegrating tablet formulation containing a hydrophobic drug. *Pharm Dev Technol.* 2015;20(1):60–64.
- Gohel M, Patel M, Amin A, Agrawal R, Dave R, Bariya N. Formulation design and optimization of mouth dissolve tablets of nimesulide using vacuum drying technique. *AAPS PharmSciTech.* 2004;5(3):e36.
- Awasthi R, Sharma S, Dua K, Kulkarni GT. Formulation of fast disintegrating drug delivery system. *J Chronother Drug Deliv.* 2013;4(1):15–18.
- Liang AC, Chen LH. Fast-dissolving intraoral drug delivery systems. *Expert Opin Ther Patents.* 2001;11(6):981–986.
- Morita Y, Tsusima Y, Yasui M, Termoz R, Ajioka J, Takayama K. Evaluation of disintegration time of rapidly disintegrating tablets via a novel method utilizing a CCD camera. *Chem Pharm Bull.* 2002;50(9):1181–1186.
- Fu Y, Yang S, Jeong SH, Kimura S, Park K. Orally fast disintegrating tablets. Developments technologies, taste-masking and clinical studies. *Crit Rev Ther Drug Carrier Syst.* 2004;21(6):433–475.

7. Bircan Y, Comoglu T. Formulation technologies of orally fast disintegrating tablets. *J Pharm Marmara Univ.* 2012;2(16):77–81.
8. Chang RK, Guo X, Burnside BA, Couch RA. Fast dissolving tablets. *Pharm Technol.* 2000;24:52–58.
9. Sharma D. Formulation development and evaluation of fast disintegrating tablets of salbutamol sulphate for respiratory disorders. *ISRN Pharm.* 2013;2013:674507.
10. Goel H, Rai P, Rana V, Tiwary AK. Orally disintegrating systems: Innovations in formulation and technology. *Recent Pat Drug Deliv Formul.* 2008;2(3):258–274.
11. Parkash V, Maan S, Deepika, Yadav SK, Hemlata, Jogpal V. Fast disintegrating tablets: Opportunity in drug delivery system. *J Adv Pharm Technol Res.* 2011;2(4):223–235.
12. Madan JR, Kamate VJ, Awasthi R, Dua K. Formulation, characterization and in-vitro evaluation of fast dissolving tablets containing gli-clazide hydrotropic solid dispersions. *Recent Pat Drug Deliv Formul.* 2017;11(2):147–154.
13. Cirri M, Rangoni C, Maestrelli F, Corti G, Mura P. Development of fast dissolving tablets of flurbiprofen–cyclodextrin complexes. *Drug Dev Ind Pharm.* 2005;31(7):697–707.
14. Dua K, Pabreja K, Ramana MV, Lather V. Dissolution behavior of  $\beta$ -cyclodextrin molecular inclusion complexes of aceclofenac. *J Pharm Bioallied Sci.* 2011;3(3):417–425.
15. Dua K, Ramana MV, Sara UV, et al. Investigation of enhancement of solubility of norfloxacin beta-cyclodextrin in presence of acidic solubilizing additives. *Curr Drug Deliv.* 2007;4(1):21–25.
16. Malipeddi VR, Dua K, Awasthi R. Development and characterization of solid dispersion-microsphere controlled release system for poorly water-soluble drug. *Drug Deliv Transl Res.* 2016;6(5):540–550.
17. Gorajana A, Rajendran A, Yew LM, Dua K. Preparation and characterization of cefuroxime axetil solid dispersions using hydrophilic carriers. *Int J Pharm Investig.* 2015;5(3):171–178.
18. Lyn LY, Sze HW, Rajendran A, Adinarayana G, Dua K, Garg S. Crystal modifications and dissolution rate of piroxicam. *Acta Pharm.* 2011;61(4):391–402.
19. Awasthi R, Kulkarni GT. Development and characterization of amoxicillin loaded floating microballoons for the treatment of *Helicobacter pylori* induced gastric ulcer. *Asian J Pharm Sci.* 2013;8:174–180.
20. Dhiman N, Awasthi R, Jindal S, Khatri S, Dua K. Development of bilayer tablets with modified release of selected incompatible drugs. *Polim Med.* 2016;46(1):5–15.
21. Comoglu T. Formulation and evaluation of carbamazepine fast disintegrating tablets. *Pharm Ind.* 2010;72(1):150–158.
22. Sunada H, Bi Y. Preparation, evaluation and optimization of rapidly disintegrating tablets. *Powder Technol.* 2002;122(2–3):188–198.
23. Lai F, Pini E, Angioni G, et al. Nanocrystals as tool to improve piroxicam dissolution rate in novel orally disintegrating tablets. *Eur J Pharm Biopharm.* 2011;79(3):552–558.
24. United States Pharmacopeia, 24<sup>th</sup> revision, Asian Edition. United States Pharmacopoeial Convention, Inc.: Rockville, MD; 2000.
25. Desai PM, Liew CV, Heng PW. Review of disintegrants and the disintegration phenomena. *J Pharm Sci.* 2016;105(9):2545–2555.



# Starch nanoparticles in drug delivery: A review

Michael Ayodele Odeniyi<sup>A–F</sup>, Omobolanle A. Omotoso<sup>B–D</sup>, Adewale O. Adepoju<sup>B–D</sup>, Kolawole T. Jaiyeoba<sup>E,F</sup>

Department of Pharmaceutics and Industrial Pharmacy, University of Ibadan, Nigeria

A – research concept and design; B – collection and/or assembly of data; C – data analysis and interpretation;  
D – writing the article; E – critical revision of the article; F – final approval of the article

Polymers in Medicine, ISSN 0370-0747 (print), ISSN 2451-2699 (online)

*Polim Med.* 2018;48(1):41–45

## Address for correspondence

Michael Ayodele Odeniyi  
E-mail: deleodeniya@gmail.com

## Funding sources

None declared

## Conflict of interest

None declared

Received on August 1, 2018

Reviewed on October 30, 2018

Accepted on November 26, 2018

## Abstract

The uptake and specificity of drugs and the bioavailability of poorly soluble drugs has been improved by means of targeted drug delivery using nanoparticles. Many platforms have been used for nanoparticulate drug delivery and these include liposomes, polymer conjugates, metallic nanoparticles, polymeric micelles, dendrimers, nanoshells, and protein and nucleic acid-based nanoparticles. Starch is the 2<sup>nd</sup> most abundant natural polymer and has found wide use in drug delivery systems as binder, disintegrant and filler. However, its application is limited by the poor functional properties of native starch. Starch nanocrystals of different shapes and sizes can be obtained based on the starch origin and isolation process involved. Nanocrystals with varying morphology have been reported; from nanocrystals of platelet-like shaped waxy maize starch with 5–7 nm thickness and 15–40 nm diameters, to those with round and grape-like shape from potato starch granules, with sizes ranging from 40 nm to 100 nm. This review describes different methods of obtaining starch nanoparticles, their modification and application in drug delivery.

**Key words:** drug delivery, starch modification, starch nanoparticles

## Cite as

Odeniyi MA, Omotoso OA, Adepoju OA, Jaiyeoba KT.  
Starch nanoparticles in drug delivery: A review.  
*Polim Med.* 2018;48(1):41–45. doi:10.17219/pim/99993

## DOI

10.17219/pim/99993

## Copyright

© 2018 by Wrocław Medical University  
This is an article distributed under the terms of the  
Creative Commons Attribution Non-Commercial License  
(<http://creativecommons.org/licenses/by-nc-nd/4.0/>)

## Introduction

Nanoparticles, with a dimension range of 1–100 nm, are used as drug delivery systems.<sup>1,2</sup> They are able to deliver a large quantity of substances to various sites of the body and for a longer time. In nanoparticle-based drug delivery, the most critical factors are particle size, particle surface properties, and the release of drugs or the active ingredients.<sup>3,4</sup> The uptake and specificity of drugs and the bioavailability of poorly soluble drugs has been improved by means of targeted drug delivery using nanoparticles.<sup>5,6</sup> Several platforms have been used for nanoparticulate drug delivery. These include liposomes, polymer conjugates, metallic nanoparticles, polymeric micelles, dendrimers, nanoshells, and protein and nucleic acid-based nanoparticles.<sup>7–9</sup> This review examines the use of starch nanoparticles in drug delivery, the effect of different methods of nanoparticle preparation and the effect of physical and chemical modifications of various starches on their functional properties and their potential for use as excipients in drug delivery.

## Starch

Starch is one of the most abundant biomass materials in nature.<sup>10</sup> Many plants store starch as a source of energy, as a natural, biocompatible, renewable, and biodegradable polymer. Starch is obtained from various classes of plants such as cereals or grains, roots, tubers, legumes, and fruits. Cereals have the highest percentage of starch.<sup>11</sup> Plant cells synthesize starch in 2 forms of polymers: amylopectin and amylose. Amylopectin is made of linear chains of glucose units linked by  $\alpha$ -1,4 glycosidic bonds. It is highly branched at the  $\alpha$ -1,6 positions by small glucose chains at intervals of 10 nm along the molecule's axis and represents between 70% and 85% of common starch.<sup>12</sup> Amylose is a linear chain of  $\alpha$ -1,4 glucans with partial branching points at the  $\alpha$ -1,6 positions and constitutes 15–30% of common starch. Wet grinding, sieving and drying are major ways of extracting and refining starch in the industry. It can be utilized in the natural form after extraction from plant "native starch" or undergo 1 or more modifications (physical, mechanical and/or chemical) to achieve targeted properties and become "modified starch".

## Starch nanoparticles

Several components such as quantum dots, liposomes, starch, and other newly developed materials were used in the development of nanoparticle-based delivery systems.<sup>13–21</sup> Nanoparticles,<sup>22</sup> nanocolloids<sup>23</sup> and nanocrystals<sup>24</sup> have been prepared from starches.

Starch nanocrystals are derived from starch granule crystallites as a result of disrupting the semicrystalline structure of granules at temperatures below gelatinization

temperature.<sup>25</sup> Starch nanocrystals are also called starch crystallite, starch microcrystalline and hydrolyzed starch. It is important to note that starch nanocrystals are different from starch nanoparticles, which can be amorphous. While starch crystallite develops as a result of the disruption of non-crystalline domains from semi-crystalline granules by acid hydrolysis, starch nanoparticles are generated from congealed starch.<sup>26</sup>

Both the crystalline and non-crystalline regions coexist in the structure of the native starch but it is noteworthy to underscore the responsibility of the amylopectin chains in the formation of the crystalline regions due to the stacking of the nanometric sub-units of the amylopectin chain blocks, which eventually form the starch nanocrystals.<sup>27</sup> As the native starch is subjected to acid hydrolysis, the starch granule begins to dissolve at the regions of low lateral order non-crystalline phases (amylose region), while changes do not occur at the highly crystalline water-insoluble lamellae.<sup>28</sup>

Le Corre et al.<sup>29</sup> established that starches of the same amylose content but different botanical sources, e.g., maize, potato and wheat starches, show similar crystal size. However, differences in size were more pronounced with starches of the same botanical source but with different amylose content. This underlines the strong influence of the composition and molecular structure on the resulting crystallite dimensions that can be obtained when preparing starch nanocrystals. Low hydrolysis temperature ranging usually between 35°C and 45°C has been reported and is required to block starch congealing and consequent disruption of the starch crystalline structure.<sup>30</sup>

Starch nanocrystals of different shapes and sizes can be obtained depending on the starch origin and isolation process involved. Though the shape and size of the granules may vary between starches, there may be no discernable difference in the shape of starch nanocrystals from different sources.<sup>31</sup> Xu et al.<sup>24</sup> found that the structure and morphology of obtained nanocrystals are influenced by several factors, such as the type of crystalline, amylose relative portion, amylopectin, botanical origin, and morphology of starch granule.

Nanocrystals with varying morphology and size have been reported. These include nanocrystals from platelet-like shaped waxy maize starch with 5–7 nm thickness and 15–40 nm diameter,<sup>32</sup> to those from potato starch granules with round and grape-like shape, with sizes ranging from 40 nm to 100 nm observed under transmission electron microscope (TEM).<sup>33</sup>

## Preparation protocols for starch nanocrystals

Three different methods are used to prepare starch nanocrystals and other nanoparticles: acid or enzymatic hydrolysis, regeneration and mechanical treatment.<sup>34</sup> Different protocols for the preparation of nanocrystals from

starches are employed with their attending challenges, chief of which is low or limited percent yield even after prolonged (days) acid hydrolysis. Another challenge is related to the onion-like structure of starch which hinders its hydrolysis.<sup>31</sup>

## Acid hydrolysis kinetic

Starch is hydrolyzed using either dilute HCl or dilute H<sub>2</sub>SO<sub>4</sub> at 25–55°C for different durations to manufacture acid-thinned starches, microcrystalline starch or starch nanocrystals.<sup>35,36</sup> All types of starch experience a 2-stage hydrolysis profile, comprising an initial fast hydrolysis step, presumably due to the hydrolysis of the non-crystalline regions of starch granules, and a 2<sup>nd</sup> slower step, presumably due to the hydrolysis of the crystalline regions.<sup>37</sup> The dense packing of the starch in the crystalline region, which does not allow for the penetration of H<sub>3</sub>O<sup>+</sup>A, leads to the slower hydrolysis rate of the crystalline region.<sup>36</sup>

A theory suggested that the dense packing of the starch in the crystalline region which does not allow for the penetration of H<sub>3</sub>O<sup>+</sup>A led to the slower hydrolysis rate of the crystalline region.<sup>36</sup> The other theory is based on the hydrolysis of the glycosidic bonds requiring a change or transformation from the chair to half-chair conformation which is required for hydrolysis of the bonds. This is an action that occurs slowly due to immobilization of the sugars in the starch crystallites.<sup>38,39</sup>

Some major factors affecting acid hydrolysis kinetics include time, acid type, acid concentration, and temperature.<sup>22</sup> The rate of hydrolysis increases at a constant temperature of 50°C with increasing acid concentration.<sup>39</sup> Another study assumed that the optimum temperature and acid concentration for starch nanocrystal production should be 40°C and 3.16M, respectively.<sup>35</sup>

Acid concentration, extent of hydrolysis<sup>40</sup> and the separation technique used have all been implicated in the low yield of nanocrystals from acid hydrolysis of starches.<sup>22,37,40</sup> Le Corre et al.<sup>40</sup> showed that starch nanocrystals are mixed with other microparticles and some nanocrystals were converted to sugar at the end of the production process. This fact results in the observed low yields. They suggested that the amount of starch nanocrystals in the final suspension may depend on the extent of hydrolysis. The study concluded that during the course of hydrolysis both micro- and nanoscale particles are present in the system. Also, differential centrifugation was not suitable for fractionation due to hydrogen bonding and different densities within starch granules. A continuous extraction technique such as microfiltration was suggested as the appropriate separation technique.<sup>40</sup>

A dispersion of uniform starch nanocrystals was obtained using another technique which combined hydrolysis process with ultrasonication.<sup>41</sup> Breaking up the aggregates of nanoparticles formed through hydrogen

bonds was observed to be effective by ultrasonic treatment at 60% vibration amplitude for 3 min. However, the starch nanocrystals treated by ultrasonication may have decreased crystallinity.

An innovative solution to address the limitations of the current processes for generating starch nanocrystals was developed by Le Corre et al.<sup>42</sup> It involved the use of a microfiltration unit equipped with ceramic membranes for the filtration of hydrolysates obtained from wheat starch. Microfiltration limited the conversion of starch nanocrystals into oligo- or monosaccharides. During the 1<sup>st</sup> day of hydrolysis, the nanoparticles produced were more crystalline and mostly B-type particles. The critical factor in the development of nanocrystals from starch is to maintain the crystalline structure of the starch while completely removing the non-crystalline region of starch granules.

Practical application of SNCs acquired using the usual acid hydrolysis method is limited because the conventional preparation method is time-consuming and results in low yield. Ball milling is a cheap and environment-friendly physical processing method that has been confirmed capable of changing properties of starch.

## Enzymatic hydrolysis method

This method involves the use of enzymes, such as  $\alpha$ -amylase, as a pretreatment to boost the efficiency of preparation. Starch nanocrystals were prepared from waxy rice starch with average diameters of 500 nm using selective enzymatic hydrolysis.<sup>42</sup> Recent developments are now focused on this method with an aim to mitigate the limitations of acid hydrolysis of starches in the preparation of starch nanocrystals.

Enzyme treatment before acid hydrolysis has been proposed to in order decrease the duration of starch nanocrystals preparation.<sup>34</sup> Studies have shown that nanocrystals with platelet-like structure and length of 20–40 nm with a thickness of 4–7 nm were produced using this method.<sup>43</sup>

## Regeneration method

Starch nanoparticles have been obtained from starch solutions using precipitation with organic solvents. Ethanol was used to precipitate starch nanoparticles in the range of 50–100 nm from pre-cooked native starch.<sup>44</sup>

## Mechanical treatment method

Mechanical and thermal treatment of starch granules can be used to generate starch nanoparticles. A simplified technique involving high-pressure homogenization method was proposed.<sup>23</sup> A specially designed microfluidizer was used through which a 5% starch slurry was

passed several times under high shear pressure. Starch particles of sizes reduced into the range between 3–6  $\mu\text{m}$  and 10–20 nm were obtained after 20 passes.

By combining a high-pressure homogenization technique with mini-emulsion cross-linking, sodium trimetaphosphate cross-linked starch nanoparticles were produced.<sup>44</sup> This method is environment-friendly because the mechanical treatment procedure is carried out within a water system. However, the efficiency process is limited as only low concentration starch slurry can be use processed for homogenization, thereby giving a relatively low yield.

## Common modifications to starch and starch nanoparticles

Starch has limited application in industry because of poor solubility and high viscosity. Improvement in certain properties and the addition of more functional groups to starch is possible using chemical modifications. Glucose units making up the chain provide sites to be modified with multifunctional groups due to the abundant hydroxyl groups. Improvement of specific functions of the polymer and consequent applications of starch nanocrystals is the main objective of chemical modification. Three approaches have been commonly used for starch nanocrystals modification. These include modification with chemical reaction with small molecules, grafting onto polymer chains with coupling agents and grafting from polymer chains with polymerization of a monomer.<sup>45</sup>

Elemental analysis, infrared spectroscopy analysis (FTIR) and X-ray photoelectron spectrometry (XPS) can be used to prove that modification occurred. Monitoring changes in the morphology and size, solubility or polarity, surface properties, and thermal properties can also be used to determine the effects of chemical modification of starch nanocrystals. The integrity of the starch nanocrystal crystalline structure must be intact regardless of the modification method used.

## Conclusions

There is an increased interest in applications of starch nanocrystal and nanoparticle derivatives as drug delivery platforms due to their biocompatibility, improved mechanical properties, thermal properties, barrier properties, absorption properties, and ability to be modified for specific functional properties.

### References

- Soppimath KS, Aminabhavi TM, Kulkarni AR, Rudzinski WE. Biodegradable polymeric nanoparticles as drug delivery devices. *J Control Release*. 2001;70(1–2):1–20.
- Mohanraj VJ, Chen Y. Nanoparticles: A review. *Trop J Pharm Res*. 2006;5:561–573.
- Vila A, Sanchez A, Tobio M, Calvo P, Alonso MJ. Design of biodegradable particles for protein delivery. *J Control Release*. 2002;78(1–3):15–24.
- Mu L, Feng SS. A novel controlled release formulation for the anti-cancer drug paclitaxel (Taxol®): PLGA nanoparticles containing vitamin E TPGS. *J Control Release*. 2003;86(1):33–48.
- Ould-Ouali L, Noppe M, Langlois X, et al. Self-assembling PEG-p(CL-co-TMC) copolymers for oral delivery of poorly water-soluble drugs: A case study with risperidone. *J Control Release*. 2005;102(3):657–668.
- Kipp JE. The role of solid nanoparticle technology in the parenteral delivery of poorly water-soluble drugs. *Int J Pharm*. 2004;284(1–2):109–122.
- Pathak Y, Thassu D. *Drug Delivery Nanoparticles Formulation and Characterization*. Rijeka, Croatia: PharmaceuTech Inc.; 2009:1–393.
- Zhang L, Gu FX, Chan JM, Wang AZ, Langer RS, Farokhzad OC. Nanoparticles in medicine: Therapeutic applications and developments. *Clin Pharmacol Ther*. 2008;83(5):761–769.
- Davis ME, Chen ZG, Shin DM. Nanoparticle therapeutics: An emerging treatment modality for cancer. *Nat Rev Drug Discov*. 2008;7(9):771–782.
- Smith AM. The biosynthesis of starch granules. *Biomacromolecules*. 2001;2(2):335–341.
- Santana AL, Meireles MAA. New starches are the trend for industry applications: A review. *Food Public Health*. 2014;4:229–241.
- Durrani CM, Donald AM. Physical characterization of amylopectin gels. *Polymer Gels Networks*. 1995;3(1):1–27.
- Baptista PV. Cancer nanotechnology: Prospects for cancer diagnostics and therapy. *Curr Cancer Ther Rev*. 2009;4(5):80–88.
- Kim JY, Lim ST. Preparation of nano-sized starch particles by complex formation with *n*-butanol. *Carbohydr Polym*. 2009;76:110–116.
- Riehemann K, Schneider SW, Luger TA, Godin B, Ferrari M, Fuchs H. Nanomedicine – challenge and perspectives. *Angew Chem Int Ed Engl*. 2009;48(5):872–897.
- Petros RA, DeSimone JM. Strategies in the design of nanoparticles for therapeutic applications. *Nat Rev Drug Discov*. 2010;9(8):615–627.
- Bae KH, Chung HJ, Park TG. Nanomaterials for cancer therapy and imaging. *Mol Cells*. 2011;31(4):295–302.
- Taylor A, Wilson KM, Murray P, Fernig DG, Levy R. Long-term tracking of cells using inorganic nanoparticles as contrast agents: Are we there yet? *Chem Soc Rev*. 2012;41(7):2707–2717.
- Villalonga-Barber C, Micha-Screttas M, Steele BR, Georgopoulos A, Demetzos C. Dendrimers as biopharmaceuticals: Synthesis and properties. *Curr Top Med Chem*. 2008;8(14):1294–1309.
- Clift MJ, Stone V. Quantum dots: An insight and perspective of their biological interaction and how this relates to their relevance for clinical use. *Theragnostic*. 2012;2(7):668–680.
- Yamashita T, Yamashita K, Nabeshi H, et al. Carbon nanomaterials: Efficacy and safety for nanomedicine. *Materials (Basel)*. 2012;5(2):350–363.
- Singh V, Ali SZ. Properties of starches modified by different acids. *Int J Food Properties*. 2008;11:495–507.
- Liu D, Wu, Q, Chen H, Chang PR. Transitional properties of starch colloid with particle size reduction from micro to nanometer. *J Colloid Interface Sci*. 2009;339(1):117–124.
- Xu Y, Ding W, Liu J, et al. Preparation and characterization of organic-soluble acetylated starch nanocrystals. *Carbohydr Polym*. 2010;80:1078–1084.
- Dufresne A. Processing of polymer nanocomposites reinforced with polysaccharide nanocrystals. *Molecules*. 2010;15(6):4111–4128.
- Le Corre D, Bras J, Dufresne A. Starch nanoparticles: A review. *Biomacromolecules*. 2010;11(5):1139–1153.
- Gallant DJ, Bouchet B, Baldwin PM. Microscopy of starch: Evidence of a new level of granule organization. *Carbohydr Polym*. 1997;32:177–191.
- Song S, Wang C, Pan Z, Wang X. Preparation and characterization of amphiphilic starch nanocrystals. *J Appl Polym Sci*. 2008;107(1):418–422.
- Le Corre D, Bras J, Dufresne A. Influence of botanic origin and amylose content on the morphology of starch nanocrystals. *J Nanopart Res*. 2011;13:7193–7208.
- Lin N, Huang J, Chang PR, Anderson DP, Yu JJ. Preparation, modification and application of starch nanocrystals in nanomaterials: A review. *Nanomater*. 2011. doi:10.1155/2011/573687

31. Ghasemlou M, Taghi Gharibzhehedi SM, Cran MJ. Preparation and characterization of starch nanocrystals. In: *Starch-Based Blends, Composites and Nanocomposites*. Visakh PM, Yu L, eds. London, UK: The Royal Society of Chemistry; 2016:60–108.
32. Putaux JL, Molina-Boisseau S, Momaur T, Dufresne A. Platelet nanocrystals resulting from the disruption of waxy maize starch granules by acid hydrolysis. *Biomacromolecules*. 2003;4(5):1198–1202.
33. Chen G, Wei M, Chen J, Huang J, Dufresne A, Chang PR. Simultaneous reinforcing and toughening: New nanocomposites of waterborne polyurethane filled with low loading level of starch nanocrystals. *Polymer*. 2008;49(7):1860–1870.
34. Le Corre D, Vahanian E, Dufresne A. Enzymatic pretreatment for preparing starch nanocrystals. *Biomacromolecules*. 2012;13(1):132–137.
35. Angellier H, Choïnard L, Molina-Boisseau S, Ozil P, Dufresne A. Optimization of the preparation of aqueous suspensions of waxy maize starch nanocrystals using a response surface methodology. *Biomacromolecules*. 2004;5(4):1545–1551.
36. Li W, Corke H, Beta T. Kinetics of hydrolysis and changes in amylose content during preparation of microcrystalline starch from high-amylose maize starches. *Carbohydr Polym*. 2007;69:398–405.
37. Biliaderis CG, Grant DR, Vose JR. Structural characterization of legume starches I. Studies on amylose, amylopectin, and beta-limit dextrins. *Cereal Chem*. 1981;58:496–502.
38. Whistler RL, BeMiller JN. *Carbohydrate Chemistry for Food Scientists*. St. Paul, MN: American Association of Cereal Chemists; 1997:1–140.
39. Wang Y-J, Truong V-D, Wang L. Structures and rheological properties of corn starch as affected by acid hydrolysis. *Carbohydr Polym*. 2003;52:327–333.
40. Le Corre D, Bras J, Dufresne A. Evidence of micro- and nanoscaled particles during starch nanocrystals preparation and their isolation. *Biomacromolecules*. 2011;8(12):3039–3046.
41. Kim HY, Lee JH, Kim JY, Lim WJ, Lim ST. Characterization of nanoparticles prepared by acid hydrolysis of various starches. *Starch/Starke*. 2012;64:367–373.
42. Le Corre D, Bras J, Dufresne A. Ceramic membrane filtration for isolating starch nanocrystals. *Carbohydr Polym*. 2011;86:1565–1572.
43. Dufresne A. Polysaccharide nanocrystals reinforced nanocomposites. *Can J Chem*. 2008;86(6):484–494.
44. Ma X, Jian R, Chang PR, Yu J. Fabrication and characterization of citric acid-modified starch nanoparticles/plasticized-starch composites. *Biomacromolecules*. 2008;9(11):3314–3320.
44. Shi AM, Li D, Wang LJ, Li BZ, Adhikari B. Preparation of starch-based nanoparticles through high-pressure homogenization and miniemulsion cross-linking: Influence of various process parameters on particle size and stability. *Carbohydr Polym*. 2011;83:1604–1610.
45. Angellier H, Putaux J-L, Molina-Boisseau S, Dupeyre D, Dufresne A. Starch nanocrystal fillers in an acrylic polymer matrix. *Macromolecular Symposia*. 2005;221:95–104.



# Ocena bezpieczeństwa collamerowych wszczepów fakijnych w korekcji wad wzroku

## Safety assessment of using collamer phakic implants in the correction of refractive errors

Krystyna Grzebieluch-Reichert<sup>1,A–F</sup>, Jarosław Marek<sup>1,A,E,F</sup>, Marta Misiuk-Hojoła<sup>2,E,F</sup>

<sup>1</sup> Ośrodek Okulistyki Klinicznej Spektrum, Wrocław, Polska

<sup>2</sup> Katedra i Klinika Okulistyki, Wydział Lekarski Kształcenia Podyplomowego, Uniwersytet Medyczny we Wrocławiu, Polska

A – koncepcja i projekt badania, B – gromadzenie i/lub zestawianie danych, C – analiza i interpretacja danych, D – napisanie artykułu, E – krytyczne zrecenzowanie artykułu, F – zatwierdzenie ostatecznej wersji artykułu

Polymers in Medicine, ISSN 0370-0747 (print), ISSN 2451-2699 (online)

Polim Med. 2018;48(1):47–51

### Adres do korespondencji

Krystyna Grzebieluch-Reichert  
E-mail: kgrzebieluch@wp.pl

### Źródła finansowania

Brak

### Konflikt interesów

Nie występuje

Praca wpłynęła do Redakcji: 4.01.2019 r.

Po recenzji: 14.01.2019 r.

Zaakceptowano do druku: 14.01.2019 r.

### Streszczenie

**Wprowadzenie.** Coraz więcej pacjentów z refrakcyjnymi wadami wzroku, u których korekcja okularowa lub soczewkami kontaktowymi jest niewystarczająca, rozważa zabieg chirurgii refrakcyjnej. Dla pacjentów niekwalifikujących się do korekcji laserowej alternatywą są wszczepy fakijne.

**Cel pracy.** Celem pracy jest ocena bezpieczeństwa stosowania collamerowych wszczepów fakijnych w korekcji wad wzroku podczas rocznej obserwacji.

**Materiał i metody.** Zbadano 24 oczu 12 pacjentów, którym w celu korekcji krótkowzroczności wszczepiono soczewki fakijne tylnokomorowe Visian ICL. Przed zabiegiem wykonano refraktometrię obiektywną, ocenę ostrości do dali z najlepszą korekcją, pomiar ciśnienia wewnątrzgałkowego, ocenę śródbłonna, topografię rogówki oraz pomiar głębokości komory przedniej. Końcowe badanie obejmowało ostrość widzenia, refrakcję, ciśnienie wewnątrzgałkowe, położenie wszczepu, mikroskopię śródbłonna oraz badanie dna oka.

**Wyniki.** Średnia refrakcja obiektywna przed operacją wynosiła: sfera  $-7,77 \pm 3,55$  dioptrii, a cylinder  $1,18 \pm 0,87$  dioptrii. Korekcją okularową uzyskiwano średnią ostrość  $0,91 \pm 0,20$  (tablica Snellena). W okresie rocznej obserwacji średnia moc sfery wyniosła  $0,475 \pm 0,390$  dioptrii, cylinder  $0,46 \pm 0,27$  dioptrii, a ostrość widzenia po zabiegu  $1,05 \pm 0,22$  (tablica Snellena). Porównanie wyników w ocenie 12-miesięcznej wykazało istotnie statystycznie większą poprawę po zastosowaniu soczewki fakijnej w stosunku do korekcji okularowej ( $p < 0,05$ ). Nie wykazano istotnych różnic w gęstości komórek śródbłonna w ocenie przed zabiegiem i po nim ( $p < 0,05$ ). Zarówno w trakcie leczenia, jak i całego okresu obserwacji nie stwierdzono powikłań pooperacyjnych.

**Wnioski.** Ocena bezpieczeństwa prawidłowo wszczepionych soczewek fakijnych ICL wskazuje na dobrą tolerancję implantu collamerowego w komorze tylnej. Implant nie wykazuje negatywnego wpływu na struktury przedniego odcinka, ze szczególnym uwzględnieniem śródbłonna rogówki i soczewki. Ostrość wzroku skorygowana metodą soczewki ICL nie ustępuje ostrości skorygowanej okularami, a w wielu przypadkach może być lepsza. Collamerowe wszczepy fakijne ICL mogą być stosowane jako alternatywa dla soczewek kontaktowych oraz refrakcyjnej wymiany przeziernicy soczewki.

**Słowa kluczowe:** krótkowzroczność, collamer, soczewka fakijna

### Cytowanie

Grzebieluch-Reichert K, Marek J, Misiuk-Hojoła M.  
Ocena bezpieczeństwa collamerowych wszczepów fakijnych w korekcji wad wzroku. *Polim Med.* 2018;48(1):47–51.  
doi:10.17219/pim/102975

### DOI

10.17219/pim/102975

### Copyright

© 2019 by Wrocław Medical University  
This is an article distributed under the terms of the  
Creative Commons Attribution Non-Commercial License  
(<http://creativecommons.org/licenses/by-nc-nd/4.0/>)

## Abstract

**Background.** An increasing number of patients with refractive visual impairments, in whom the correction using spectacles or contact lenses does not meet expectations, consider the possibility of undergoing refractive surgery. Phakic implants are an alternative for patients who are not eligible for laser correction.

**Objectives.** The aim of the study is to assess the safety of using collamer phakic implants in the correction of vision defects during the annual follow-up.

**Material and methods.** The study included 24 eyes in 12 patients who were implanted with Visian ICL phakic posterior chamber lenses in order to correct myopia. The examinations carried out before the surgery were as follows: objective refractometry, the assessment of distant visual acuity with the best correction, intraocular pressure measurement, evaluation of the endothelium, corneal topography, and depth of the anterior chamber measurement. The final examinations included visual acuity, refraction, intraocular pressure, implant placement, endothelial microscopy, and funduscopy examination.

**Results.** Mean objective refraction was: sphere  $-7.77 \pm 3.55$  diopters and cylinder  $1.18 \pm 0.87$  diopters. Spectacle correction produced the mean visual acuity of  $0.91 \pm 0.20$  (Snellen). During the period of 1-year follow-up, the mean spherical power was  $0.475 \pm 0.39$  diopters, cylinder  $0.46 \pm 0.27$  diopters and the visual acuity after the procedure  $1.05 \pm 0.22$  (Snellen). The results of the 12-month evaluation showed a statistically significant greater improvement in patients using phakic implants compared to those subjected to spectacle correction ( $p < 0.05$ ). The pre- and post-operative evaluation demonstrated no significant differences in endothelial cell density ( $p < 0.05$ ). No complications were reported both during the surgery and the entire follow-up period.

**Conclusions.** The results of the safety assessment of using properly implanted ICL phakic lenses show good tolerance of collamer implants in the posterior chamber. They do not have a negative effect on the structures located in the anterior segment of the eye, including the corneal endothelium and the lens.

**Key words:** myopia, collamer, phakic lens

## Wprowadzenie

Coraz większa liczba pacjentów z refrakcyjnymi wadami wzroku, u których korekcja okularowa lub soczewkami kontaktowymi jest niewystarczająca bądź nie jest możliwa ze względów zawodowych, rozważa zabieg chirurgii refrakcyjnej.<sup>1</sup> Dla osób niekwalifikujących się do korekcji laserowej z powodu zbyt dużej wady i cienkiej rogówki alternatywą są wszczepy fakijne. Ich ogromną zaletą jest odwracalność procedury (możliwość usunięcia z oka).<sup>2</sup> Wszczepy fakijne umożliwiają skorygowanie krótkowzroczności, nadwzroczności i astygmatyzmu przy zachowaniu własnej akomodującej soczewki.<sup>3</sup> Wcześniej stosowano wszczepy przedniokomorowe, które ze względu na możliwość negatywnego wpływu na śródbłonek rogówki zostały wycofane.

Soczewki fakijne tylnokomorowe ICL (ang. *implantable collamer lens*) są wszczepiane na całym świecie od ponad 20 lat,<sup>1</sup> w Polsce stosuje się je dopiero od paru lat.

Wszczepy tylnokomorowe Visian ICL (STAAR Surgical AG) są zbudowane z biokompatybilnego collameru. W skład collameru wchodzi kolagen, kopolimer poli-HEMA i chromofor benzofenon. Collamer jest hydrofilny, charakteryzuje się 40% zawartością wody. Współczynnik refrakcji wynosi 1,44. Soczewki wykonane z collameru są wysoce biozgodne, głównie za sprawą dodatku kolagenu. Kolagen przyciąga naturalnie występującą w oku fibronektynę, która tworzy ochronną warstwę wokół soczewki.<sup>4</sup>

Soczewki ICL były wielokrotnie modyfikowane w celu zwiększenia bezpieczeństwa ich stosowania oraz poprawy właściwości optycznych. Podczas wszczepiania

poprzednich modeli należało wykonać irydotomię laserową, aby zapobiec wzrostowi ciśnienia wewnątrzgałkowego oraz powstaniu bloku źrenicznego. Ponadto istniało ryzyko powstania zaćmy przedniej podtorebkowej w wyniku kontaktu wszczepu z soczewką własną z powodu zbyt małej odległości między nimi (ang. *vault*) powodującej zaburzenie przepływu cieczy wodnistej.<sup>5</sup> Przełomową modyfikacją jest centralny otwór 0,36 mm KS-Aquaport w modelu V4 Visian ICL (STAAR Surgical AG), który umożliwia przepływ cieczy wodnistej do komory przedniej przez źrenicę. Zmiana w budowie wyeliminowała konieczność wykonania irydotomii laserowej oraz zmniejszyła ryzyko jaskry wtórnej związanej z blokiem źrenicznym.<sup>6</sup>

Metoda korekcji wady z użyciem soczewek Visian ICL znajduje zastosowanie u pacjentów w przypadku: krótkowzroczności od  $-0,5$  do  $-20$  dioptrii, nadwzroczności od  $+0,5$  do  $+10$  dioptrii, astygmatyzmu do 6 dioptrii.<sup>7,8</sup> Przeciwwskazania okulistyczne do zabiegu obejmują: jaskrę, patologie płamki, dystrofię rogówki, anomalie tęczówki, retinopatię cukrzycową, odwarstwienie siatkówki lub stan po leczeniu odwarstwienia, przewlekłe lub nawracające zapalenie błony naczyniowej. Wszczepienia ICL nie powinno się przeprowadzać, gdy gęstość komórek śródbłonna wynosi  $<2000 \text{ mm}^2$ , głębokość komory przedniej to  $<2,8 \text{ mm}$ , a także przy braku stabilności wady. Ogólne przeciwwskazania to: cukrzyca, choroby endokrynologiczne, kolagenozy oraz choroby nowotworowe.<sup>9,10</sup>

Celem pracy była ocena bezpieczeństwa stosowania collamerowych soczewek fakijnych tylnokomorowych, które zostały prawidłowo wszczepione, zgodnie z zalecanymi kryteriami kwalifikacji.



## Materiał i metody

Badania przeprowadzono zgodnie z zasadami i wytycznymi *Deklaracji helsińskiej*. Przed przystąpieniem do badań wszyscy pacjenci zostali poinformowani o celu i sposobie badania oraz podpisali świadomą zgodę na zabieg.

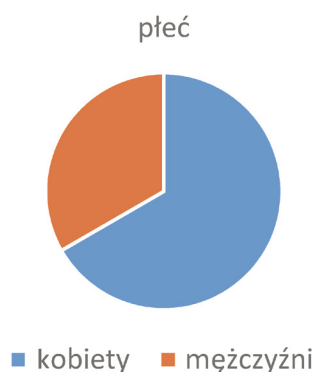
Zabiegi zostały przeprowadzone w latach 2015–2017 w Ośrodku Okulistyki Klinicznej Spektrum we Wrocławiu.

Badania miały charakter retrospektywnych badań obserwacyjnych (badania kohortowe).

Do badania kwalifikowano pacjentów, którym wszczepiono soczewki faliżne tylnokomorowe Visian ICL w latach 2015–2017, a okres obserwacji był nie krótszy niż rok. Przeanalizowano dokumentację 24 oczu 12 pacjentów spełniających kryteria włączenia, czyli: krótkowzroczność od  $-3$  do  $-16$  dioptrii i astygmatyzm krótkowzroczny od  $-0,5$  do  $-3,0$  dioptrii, wiek 19–39 lat, badanie kontrolne po upływie roku. Przebadano 8 kobiet i 4 mężczyzn (ryc. 1; średni wiek: 26,8 roku  $\pm 6,12$  roku). Przed zabiegiem wykonywano refraktometrię obiektywną (autorefraktometr Topcon TRK-2P), ocenę ostrości do dali z najlepszą korekcją BCDVA (ang. *best corrected distance visual acuity*) za pomocą standardowych tablic Snellena z odległości 5 m, wynik podano w skali dziesiętnej, wykonano pomiar gęstości śródbłonna (aparat Topcon), topografię rogówki (Tommy Version 4.2 F TMS-4), zmierzono głębokość komory przedniej Visiante OCT Zeiss. Moc wszczepu obliczono za pomocą oprogramowania dostarczonego przez producenta. Zabieg został wykonany w znieczuleniu miejscowym przez cięcie w przezroczystej rogówce.

Operacja drugiego oka odbyła się po 7–21 dniach od pierwszego zabiegu. Pierwsze badanie kontrolne odbyło się dzień po zabiegu, następnie: po tygodniu, po miesiącu, po 3, 6 i 12 miesiącach od operacji. Sprawdzano ostrość widzenia, ciśnienie śródgałkowe, refrakcję, oceniano w lampie szczelinowej przedni odcinek, położenie wszczepu w stosunku do własnej soczewki (ang. *vault*), mikroskopię śródbłonna oraz dno oka.

Analiza statystyczna została wykonana przy wykorzystaniu programu TIBCO Statistica (TIBCO Software Inc., Palo Alto, USA) i Microsoft Excel z pakietu Micro-



Ryc. 1. Płeć chorych  
Fig. 1. Patients' sex

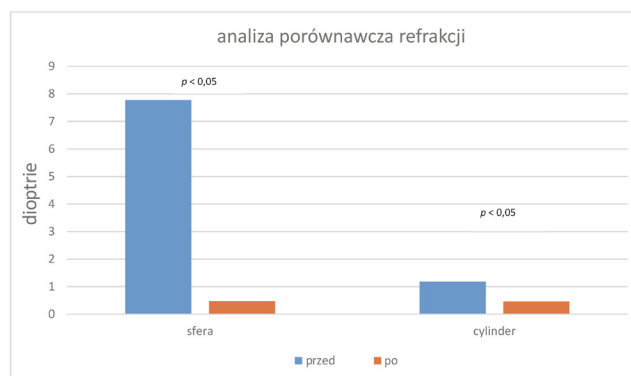
soft Office 365 Personal (Microsoft Corporation, Redmond, USA).

Obliczono średnią arytmetyczną i odchylenie standardowe dla następujących badanych parametrów: sfera, cylinder, ostrość wzroku. Wykonano test Shapiro–Wilka dla zbadania normalności rozkładu analizowanych parametrów. W porównaniu pomiędzy oczami u tego samego pacjenta wykorzystano parametryczny test *t* Studenta dla grup zależnych. W porównaniu pomiędzy badanymi grupami wykorzystano parametryczny test *t* Studenta dla grup niezależnych. Poziom istotności statystycznej oznaczono jako  $p < 0,05$ .

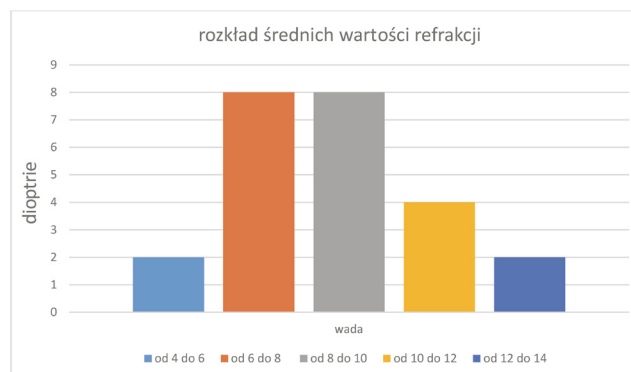
## Wyniki

Średnia refrakcja obiektywna przedoperacyjna wynosiła: sfera  $-7,77 \pm 3,55$  dioptrii; cylinder  $1,18 \pm 0,87$  dioptrii (ryc. 2). Największa grupa pacjentów miała wadę pomiędzy 6 a 8 dioptrii (ryc. 3). Korekcją okularową uzyskiwano średnią ostrość  $0,91 \pm 0,20$  (tablica Snellena). W okresie rocznej obserwacji średnia moc sfery wyniosła  $0,475 \pm 0,39$  dioptrii, cylinder  $0,46 \pm 0,27$  dioptrii, ostrość po zabiegu  $1,05 \pm 0,22$  (tablica Snellena) (ryc. 2).

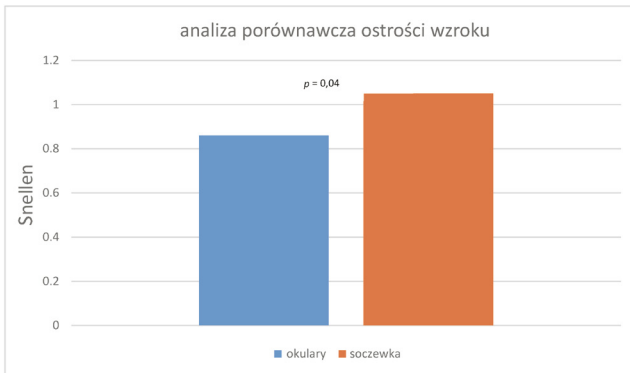
Porównanie wyników w ocenie 12-miesięcznej wykazało istotnie statystycznie większą poprawę po zastosowaniu soczewki faliżnej w stosunku do korekcji okularowej ( $p < 0,05$ ; ryc. 4, tabela 1).



Ryc. 2. Analiza porównawcza obiektywnej refrakcji przed zabiegiem i po nim  
Fig. 2. Comparison of objective refraction before and after surgery



Ryc. 3. Średnia wartość refrakcji  
Fig. 3. Mean value of objective refraction



Ryc. 4. Analiza porównawcza ostrości wzroku w najlepszej korekcji okularowej i po zabiegu

Fig. 4. Comparison between BCDVA and visus after surgery

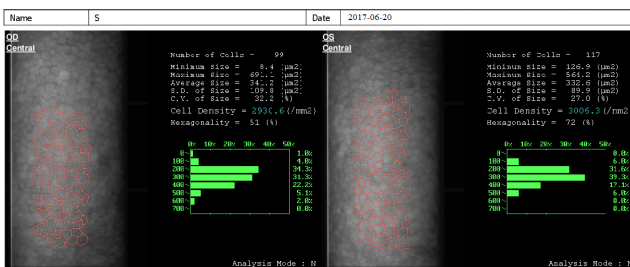
Tabela 1. Wyniki mocy sferycznej, cylindrycznej i BCDVA przed wszczepieniem soczewki i po nim

Table 1. Results of spherical power, cylinder power and BCDVA before and after surgery

Oceniane parametry	Przed wszczepieniem soczewki	Po wszczepieniu soczewki	p
Moc sferyczna	7,77 ±3,55	0,475 ±0,27	<0,01
Moc cylindryczna	1,18 ±0,87	0,46 ±0,27	<0,01
BCDVA	0,91 ±0,20	1,05 ±0,22	0,04

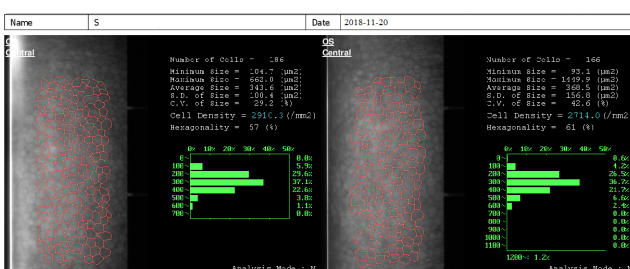
Średnia gęstość komórek śródbłonna przed operacją wynosiła  $2999 \pm 312$  komórek/mm<sup>2</sup>, a po zabiegu  $2953 \pm 105$  komórek/mm<sup>2</sup>. Nie wykazano istotnych różnic w gęstości komórek śródbłonna w ocenie przed zabiegiem i po nim ( $p < 0,04$ ; ryc. 5, 6).

W trakcie leczenia chirurgicznego oraz całego okresu obserwacji nie stwierdzono powikłań pooperacyjnych.



Ryc. 5. Obraz śródbłonna rogówki obu oczu przed wszczepieniem soczewki

Fig. 5. Image of endothelial cells of both eyes before the treatment



Ryc. 6. Obraz śródbłonna rogówki obu oczu po wszczepieniu soczewki

Fig. 6. Image of endothelial cells of both eyes after the treatment

## Omówienie

W materiale własnym średnia wartość refrakcji wynosiła  $-7,77 \pm 3,55$  dioptrii, co jest podobne z badaniem Shimizu et al. Autorzy ci przebadali 64 oczu 32 pacjentów, którym do jednego oka wszczepili model Visian ICL V4, a do drugiego – ICL konwencjonalny. Średnia wartość refrakcji przed zabiegiem wyniosła  $-7,53 \pm 2,39$  dioptrii.<sup>11</sup>

Fernández-Vega-Cueto et al.<sup>6</sup> poddali obserwacji 184 oczu 92 pacjentów w ciągu 3 lat po wszczepieniu ICL V4 z powodu krótkowzroczności. Zaobserwowali zmianę średniej refrakcji z  $-8,30 \pm 2,98$  dioptrii przed operacją do  $-0,37 \pm 0,47$  dioptrii po zabiegu. Liczba komórek śródbłonna na milimetr kwadratowy przed zabiegiem wynosiła  $2742 \pm 340$ , a po wszczepieniu soczewki  $2663 \pm 366$ .

W przeciwieństwie do Shimizu et al., którzy przeprowadzili 5-letnią obserwację, nie stwierdziliśmy zaćmy podtorebkowej przedniej. Wytłumaczeniem może być to, że w przypadku V4c ICL ciecz wodnista przepływająca przez otwór przesuwając soczewkę i oddziela ją od ICL, natomiast u pacjenta z konwencjonalnym wszczepem stwierdzono bezobjawową zaćmę podtorebkową przednią.<sup>11,12</sup>

Według Dougherty i Privera średnia przedoperacyjna refrakcja sferyczna wynosiła  $-6,96 \pm 1,60$  dioptrii, a cylinder  $1,03 \pm 0,88$  dioptrii. Ostrość wzroku (ang. *corrected distance visual acuity* – CDVA) wynosiła 20/20 (zakres 20/15 do 20/80) i podobne wartości stwierdzono na końcowej wizycie. Podczas ostatniej kontroli lekarskiej po operacji sferyczny ekwiwalent wynosił  $-0,08 \pm 0,01$  dioptrii, a cylinder  $0,29 \pm 0,71$  dioptrii.<sup>13</sup> Porównanie pooperacyjnej nieskorygowanej ostrości wzroku (ang. *uncorrected distance visual acuity* – UCDVA) z przedoperacyjną CDVA wykazało, że 27 oczu (26%) miało lepszą pooperacyjną UCDVA i 61 oczu (59%) miało UDVA odpowiadającą przedoperacyjnej CDVA. Nie odnotowano powikłań śródoperacyjnych. Podczas ostatniego badania nie stwierdzono zmętnienia soczewki.<sup>13</sup>

Gimbel et al. przeanalizowali rezultaty wszczepienia Visian V4 ICL w oczach pacjentów krótkowzrocznych, okres obserwacji wahał się w granicach 2–14 lat. Wspomniane retrospektywne badanie wykazało, że odsetek rozwijającej się zaćmy przedniej podtorebkowej był dodatnio skorelowany z wiekiem.<sup>14</sup>

Karandikar et al. przeprowadzili obserwację roczną 34 oczu pacjentów z krótkowzrocznością  $\geq 6$  dioptrii, którym wszczepiono V4 ICL. Średnia refrakcja przed zabiegiem wynosiła  $-9,24 \pm 2,4$  dioptrii, a po zabiegu zmniejszyła się do  $-0,19 \pm 1,18$  dioptrii. Dla astygmatyzmu wyniki były następujące:  $-1,9 \pm 1,6$  dioptrii przed zabiegiem i  $-0,9 \pm 0,3$  dioptrii po nim. Średnia utrata komórek śródbłonna wyniosła 7,1%, nie zaobserwowano wzrostu ciśnienia wewnątrzgałkowego.<sup>15</sup>

Przeprowadziliśmy badanie gęstości śródbłonna, które nie wykazało żadnej istotnej zmiany po roku. Jest to odmienna obserwacja od wyników innych autorów od-

notowanych podczas stosowania wszczepów przednio-komorowych. Wszczepy te mocowano na przedniej powierzchni tęczówki, co mogło spowodować uszkodzenie komórek śródbłonna. Obecnie stosowany model dotyka tylnej powierzchni tęczówki.<sup>15</sup>

W trakcie całego okresu obserwacji nie stwierdzono odczynu zapalnego, nie wystąpiło zakażenie ani inne powikłania pooperacyjne, tak samo jak w przypadku badań Alfonso et al.<sup>16</sup>

Collamerowe wszczepy fakijne są dobrze tolerowane, sprawdzają się w przypadku dużych wad wzroku, zwłaszcza u pacjentów pracujących w określonych warunkach (zapylenie, wilgotność, zmiana temperatur, praca na wysokości) oraz u zawodowych sportowców. Istotną zaletą jest odwracalność zabiegu – wszczep można usunąć i przywrócić stan sprzed operacji.

Jak wskazał Packer w niedawno opublikowanej metaanalizie i przeglądzie 37 badań klinicznych z 5-letnim okresem obserwacji, nowy model ICL V4 z centralnym otworem zapewnia znaczną poprawę widzenia i jakości życia.<sup>17</sup> Badania własne również wykazały znaczną poprawę ostrości wzroku, natomiast jakość życia nie była przez nas oceniana.

Należy podkreślić, że w niniejszym badaniu zaprezentowano wyniki wstępne, okres obserwacji był krótki, ponadto ograniczenie naszej metody stanowiła niewielka grupa pacjentów. W przyszłości badania powinny uwzględniać omówienie jakości życia pacjentów oraz być uzupełnione o długoterminową ocenę wpływu implantu na korekcję astygmatyzmu i innych aberracji układu optycznego oka.

## Wnioski


Ocena bezpieczeństwa prawidłowo wszczepionych soczewek fakijnych ICL wskazuje na dobrą tolerancję implantu collamerowego w komorze tylnej.

Nie wykazano negatywnego wpływu na struktury przedniego odcinka ze szczególnym uwzględnieniem śródbłonna rogówki i soczewki.


Ostrość wzroku skorygowana soczewką Visian ICL nie ustępuje ostrości skorygowanej okularami, a w wielu przypadkach może być lepsza.

Collamerowe wszczepy fakijne ICL mogą być stosowane jako alternatywa dla soczewek kontaktowych oraz refrakcyjnej wymiany przezierniej soczewki.

## ORCID iDs

Krystyna Grzebieluch-Reichert  <https://orcid.org/0000-0003-3711-5672>

Jarosław Marek  <https://orcid.org/0000-0003-1547-5204>

Marta Misiuk-Hojto  <https://orcid.org/0000-0002-4020-3203>

## Piśmiennictwo

- Dolgin E. The myopia boom. *Nature*. 2015;519(7543):276–278. doi:10.1038/519276a
- Nam SW, Lim DH, Hyun J, Chung ES, Chung TY. Buffering zone of implantable collamer lens sizing in V4c. *BMC Ophthalmol*. 2017;17(1):260. doi:10.1186/s12886-017-0663-4
- Chen X, Miao H, Naidu RK, Wang X, Zhou X. Comparison of early changes in and factors affecting vault following posterior chamber phakic Implantable Collamer Lens implantation without and with a central hole (ICL V4 and ICL V4c). *BMC Ophthalmol*. 2016;16(1):161. doi:10.1186/s12886-016-0336-8
- Tian Y, Jiang HB, Jiang J, Wen D, Xia XB, Song WT. Comparison of implantable collamer lens visian ICL V4 and ICL V4c for high myopia: A cohort study. *Medicine (Baltimore)*. 2017;96(25):e7294. doi:10.1097/MD.00000000000007294
- Alfonso JF, Lisa C, Abdelhamid A, Fernandes P, Jorge J, Montés-Micó R. Three-year follow-up of subjective vault following myopic implantable collamer lens implantation. *Graefes Arch Clin Exp Ophthalmol*. 2010;248(12):1827–1835. doi:10.1007/s00417-010-1322-0
- Fernández-Vega-Cueto L, Lisa C, Esteve-Taboada JJ, Montés-Micó R, Alfonso JF. Implantable collamer lens with central hole: 3-year follow-up. *Clin Ophthalmol*. 2018;12:2015–2029. doi:10.2147/OPHTH.S171576
- Lee H, Kang DS, Ha BJ, et al. Effect of accommodation on vaulting and movement of posterior chamber phakic lenses in eyes with implantable collamer lenses. *Am J Ophthalmol*. 2015;160(4):710–716.e1. doi:10.1016/j.ajo.2015.07.014
- Lovisol CF, Reinsteinst DZ. Phakic intraocular lenses. *Surv Ophthalmol*. 2005;50(6):549–587. doi:10.1016/j.survophthal.2005.08.011
- Chang DH, Davis EA. Phakic intraocular lenses. *Curr Opin Ophthalmol*. 2006;17(1):99–104. doi:10.1097/01.cco.0000188624.54743.c7
- Rosen E, Gore C. Staar collamer posterior chamber phakic intraocular lens to correct myopia and hyperopia. *J Cataract Refract Surg*. 1998;24(5):596–606.
- Shimizu K, Kamiya K, Igarashi A, Shiratani T. Intraindividual comparison of visual performance after posterior chamber phakic intraocular lens with and without a central hole implantation for moderate to high myopia. *Am J Ophthalmol*. 2012;154(3):486–494.e1. doi:10.1016/j.ajo.2012.04.001
- Kamiya K, Shimizu K, Ando W, Igarashi A, Iijima K, Koh A. Comparison of vault after implantation of posterior chamber phakic intraocular lens with and without a central hole. *J Cataract Refract Surg*. 2015;41(1):67–72. doi:10.1016/j.jcrs.2014.11.011
- Dougherty PJ, Priver T. Refractive outcomes and safety of the implantable collamer lens in young low-to-moderate myopes. *Clin Ophthalmol*. 2017;11:273–277. doi:10.2147/OPHTH.S120427
- Gimbel HV, LeClair BM, Jabo B, Marzouk H. Incidence of implantable collamer lens-induced cataract. *Can J Ophthalmol*. 2018;53(5):518–522. doi:10.1016/j.jcjo.2017.11.018
- Karandikar S, Bhandari V, Reddy J. Outcomes of implantable collamer lens V4 and V4c for correction of high myopia: A case series. *Nepal J Ophthalmol*. 2015;7(14):164–172. doi:10.3126/nepjoph.v7i2.14967
- Alfonso JF, Fernández-Vega L, Lisa C, Fernandes P, González-Mejome J, Montés-Micó R. Long-term evaluation of the central vault after phakic collamer lens (ICL) implantation using OCT. *Graefes Arch Clin Exp Ophthalmol*. 2012;250(12):1807–1812. doi:10.1007/s00417-012-1957-0
- Packer M. Meta-analysis and review: Effectiveness, safety, and central port design of the intraocular collamer lens. *Clin Ophthalmol*. 2016;10:1059–1077. doi:10.2147/OPHTH.S111620



# Polyethylene terephthalate tape augmentation as a solution in recurrent quadriceps tendon ruptures

Maciej Leciejewski<sup>1,A,C,D</sup>, Aleksandra Królikowska<sup>2,E</sup>, Paweł Reichert<sup>3,C,E,F</sup>

<sup>1</sup> Department of Trauma and Orthopedic Surgery, District Hospital, Puszczykowo, Poland

<sup>2</sup> College of Physiotherapy, Wrocław, Poland

<sup>3</sup> Division of Sports Medicine, Wrocław Medical University, Poland

A – research concept and design; B – collection and/or assembly of data; C – data analysis and interpretation;

D – writing the article; E – critical revision of the article; F – final approval of the article

Polymers in Medicine, ISSN 0370-0747 (print), ISSN 2451-2699 (online)

*Polim Med.* 2018;48(1):53–56

## Address for correspondence

Maciej Leciejewski

E-mail: [leciej@gmail.com](mailto:leciej@gmail.com)

## Funding sources

None declared

## Conflict of interest

None declared

Received on October 29, 2018

Reviewed on December 9, 2018

Accepted on January 16, 2019

## Abstract

Quadriceps tendon rupture is a severe and demanding problem in knee surgery, especially when it is recurrent and when elderly patients are involved. It can have a devastating impact when it is a complication following knee arthroplasty. There are many procedures for dealing with this problem, but none of them offer reliable results. The most popular methods of treatment are traditional transosseous sutures and suture anchors, often in combination with semitendinosus augmentation. In cases of osteoporotic bone or hamstring insufficiency, these solutions are not appropriate. One way to manage quadriceps tendon rupture is to use polyethylene terephthalate tape (poly tape) as scaffolding for tissue ingrowth. Because of its structure, poly tape provides adequate strength and allows early mobilization. Besides being durable, multifilament high tenacity polyethylene terephthalate is flexible. Poly tape augmentation is particularly recommended in the following cases: recurrent rupture of the quadriceps tendon; extensor apparatus damage following total knee arthroplasty (TKA); delayed diagnosis of quadriceps tendon rupture; and in elderly patients (with weak bones and poor ligament quality). The surgical technique is simple and the procedure has a low complication rate. There have been many studies confirming the security of polyethylene terephthalate use in the human body. There is also a great deal of evidence concerning tissue ingrowth in the mesh structure of poly tape. Allergic reactions and inflammatory responses are rare.

**Key words:** quadriceps tendon rupture, poly tapes, ligament augmentation

## Cite as

Leciejewski M, Królikowska A, Reichert P.

Polyethylene terephthalate tape augmentation as a solution in recurrent quadriceps tendon ruptures.

*Polim Med.* 2018;48(1):53–56. doi:10.17219/pim/102977

## DOI

10.17219/pim/102977

## Copyright

© 2018 by Wrocław Medical University

This is an article distributed under the terms of the

Creative Commons Attribution Non-Commercial License

(<http://creativecommons.org/licenses/by-nc-nd/4.0/>)

## Introduction

The quadriceps tendon attaches all 4 quadriceps femoris muscles (QMFs) to the proximal part of the patella. In more than 50% of cases, the QMF tendon consists of 3 layers.<sup>1</sup> The most superficial layer is formed by the rectus femoris muscle, which passes above the patella to form the patellar tendon. The intermediate layer arises from the vastus lateralis and the vastus medialis muscles, which also form the lateral and medial patellar retinacula and play a very important role in patellofemoral joint stability. The deepest layer of the QMF tendon originates from the vastus intermedius muscle. The articularis genus muscle, which makes up the deepest part of the intermedius, is also in this vicinity,<sup>2</sup> but because it varies greatly in terms of size and number of fibers, it is often not mentioned.

Variations in the structure of the QMF tendon is quite common; it sometimes consists of 4 layers (6%) or of 2 layers (30%), and in some cases the layers are hard to identify. The medial and lateral muscles may themselves be 2-ply. The longitudinal fibers may be crossed by oblique portions of the muscles. The patellofemoral ligaments also vary a great deal; the medial patellofemoral ligament (MPFL) is more common than the lateral patellofemoral ligament (LPFL).<sup>3</sup>

The QMF is the largest human muscle and the forces transmitted through its tendon are extremely large. Calculated per square centimeter, its mechanical capacities are very similar to those of the anterior cruciate ligament (ACL). In many studies, the QMF is described as good material for ACL grafting.<sup>4</sup>

## Epidemiology of and risk factors for quadriceps tendon rupture

Knee extensor apparatus ruptures as a whole are rare. Quadriceps tendon ruptures, with an incidence of 1.37/100,000, are more common than patellar tendon ruptures (0.68/100,000), but much less frequent than patella fractures (13.1/100,000). Quadriceps femoris muscles tendon ruptures usually occur in patients over 40 years of age and are much more frequent in males than in females (8:1).<sup>5</sup>

The most important risk factors for QMF tendon rupture is overweight (mean BMI  $30.0 \pm 6.05$  kg/m<sup>2</sup>).<sup>5</sup> Medical comorbidities are common in tendon ruptures, especially among women. Most frequent are diabetes, rheumatoid arthritis (steroid use), renal failure,<sup>6</sup> and connective tissue disorders. A history of intra-articular injections and the use of statins are also proven risk factors.<sup>7</sup>

The frequency of recurrent QMF tendon rupture is hard to estimate. Few trials have addressed this problem, so data is scarce; most published reports are case studies.

## Clinical problems

Standard techniques used to repair QMF tendon rupture have some disadvantages<sup>8,9</sup>; they lack sufficient strength to permit patients to exercise the full range of motion. There is no consensus regarding rehabilitation protocol. In the past, after QMF tendon repair the knee was immobilized for 6 weeks in full extension, resulting in muscle mass loss, stiffness, limited range of motion, and a very long rehabilitation period after that. On the other hand, although early movement and flexion exercises may improve the rehabilitation process, some authors suggest that a protective cast is necessary.<sup>10</sup> In elderly patients, especially in recurrent cases, or in patients with tendon ruptures following knee arthroplasty, a long cast and immobility have a negative impact on further treatment. Because of age-related comorbidities, many additional complications may occur (deep vein thrombosis, skin lacerations, muscular dystrophy, joint contracture, stiffness). A better solution is therefore needed. There have been many attempts to use grafts to strengthen the damaged area, including grafts from the semitendinosus (gracilis) tendon<sup>11,12</sup> or the Achilles tendon.<sup>13</sup> However, in elderly patients such autografts are weak and morbidity at the donor site may be dangerous. The use of allografts has its own risks (e.g., transmission of infectious diseases) and there are frequent problems with availability.<sup>14</sup> Nowadays total knee arthroplasty (TKA) is so common that the number of patient suffering from QMF tendon rupture following arthroplasty is increasing.<sup>15,16</sup>

The aim of using polyethylene terephthalate tape (poly tape) is to enhance the ruptured tendon and allow the patient early mobilization.<sup>17-21</sup> The tape provides intrinsic strength, enabling the tendon to work against tensile forces.

## Surgical technique

The patient is in a supine position and the leg is free, without a tourniquet (to avoid compressing the QMF and shortening the tendon stump). A midline approach is usually recommended. Scar tissue in the area of the injury is debrided, and the proximal part of the patella is refreshed. The QMF is mobilized. In cases of contracture, release may be needed. There are often adhesions that need to be released; sometimes the rectus femoris muscle must be lengthened (by the V-Y technique or Z-plasty). After these preparatory stages, the first step is to pass poly tape under the distal end of the patella (Fig. 1), where it is connected to the patellar tendon. The tape should not be too deep, to avoid joint penetration. It should be securely anchored in the midsubstance of the patellar tendon. The 2 ends of the tape are then brought up and crossed over the kneecap (the anterior aspect of the patella), keeping the tape flat; additional tacking sutures are used to attach the poly tape to the surrounding tissues and to itself at the crossing point.

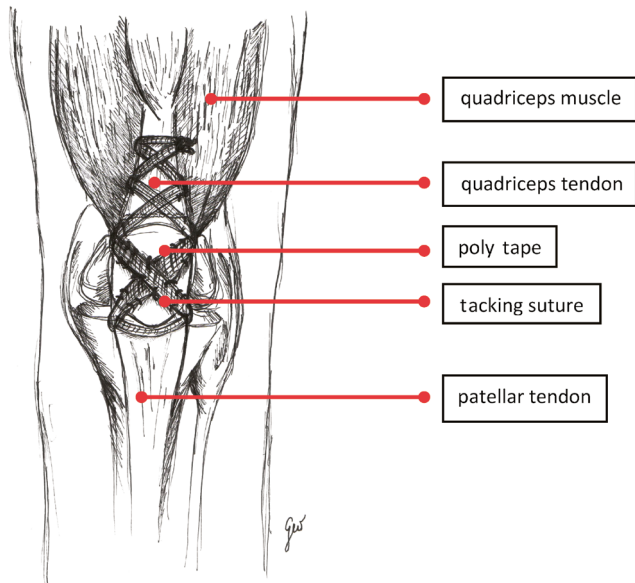


Fig. 1. Schematic poly tape placement on extensor apparatus of the knee (author's own illustration)

The distal end of the quadriceps tendon must be approximate to the patella, and then the tape is passed through the tendon as in a Bunnell suture. Because of the length of the tape, (30 × 800 mm), the number of loops is rather arbitrary (Fig. 2). To prevent secondary ischemic damage, it is essential to ensure that the tape is not too tight; the stability of the extensor apparatus should be achieved through the appropriate placement of additional sutures joining the tape and tendon/muscle tissue rather than by putting pressure on the tendon with the tape. Finally, the proximal ends of the tape are knotted and hidden in the muscle. A protective suture is added to avoid knot failure. After that the tape should smoothly interlace the tendon, and any unevenness should be flattened by sutures. It is good to make sure knee flexion in the range of 0–60° is safe, causing no discontinuity of the extensor apparatus. The wound is closed in the standard way.



Fig. 2. Poly tape, 30 mm x 800 mm (photo courtesy of Komak sp. z o.o.)

## Rehabilitation protocol

Despite augmentation of the extensor mechanism with poly tape, the rehabilitation protocol is cautious and must be adapted to suit each patient. The use of a cast is not advised; we prefer a brace with an adjustable range of motion. Just after surgery, the brace is fixed in full extension for 2 weeks. During this period the patient is taught how to exercise the QMF isometrically. Walking distances are not limited, but the patient uses 2 crutches. After 2 weeks of immobilization, the range of motion is increased gradually by 30° of flexion per 2-week periods (0–30°: 2–4 weeks; 0–60°: 4–6 weeks; 0–90°: 6–8 weeks). The patient is advised to try to use 1 crutch in the opposite hand at this stage. Movement is achieved passively; active flexion of the knee is allowed 6 weeks after the reconstructive procedure. Active extension is initiated after 8 weeks. The brace is no longer needed. Strengthening of the quadriceps muscle continues, along with gait training. An important part of the protocol is the reinforcement of the proximal and core musculature (gluteal muscles, paraspinal muscles and abdominal muscles). Proprioception and balance training are also crucial. Sometimes an imbalance between the lateral and medial stabilizers of the patella may occur. Special care must be taken of vastus medialis obliquus (VMO), which is naturally the smallest part of the quadriceps and it frequently atrophies after an injury. Training the VMO is essential for proper patellofemoral tracking and painless flexion. Patellar mobilization is done throughout the rehabilitation process and patients are taught how to do it by themselves.<sup>22</sup>

## Discussion

Because of aging societies and the increasing number of degenerative diseases, there are new demands on modern medicine. There is a need to look for materials that provide good structural support and are safe in widespread use. Along with metallic and ceramic materials, polymers play a key role.<sup>23</sup> Polymers are used as acrylic bone cements (to anchorage prostheses to the bone), as polyethylene inserts in acetabular cups in hip prostheses or as silicone elastomers that replace small joints. The next generation of polymers might be bioabsorbable and useful for bone and other tissue defects. In ligament diseases and discontinuity, a material is required that acts as 3-dimensional scaffold. Poly tape is made of woven multifilament high-tenacity polyester fiber. The open-weave structure acts as a matrix and leaves space for tissue ingrowth. The parallel fibers provide a high degree of strength. The mesh is made of pure polyethylene terephthalate (PET), without any additions. It consists of repeating units of the monomer ethylene terephthalate (C<sub>10</sub>H<sub>8</sub>O<sub>4</sub>). Its physical properties are as follows: tensile strength 55–75 MPa; elastic limit 50–150%; glass transition temperature 67–81°C,


with a softening point of 265°C. It is lightweight, strong and impact-resistant, as well as hygroscopic (absorbing water from its surroundings).


Years of experience with similar polymers provide reproducible results. Long-term outcomes in strengthening the abdominal wall in hernias are good or even excellent.<sup>24</sup> The infection rate is very low and recurrence is rare. Hypersensitivity to implant materials occurs infrequently. That is why use of tape in tendon/muscle injury seems to be safe. There is no data suggesting heterotopic ossification or muscle fibrosis. In comparison to other techniques, it offers the possibility of early movement and immediate isometric exercises. Reconstruction of the extensor apparatus with poly tape is worth considering in difficult recurrent cases.

The use of poly tape in patellar tendon rupture is also promising. The technique is similar to what has been described above, likewise reproducible and not difficult. It can be even applied when the extensor apparatus needs to be reconstructed following patellectomy.

In the future, poly tape may be applied in the reconstruction of other tendons, i.e., in the biceps brachii tendon or the Achilles tendon. Because of good clinical results, the use of poly tapes in ligament surgery is likely to gain popularity.

#### ORCID iDs

Maciej Leciejewski  <https://orcid.org/0000-0002-2081-8788>

Aleksandra Królikowska  <https://orcid.org/0000-0002-6283-5500>

Paweł Reichert  <https://orcid.org/0000-0002-0271-4950>

#### References

- Zeiss J, Saddemi SR, Ebraheim NA. MR imaging of the quadriceps tendon: Normal layered configuration and its importance in cases of tendon rupture. *AJR Am J Roentgenol*. 1992;159(5):1031–1034.
- Grob K, Gilbey H, Manestar M, Ackland T, Kuster MS. The anatomy of the articularis genus muscle and its relation to the extensor apparatus of the knee. *JBJS Open Access*. 2017;2(4):e0034.
- Waligora AC, Johanson NA, Hirsch BE. Clinical anatomy of the quadriceps femoris and extensor apparatus of the knee. *Clin Orthop Relat Res*. 2009;467(12):3297–3306.
- Hurley ET, Calvo-Gurry M, Withers D, Farrington SK, Moran R, Moran CJ. Quadriceps tendon autograft in anterior cruciate ligament reconstruction: A systematic review. *Arthroscopy*. 2018;34(5):1690–1698.
- Garner MR, Gausden E, Berkes MB, Nguyen JT, Lorich DG. Extensor mechanism injuries of the knee: Demographic characteristics and comorbidities from a review of 726 patients records. *J Bone Joint Surg Am*. 2015;97(19):1592–1596.
- Lim CH, Landon KJ, Chan GM. Bilateral quadriceps femoris tendon rupture in a patient with chronic renal insufficiency: A case report. *J Emerg Med*. 2016;51(4):e85–e87.
- Deren ME, Klinge SA, Mukand NH, Mukand JA. Tendinopathy and tendon rupture associated with statins. *JBJS Rev*. 2016;4(5). doi:10.2106/JBJS.RVW.15.00072
- Plessner S, Keilani M, Vekszler G, et al. Clinical outcomes after treatment of quadriceps tendon ruptures show equal results independent of suture anchor or transosseous repair technique used: A pilot study. *PLoS One*. 2018;13(3):e0194376.
- Brossard P, Le Roux G, Vasse B; Orthopedics, Traumatology Society of Western France (SOO). Acute quadriceps tendon rupture repaired by suture anchors: Outcomes at 7 years' follow-up in 25 cases. *Orthop Traumatol Surg Res*. 2017;103(4):597–601.
- Boudissa M, Roudet A, Rubens-Duval B, Chaussard C, Saragaglia D. Acute quadriceps tendon ruptures: A series of 50 knees with an average follow-up of more than 6 years. *Orthop Traumatol Surg Res*. 2014;100(2):213–216.
- Chahla J, DePhillipo NN, Cinque ME. Open repair of quadriceps tendon with suture anchors and semitendinosus tendon allograft augmentation. *Arthrosc Tech*. 2017;6(6):e2071–e2077.
- Maffulli N, Papalia R, Torre G, Denaro V. Surgical treatment for failure of repair of patellar and quadriceps tendon rupture with ipsilateral hamstring tendon graft. *Sports Med Arthrosc Rev*. 2017;25(1):51–55.
- Wise BT, Erens G, Pour AE, Bradbury TL, Roberson JR. Long-term results of extensor mechanism reconstruction using Achilles tendon allograft after total knee arthroplasty. *Int Orthop*. 2018;42(10):2367–2373.
- Ricciardi BF, Oi K, Trivellas M, Lee YY, Della Valle AG, Westrich GH. Survivorship of extensor mechanism allograft reconstruction after total knee arthroplasty. *J Arthroplasty*. 2017;32(1):183–188.
- Chhapan J, Sankineani SR, Chiranjeevi T, Reddy MV, Reddy D, Gura-va Reddy AV. Early quadriceps tendon rupture after primary total knee arthroplasty. *Knee*. 2018;25(1):192–194.
- Soong JW, Silva AN, Andrew TH. Disruption of quadriceps tendon after total knee arthroplasty: Case report of four cases. *J Orthop Surg (Hong Kong)*. 2017;25(2):2309499017717206.
- Abdel MP, Salib CG, Mara KC, Pagnano MW, Perry KI, Hanssen AD. Extensor mechanism reconstruction with Ue of Marlex mesh: A series study of 77 total knee arthroplasties. *J Bone Joint Surg Am*. 2018;100(15):1309–1318.
- Paci JM, Pawlak A. Knotless tape suture fixation of quadriceps tendon rupture: A novel technique. *Am J Orthop (Belle Mead NJ)*. 2018;47(1). doi:10.12788/ajo.2018.0002
- Nodzo SR, Rachala SR. Polypropylene mesh augmentation for complete quadriceps rupture after total knee arthroplasty. *Knee*. 2016;23(1):177–180.
- Morrey MC, Barlow JD, Abdel MP, Hanssen AD. Synthetic mesh augmentation of acute and subacute quadriceps tendon repair. *Orthopedics*. 2016;39(1):e9–13.
- Rehman H, Kovacs P. Quadriceps tendon repair using hamstring, prolene mesh and autologous conditioned plasma augmentation: A novel technique for repair of chronic quadriceps tendon rupture. *Knee*. 2015;22(6):664–668.
- Langenhan R, Baumann M, Ricart P. Postoperative functional rehabilitation after repair of quadriceps tendon ruptures: A comparison of two different protocols. *Knee Surg Sports Traumatol Arthrosc*. 2012;20(11):2275–2278.
- Navarro M, Michiardi A, Castano O, Planell JA. Biomaterials in orthopedics. *JR Soc Interface*. 2008;5(27):1137–1158.
- Gordon AC, Gillespie C, Son J, Polhill T, Leibman S, Smith GS. Long-term outcomes of laparoscopic large hiatus hernia repair with nonabsorbable mesh. *Dis Esophagus*. 2018;31(5). doi:10.1093/dote/dox156



# Dialysis membranes: A 2018 update

Piotr Olczyk<sup>1,A–D</sup>, Artur Małyszczak<sup>1,A–D</sup>, Mariusz Kuzstal<sup>2,E,F</sup>

<sup>1</sup> Faculty of Medicine, Wrocław Medical University, Poland

<sup>2</sup> Department of Nephrology and Transplantation Medicine, Wrocław Medical University, Poland

A – research concept and design; B – collection and/or assembly of data; C – data analysis and interpretation; D – writing the article; E – critical revision of the article; F – final approval of the article

Polymers in Medicine, ISSN 0370-0747 (print), ISSN 2451-2699 (online)

*Polim Med.* 2018;48(1):57–63

## Address for correspondence

Piotr Olczyk  
E-mail: ol.piotr1994@gmail.com

## Funding sources

None declared

## Conflict of interest

None declared

Received on October 8, 2018

Reviewed on January 12, 2019

Accepted on January 16, 2019

## Abstract

Dialysis membranes are the basic element of a hemodialyzer. Synthetic and natural materials characterized by various fiber arrangements are used in their production. The most up-to-date ones are made of synthetic polymers such as polyamide, phosphatidylserine (PS), polyacrylonitrile-based fiber (PAN), polyarylether-sulfone, polyethersulfone, or polymethylmethacrylate. Dialysis membranes are characterized by the ability to remove uremic molecules, which can be divided into small water-soluble compounds, protein-bound compounds and larger “middle molecules”. Newer membranes such as medium cut off membranes (MCO) allow the removal of a wider spectrum of uremic molecules, which reduces the risk of late complications of dialysis. Dialysis membranes are used in therapy methods such as low flux, high flux or HDx therapy. An important aim in dialysis membrane development is to increase their biocompatibility. Insufficient biocompatibility can result in complement activation or platelet activation, which can lead to an increased risk of cardiovascular complications. The aim of the study is to discuss the latest reports on dialysis membranes.

**Key words:** dialysis, membranes, HDx, MCO

## Cite as

Olczyk P, Małyszczak A, Kuzstal M. Dialysis membranes: A 2018 update. *Polim Med.* 2018;48(1):57–63. doi:10.17219/pim/102974

## DOI

10.17219/pim/102974

## Copyright

© 2019 by Wrocław Medical University

This is an article distributed under the terms of the Creative Commons Attribution Non-Commercial License (<http://creativecommons.org/licenses/by-nc-nd/4.0/>)

Despite the increasing frequency of kidney transplants, the number of patients requiring hemodialysis (HD) continues to grow. According to the European Renal Association registry on December 31, 2014, 490,743 individuals in Europe were receiving renal replacement therapy for end-stage renal disease (ESRD), equating to an unadjusted prevalence of 924 patients per million population (pmp) (ranging from 157 pmp in Ukraine to 1794 pmp in Portugal). In 2016, 20,144 Polish patients required HD,<sup>1</sup> and were struggling with numerous complications caused by insufficient removal of uremic molecules.

It is worth mentioning the classifications of the European Uremic Toxin Work Group (EUTox) here: 1. small water-soluble compounds; 2. protein-bound compounds; and 3. larger “middle molecules”. High-flux dialysis and more efficient treatment techniques, like hemodiafiltration (HDF), improve the removal of uremic toxins in the middle molecular-weight range.

Currently, the most popular (and low cost) dialysis membranes are synthetic membranes, used in high-flux dialysis. In recent years, a new type of membrane – medium cut-off membranes (MCO), used in expanded HD therapy (HDx) – has been developed. Today, new MCO membranes with increased pore size allow for the removal of toxins with bigger molecular weight, such as kappa and lambda light chains and/or mediators of inflammation. Heparin-grafted membranes have been developed to reduce the risk of bleeding. Graphene membranes are at the early phase of research. This article presents an overview of the dialysis membranes currently available and those which will soon appear on the market.

## Chemical composition and its influence on membrane performance

An important aspect of the functioning of dialysis membranes is their composition. Formerly, they were divided into cellulose and noncellulosic. Nowadays, we distinguish rayon-based membranes (also known as cuprophan membranes) and other membranes such as cellulose acetate, cellulose triacetate and so on, also known as modified cellulosic membranes. The second group includes synthetic membranes made of polyamide, phosphatidylserine (PS), polyacrylonitrile-based (PAN) fibers, polyarylethersulfone, polyethersulfone, and polymethylmethacrylate. The membranes in the second group are characterized by better biocompatibility and the ability to remove substances of a bigger molecular weight. In order to reduce the side effects associated with excessive hydrophobicity and to increase the efficiency and permeability of the membrane, it is possible to use compositions of different synthetic components.<sup>2,3</sup> Excessive hydrophobicity is associated with membrane fouling, caused by adhe-

sion of plasma proteins to the surface of the membrane. It leads to platelet adhesion, aggregation and coagulation.

Cellulose membranes are considered natural. They have a symmetrical structure and the same pore size in all layers. They also have hydrophilic properties, and after contact with blood and dialysate they take the form of a homogeneous gel. Some synthetic membranes have similar construction. An asymmetric structure is characteristic only of synthetic membranes. They have a thin, selective inner layer and a thicker outer support layer. The outer layer is formed of a finely porous skin, which is the real separation barrier for solute. The inner part of the support layer is characterized by its high density, which reduces from the inside to the outside. The support layer provides mechanical stability. Under the microscope it forms a sponge-like or finger-type structure. Synthetic membranes, unlike cellulose membranes, have a strongly hydrophobic component. Their structure depends on the rate of precipitation of the polymer in the presence of a non-solvent solution.<sup>4,5</sup>

Synthetic and cellulose membranes differ also in terms of the fiber arrangement. Cellulose membranes naturally have a wave-like structure, while synthetic fibers are crimped to produce a ripple pattern for better blood and dialysate distribution. This design prevents contact or excess packing among fibers, and thus allows for better matching of blood and dialysate flows across all the sections of the fiber bundle.<sup>6,7</sup>

A clinically important parameter is molecular weight cut-off. This coefficient describes the largest molecule that can pass through the membrane. For older types of membrane, this value is about 3,000 Da, while for newer ones it is around 15,000 Da. In super high-flux dialysis, it can be as high as 65,000 Da. Effective removal of medium and large molecules is made possible through the use of a more uniform pore size and by increasing the average pore size. An additional benefit is the sharper cut-off in the sieving coefficient, which facilitates the passage of low molecular-weight proteins and decreases albumin loss.<sup>8,9</sup>

## The most popular materials used in dialysis membranes

Polysulfone-based membranes (PSf) are characterized by good mechanical strength and high resistance to chemicals and to temperature. The most important advantages that make PSf useful in HD are:

- high biocompatibility;
- high permeability for low molecular-weight proteins;
- high retention of endotoxins;
- the possibility of trouble-free sterilization.<sup>10</sup>

Such membranes also have some disadvantages. They can cause protein accumulation on the surface of the membrane, which results in reduced flow and changes in membrane selectivity. Additionally, the accumulated protein may cause activation of the immune system.<sup>11</sup>

Polyethersulfone (PES) is one of the most common materials used in the production of dialysis membranes. It is characterized by high oxidative, chemical and thermal resistance and has appropriate mechanical properties. Polyethersulfone does not change after sterilization. One of the most important features of PES as a material for HD membranes is its high permeability for low-molecular weight proteins. The main problem is the hydrophobic nature of this material, which contributes to membrane fouling. Nowadays, hydrophilic polymers are added to PES to minimize this phenomenon. The most popular combination is PES with polyvinylpyrrolidone (PVP).<sup>12</sup>

Cellulose triacetate (CTA) is a compound formed by replacing the hydroxyl groups of cellulose with a carboxylic group. It is characterized by high diffusion efficiency and structural homogeneity.<sup>13</sup> Cellulose triacetate and synthetic membranes have similar permeability for small molecular uremic toxins,  $\beta$ 2-microglobulin ( $\beta$ 2M) and small molecules associated with proteins. Another important property of CTA is its low thrombogenic potential.<sup>14</sup>

The asymmetric triacetate membrane (ATA), which was created by modifying CTA, is a new compound developed by the Nipro Corporation (Osaka, Japan). Its main properties are its asymmetrical structure and smooth surface, resulting in high permeability during massive filtration, less variation in permeation time, better biocompatibility, and lower protein adsorption.<sup>15</sup>

Polymethyl methacrylate (PMMA) gives membranes high biocompatibility and high permeability. The PMMA-based membranes have the ability to remove protein through permeation and adsorption. This allows the removal of high-weight molecules like the free light chain of immunoglobulins (56,000 Da). Polymethyl methacrylate can be used to reduce inflammation in patients during HD by removing cationic compounds and cytokines. It also contributes to the preservation of muscle mass in the elderly (probably due to a decreased loss of amino acids) and a reduction in pruritus.<sup>16</sup>

Polyester polymer alloy (PEPA) is a polymer based on polyarylate and PES. It is comprised of 3 layers: an inner skin layer, a porous layer and an outer skin layer. An important feature of PEPA is its ability to filter endotoxins through the outer layer. The addition of PVP allows increased  $\beta$ 2M excretion and reduced albumin loss.<sup>17</sup>

The creation of ethylene vinyl alcohol co-polymer (EVOH) is another attempt to reduce HD-related complications. The EVOH-based membranes are characterized by reduced neutrophil activation and thus a reduction in oxidative stress. The activation of platelets and generation of reactive oxygen species by activated neutrophils on the surface of EVOH-based membranes is lower than on PSf membranes; EVOH is associated with lower inflammation rates and reduced atherogenesis progression, which results in better peripheral blood circulation in patients. Due to their hydrophilic structure EVOH-based membranes do not require the addition of PVP. The EVOH can therefore effectively reduce the risk of cardiovascular (Cv) events in HD patients.<sup>18</sup>

Polyacrylonitrile-based membranes were designed for patients with HD-related complications such as peripheral arterial disease or poor nutritional status.<sup>19</sup> They are hydrophilic membranes characterized by high permeability and high specificity for low and medium molecular proteins.<sup>20</sup>

Heparin-grafted membranes were created for patients with a higher risk of bleeding. Classic anticoagulation therapy using unfractionated or fractionated heparin is associated with a risk of bleeding, hypoadosteronism, dyslipidemia, hyperkalemia, pruritus, and osteoporosis. Heparin-grafted membranes can provide an alternative for these patients; research indicated that they offer results no worse than classic anticoagulation therapy.<sup>21</sup> There are other methods of heparin-free HD, such as albumin priming, regional citrate anticoagulation or airless tubing. A combination of heparin-sparing methods is probably more effective than any single one. However, hard data to prove this hypothesis have not been published so far.<sup>22</sup>

The Massachusetts Institute of Technology (MIT; Cambridge, USA) is currently conducting research on graphene dialysis membranes. At the early stage of testing, these membranes are reported to offer up to 10 times higher filtration speeds than membranes currently in use. Modern dialysis membranes work fairly slowly due to their thickness, but this new graphene membrane can accelerate this process due to being less than 1 nanometer thick.<sup>23</sup>

## Solute removal

During dialysis 3 processes allow solute removal: adsorption, diffusion and convection. There are 3 main groups of uremic solutes: 1. small molecules (<500 Da), which are removed during the diffusion process; 2. middle and large molecules (50–15,000 Da), removed by high flux dialysis; and 3. molecules bound with proteins weighing 500 Da, which are hard to remove and the dissociation process is time-consuming.<sup>24</sup>

Protein-bound uremic toxins (PBUTs) are nondialyzable using currently available membranes. Toxins like indoxyl sulfate (IS, 251 kD) and *p*-cresyl sulfate (108 kD) possess a very high protein-binding capacity of 90% with albumin. The molecular complexes formed by the protein-bound aggregate are too large to pass through dialysis membranes, resulting in a low reduction rate of 35% per session regardless of membrane class. Continued systemic accumulation of these uremic toxins after HD is the main factor contributing to HD-induced cardiovascular syndrome. Due to the nondialyzability of PBUTs, other strategies reducing the generation or adsorption of PBUTs (like pre- and probiotics) have been tried. *P*-cresol is a product of protein metabolism by gut bacteria; the administration of probiotics could decrease its production.<sup>25</sup> Some modified therapies have been more effective than conventional HD at removing certain PBUTs:

1. daily HD (compared with the standard 3 times/week scheme) lowered levels of glycation-related substances and advanced glycation end products (AGEs); 2. super-flux cellulose triacetate membranes were superior to low-flux membranes for clearing IS; 3. increasing the dialyzer mass transfer area coefficient and dialysate flow improved the removal of PBUTs; and 4. the addition of activated charcoal to the dialysate resulted in greater efficiency in removing PBUTs.<sup>26</sup>

**Table 1.** Classification of solutes based on molecular weight (adapted from Azar and Canaud<sup>48</sup>)

Molecular weight range [Da]	Classification of solutes
<500	<b>small molecules</b> urea, creatinine, phosphate
500–15,000	<b>middle molecules</b> vitamin B <sub>12</sub> , vancomycin, insulin, endotoxin fragments, parathormone, $\beta$ 2-microglobulin
>15,000	<b>large molecules</b> myoglobin, retinol-binding protein (RBP), erythropoietin (EPO), albumin, transferrin

## Dialyzer characteristics

The mass-transfer area coefficient (KoA) describes the amount of solute clearance through diffusion. It is determined for each substance of a particular dialyzer. In clinical practice, the KoA for urea is used and is provided by the manufacturer. The KoA is the mass transfer coefficient and A is the surface of the membrane.

Diffusion is the movement of solutes across the membrane caused by differences in the concentration gradient. The diffusion rate depends on the characteristics of the solute (protein binding, charge, size), the concentration gradient of the solute between the dialysate and the blood, as well the dialysis membrane surface area, porosity, type, and thickness.

Convection is the movement of solutes out of the blood compartment through the dialysis membrane, with the fluid being removed during ultrafiltration. Convective transport is independent of solute concentration gradients across the membrane. The size of the membrane pores determines which solutes can be removed.

During ultrafiltration fluid flows through the dialysis membrane. This movement is forced by a difference in pressure on the 2 sides of the membrane (the pressure gradient). The ultrafiltration coefficient (KUF), which is ultrafiltration rate (QUF) / pressure gradient in the membrane ( $\Delta P$ ), describes the efficiency of the membrane for ultrafiltration.<sup>27</sup>

Absorption takes place when molecules permeate the sorbent and are subsequently taken up by it. In addition, whereas some sorbents take up molecules until they become saturated, others act primarily by exchanging one molecule for another. This phenomenon can be used to remove a specific toxin from blood. Absorption is not

used in conventional HD therapy, but work is currently underway to apply it in portable and wearable dialysis devices.<sup>28</sup>

One of the most important parameters describing a dialyzer is clearance. Urea clearance can be used to calculate the dialysis dose. In patients with elevated levels of uric acid or phosphate, uric acid clearance and phosphate clearance can be useful, but these values are not always reported.

The introduction of dialyzers with enlarged pores has resulted in increases in middle molecule clearance, leading to a need to find a middle molecule marker.  $\beta$ 2-microglobulin ( $\beta$ 2M) is now used as a middle molecule marker, because it is easy to measure. High-flux dialyzers are characterized by a KUF coefficient > 15 mL/h/mm Hg and an ability to clear  $\beta$ 2Ms at a rate of more than 20 mL/min.<sup>29</sup>  $\beta$ 2-microglobulin clearance is also the basis for the 5-level dialyzer classification system developed in Japan (Table 2). Grades 4 and 5 are characterized by clearance  $\geq$ 70 mL/min and a blood flow of 200 mL/min with a dialysate flow of 500 mL/min. Dialysis membranes used in grade 4 and 5 dialyzers are called high-performance membranes (HPMs) due to their high flux rate, permeability and biocompatibility.

High-performance membranes have larger pores than low-performance membranes, which allows the removal of not only small molecules, but also medium and large molecules, including low-molecular weight proteins (LMWPs) and small amounts of albumin. The optimal pore size should prevent a loss of albumin >3 g/session with a blood flow rate of 200 mL/min and a dialysate flow rate of 500 mL/min.<sup>30</sup> This structure makes the filtering of uremic toxins and albumin in the dialyzer similar to the human kidney.<sup>31,32</sup>

**Table 2.** Japanese dialyzer classifications

Dialyzer class	Clearance of $\beta$ 2-microglobulin of less than [mL/min]
I	10
II	30
III	50
IV	70
V	more than 70

## High-flux vs low-flux dialysis

According to a review by Palmer et al., high-flux dialysis can reduce the mortality of hemodialyzed patients due to CV events by 15%, but all-causes mortality was not significantly decreased.<sup>33</sup> Another study showed that after 3.7 years of HD, the risk of cerebrovascular disease and cardiac mortality is significantly lower in the case of high-flux dialysis than in low-flux dialysis.<sup>34</sup> Despite its many advantages, high-flux dialysis can be associated with backflow, which rarely occurs with low-flux dialysis. This can be a problem when dialysis water is contaminated

with endotoxins, because wash-out from the membrane can reach the blood side. However, nowadays it is not a common problem. In addition, high-flux dialysis may be associated with an increased risk of hypotension, especially in patients with impaired cardiac function or autonomic neuropathy.<sup>30</sup>

## Biocompatibility

High biocompatibility is crucial for the long-term survival of dialysis patients. The contact of blood with artificial material (the dialysis membrane) may cause many complications. Adsorption of plasma proteins on the membrane surface impairs the functioning of the membrane and can trigger the activation of almost any plasma or cellular component of the blood.<sup>35</sup> In the past, cuprophane membranes were used, but they were highly immunoreactive because of the large number of hydroxyl groups, responsible for complement activation and leukopenia. Technological advances made it possible to create synthetic membranes with reduced immunoreactivity. The following crucial issues are related to biocompatibility: complement activation, platelet activation and toxins.

**Complement activation:** the contact of plasma with the dialysis membrane can result in complement activation, which can lead to a pseudo-anaphylactic reaction called complement activation-related pseudoallergy (CARPA).<sup>36</sup> It has been shown that complement activation is related to the progression of cardiovascular disease (CVD). According to several studies, patients with higher C3 levels are more likely to develop CV events. Poppelaars et al. reported that patients who develop CV events have sharp C3d/C3 ratio increases after 30 min of HD.<sup>37</sup> Complement activation caused by the contact of blood with the dialysis membrane can lead to a higher frequency of thromboembolic events.<sup>38</sup>

**Platelet activation:** fibrinogen accumulates on the dialysis membrane, which results in the adhesion and activation of platelets. A decrease in the platelet count is usually observed for 15–30 min after HD and ranges from 5–15%. Studies have shown that significant thrombocytopenia (defined a priori as a post-dialysis platelet count of less than  $100 \times 10^3/\mu\text{L}$  or a post-dialysis decrease in platelet count of more than 15%) was most frequently observed in patients dialyzed with PSf membranes that were previously sterilized using an electron beam.<sup>39</sup>

**Toxins:** bisphenol A (BPA) is a component of some dialysis membranes. During HD, it is released and absorbed into the blood. In a patient with impaired kidney function, it accumulates. It can cause atherosclerosis, diabetes, metabolic syndrome, insulin resistance, obesity, and CVD. Ethylene oxide (ETO) is a sterilizing substance that can accumulate in dialyzers during contact with dialyzer components made of polycarbonates. The penetration of ETO into the blood can cause anaphylactic reactions.

Insufficient biocompatibility can lead to such clinical consequences as: pulmonary changes, worsening of renal function and dialysis-related amyloidosis.

**Pulmonary changes:** it has been suggested that less biocompatible membranes activate neutrophils and the complement system to a greater extent than newer, more biocompatible ones. The first reaction may result in the release of inflammatory mediators and reactive oxygen species (ROS) that could trigger a breakdown of pulmonary elastin fibrils, increasing the probability of developing emphysema. Increasing leukocyte sequestration in the pulmonary capillary network can lead to a serious diffusion defect. Enhanced complement activation (especially component C5) has been linked to leukotriene release, smooth muscle contraction, pulmonary hypertension, and hypoxemia. Complement C5a is an anaphylotoxin, so it promotes increases in vascular permeability and the progression of pulmonary edema. Studies have suggested that high biocompatibility plays an important role in preventing pulmonary dysfunction in HD patients, but there are also studies with contradictory results.<sup>40</sup>

**Worsening of renal function:** biocompatibility plays an important role in preserving residual renal function in HD patients. Factors like neutrophil and complement activation triggered by less biocompatible membranes can lead to a worsening of renal function. Both result in the release of vasoconstrictive compounds, which promotes ischemia, especially in the medullar region of the kidney.<sup>41</sup>

**Dialysis-related amyloidosis:**  $\beta_2\text{M}$  is a protein present in almost all nucleated cells, and is additionally released by degranulating neutrophils. Its aggregation as amyloid fibrils can lead to dialysis-related amyloidosis, a well-known pathologic process in long-term HD patients. The symptoms include pathologic fractures, arthropathy and carpal tunnel syndrome. Less biocompatible membranes, such as cellulose membranes, are known to induce this process more rapidly than PAN or PMMA membranes. The mechanisms leading to this difference include: increased release of proteases and ROS from neutrophils, which enhance the aggregation of  $\beta_2\text{M}$  into amyloid fibrils, increased synthesis of  $\beta_2\text{M}$  by mononuclear cells and the fact that cellulose membranes do not sufficiently clear  $\beta_2\text{M}$ s.<sup>42</sup>

## New types of dialysis membrane and a new type of therapy

One of the most important challenges of dialysis therapy is to reduce the number of late HD complications. Many side effects are associated with insufficient removal of middle and large molecules. Table 3 presents some of the correlations between clinical problems and uremia-retention molecules. The introduction of high-flux dialysis and HDF promised to make it possible to remove these molecules. Unfortunately, the effectiveness of these solutions remains unsatisfactory.<sup>43</sup>

**Table 3.** Associations between uremic-retention molecules and clinical problems (based on Lorenzin et al.<sup>45</sup>)

Uremic-retention molecule	Clinical problem
β2-microglobulin	dialysis-related amyloidosis
inflammatory mediators, leptin, appetite-suppressing toxins	malnutrition
parathyroid hormone, homocysteine, inflammatory cytokines	cardiovascular complications and osteodystrophy
erythropoiesis inhibitors, hepcidin	anemia
polyclonal free light chains (κ-FLC and λ-FLC)	atherosclerosis

Medium cut-off membranes are a new solution that has appeared on the market. They are characterized by a narrow molecular weight interval between cut-off and retention onset (a sieving coefficient between 0.1 and 0.9). This has been achieved by tight pore size distribution, and it allows effective removal of middle-to-high-weight molecules with little albumin loss.<sup>44</sup>

In order to utilize the potential of MCO membranes, HDx was developed. This new therapy allows increased clearance (K) of large molecules. However, due to the low diffusion coefficient of MCO membranes, they additionally require convection. This can be achieved in 2 ways: by increasing ultrafiltration (QUF) or by increasing sieving (S), since  $K = QUF \cdot S$ . In HDE, QUF is increased. As a result, in HDE, there is a need to replenish a large amount of commercially prepared fluids and to use special devices for fluid preparation. In contrast, in HDx, it is possible to maintain a lower QUF by increasing S. This technique can be performed using standard equipment for HD. Specially prepared fluids are not required due to properly balanced reverse filtration.<sup>45,46</sup>


High cut-off (HCO) membranes are characterized by an increased average pore diameter and effective removal of substances in the range from 20 kDa to 50 kDa. This modification allows the passage of larger proteins and more effective clearance of middle-molecular weight molecules, which permits the removal of excess myoglobin in trauma patients, inflammatory molecules in sepsis or free light-chain proteins in multiple myeloma. The downside of this approach is albumin loss, which limits its use in chronic HD.<sup>47</sup>


## Summary

Despite the continuous development of technology and the emergence of more and more refined dialysis membranes, no membrane functions closely enough to the human kidney. Neither ideal biocompatibility nor the removal of the full spectrum of uremic molecules has been achieved. Removing middle molecules is possible through high-flux therapy and HDE. However, the efficiency of this process is insufficient, especially for cardiotoxins among protein-bound toxins. Currently, the membranes that have the most

promising properties are MCO membranes. Their use in HDx makes efficient removal of middle molecules possible without excessive ultrafiltration. We are awaiting randomized controlled trials and long-term results of MCO membrane use in the dialysis population.

## ORCID iDs

Piotr Olczyk  <https://orcid.org/0000-0002-9447-9459>

Artur Małyszczak  <https://orcid.org/0000-0003-0167-5600>

Mariusz Kuształ  <https://orcid.org/0000-0002-6502-0374>

## References

- Dębska-Ślizień A, Rutkowski B, Rutkowski G, Korejwo R, Gellert R. Stan terapii nerkozastępczej w Polsce – 2016. *Nefrol Dial Pol.* 2018;22:1–8.
- Ronco C. Hemodiafiltration: Technical and clinical issues. *Blood Purif.* 2015;40(Suppl 1):2–11.
- Clark WR, Hamburger RJ, Lysaght MJ. Effect of membrane structure and composition on performance and biocompatibility in hemodialysis. *Kidney Int.* 1999;56(6):2005–2015.
- Ronco C, Crepaldi C, Brendolan A, et al. Evolution of synthetic membranes for blood purification: The case of the Polyflux family. *Nephrol Dial Transplant.* 2003;18(Suppl 7):10–20, discussion 55.
- Zweigert C, Neubauer M, Storr M, et al. Progress in the development of membranes for kidney-replacement therapy. In: Drioli E, Giorno L, eds. *Comprehensive Membrane Science and Engineering*. Oxford, UK: Elsevier; 2013:351–387.
- Davenport A. Membrane designs and composition for hemodialysis, hemofiltration and hemodiafiltration: Past, present and future. *Minerva Urol Nefrol.* 2010;62(1):29–40.
- Ronco C, Levin N, Brendolan A, et al. Flow distribution analysis by helical scanning in polysulfone hemodialyzers: Effects of fiber structure and design on flow patterns and solute clearances. *Hemodial Int.* 2006;10(4):380–388.
- Sakai K, Matsuda M. Solute removal efficiency and biocompatibility of the high-performance membrane from engineering point of view: High-performance membrane dialyzers. *Contrib Nephrol.* 2011;173:11–22.
- Meert N, Eloot S, Schepers E, et al. Comparison of removal capacity of two consecutive generations of high-flux dialyzers during different treatment modalities. *Nephrol Dial Transplant.* 2001;26(8):2624–2630.
- Su B-H, Shi Y, Fu P, Tao Y, Nie S, Zhao C-S. Clinical evaluation of polyethersulfone high-flux haemodialysis membrane compared to other membranes. *J Appl Polym Sci.* 2012;124(S1):91–98.
- Wenten I, Aryanti P, Khoiruddin K, Hakim A, Himma N. Advances in polysulfone-based membranes for hemodialysis. *JMSR.* 2016;2(2):78–89.
- Baihai S, Shudong S, Changsheng Z. Polyethersulfone Hollow Fiber Membranes for Hemodialysis. *Progress in Hemodialysis – From Emergent Biotechnology to Clinical Practice.* 2011. Doi:10.5772/22857.
- Sunohara T, Masuda T. Cellulose triacetate as a high-performance membrane: High-performance membrane dialyzers. *Contrib Nephrol.* 2011;173:156–163.
- Ronci M, Loporini L, Felaco P, et al. Proteomic characterization of a new asymmetric cellulose triacetate membrane for hemodialysis. *Proteom Clin Appl.* 2018;12(6):e1700140.
- Sunohara T, Masuda T. Fundamental characteristics of the newly developed ATA membrane dialyzer. *Contrib Nephrol.* 2017;189:215–221.
- Aucella F, Vigilante M, Gesuete A. Review: The effect of polymethylmethacrylate dialysis membranes on uraemic pruritus. *NDT Plus.* 2010;3(Suppl 1):i8–i11.
- Igoshi T, Tomisawa N, Hori Y, Jinbo Y. Polyester polymer alloy as a high-performance membrane. *Contrib Nephrol.* 2011;173:148–155.
- Nakano A. Ethylene vinyl alcohol co-polymer as a high-performance membrane: An EVOH membrane with excellent biocompatibility. *Contrib Nephrol.* 2011;173:164–171.
- Nakada H, Kashiwagi T, Iino Y, Katayama Y. Therapeutic effects of the long-term use of PAN membrane dialyzer in hemodialysis patients: Efficacy in old dialysis patients with mild PAD. *J Nippon Med Sch.* 2014;81(4):221–235.

20. Thomas M, Moriyama K, Ledebol AN69: Evolution of the world's first high permeability membrane. *Contrib Nephrol.* 2011;173:119–129.
21. Meijers B, Metalidis C, Vanhove T, Poesen R, Kuypers D, Evenepoel P. A noninferiority trial comparing a heparin-grafted membrane plus citrate-containing dialysate versus regional citrate anticoagulation: Results of the CiTED study. *Nephrol Dial Transplant.* 2017;32(4):707–714.
22. Szymczak A, Kanafa M, Chuć M, Kuzstal M. Hemodializa bez heparyny. *Postepy Hig Med Dosw.* 2018;72:671–677.
23. Chu J. Scientists produce dialysis membrane made from graphene. *MIT News Office.* <http://news.mit.edu/2017/scientists-produce-dialysis-membrane-made-from-graphene-0628>. Accessed October 6, 2018.
24. Aucella F, Gesuete A, Vigilante M, et al. Adsorption dialysis: From physical principles to clinical applications. *Blood Purif.* 2013;35(Suppl 2):42–47.
25. Guo J, Lu L, Hua Y, et al. Vasculopathy in the setting of cardiorenal syndrome: Roles of protein-bound uremic toxins. *Am J Physiol Heart Circ Physiol.* 2017;1:313(1):1–13.
26. Meyer TW, Peattie JW, Miller JD, et al. Increasing the clearance of protein-bound solutes by addition of a sorbent to the dialysate. *J Am Soc Nephrol.* 2007;18(3):868–874.
27. Fichoux A, Ronco C, Brunet P, Argilés À. The ultrafiltration coefficient: This old 'grand inconnu' in dialysis. *Nephrol Dial Transplant.* 2015;30(2):204–208.
28. Davenport A. Portable and wearable dialysis devices for the treatment of patients with end-stage kidney failure: Wishful thinking or just over the horizon? *Pediatr Nephrol.* 2014;30(12):2053–2060.
29. Karkar A. Advances in hemodialysis techniques. Hemodialysis, IntechOpen. <http://www.intechopen.com/books/hemodialysis/advances-in-hemodialysis-techniques>. Accessed October 6, 2018.
30. Saito A. Definition of high-performance membranes: From the clinical point of view. *Contrib Nephrol.* 2011;173:1–10.
31. Tsuchida K, Minakuchi J. Albumin loss under the use of high-performance membranes. *Contrib Nephrol.* 2011;173:76–83.
32. Niwa T. Update of uremic toxin research by mass spectrometry. *Mass Spectrom Rev.* 2011;30(3):510–521.
33. Palmer SC, Rabindranath KS, Craig JC, et al. High-flux versus low-flux membranes for end-stage kidney disease. *Cochrane Database Syst Rev.* 2012;12(9):CD005016.
34. Delmez JA, Yan G, Bailey J, et al; Hemodialysis (HEMO) Study Group. Cerebrovascular disease in maintenance hemodialysis patients: Results of the HEMO study. *Am J Kidney Dis.* 2006;47(1):131–138.
35. Pieroni L, Mortera SL, Greco V, et al. Biocompatibility assessment of haemodialysis membrane materials by proteomic investigations. *Mol Biosyst.* 2015;11(6):1633–1643.
36. Poppelaars F, Faria B, Costa MG, et al. The complement system in dialysis: A forgotten story? *Front Immunol.* 2018;9:71.
37. Poppelaars F, Gaya da Costa M, Faria B, et al. Intradialytic complement activation precedes the development of cardiovascular events in hemodialysis patients. *Front Immunol.* 2018;9:2070.
38. Lines SW, Richardson VR, Thomas B, Dunn EJ, Wright MJ, Carter AM. Complement and cardiovascular disease: The missing link in haemodialysis patients? *Nephron.* 2016;134(2):103–103.
39. Kiaii M, Djurdjev O, Farah M, et al. Use of electron-beam sterilized hemodialysis membranes and risk of thrombocytopenia. *JAMA.* 2011;306(15):1679–1687.
40. Lang SM, Becker A, Fischer R, Huber RM, Schiffel H. Acute effects of hemodialysis on lung function in patients with end-stage renal disease. *Wien Klin Wochenschr.* 2006;118(3–4):108–113.
41. Hakim RM, Wingard RL, Parker RA. Effect of the dialysis membrane in the treatment of patients with acute renal failure. *N Engl J Med.* 1994;331(20):1338–1342.
42. Hakim RM. Clinical implications of hemodialysis membrane biocompatibility. *Kidney Int.* 1993;44(3):484–494.
43. Wolley M, Jardine M, Hutchison CA. Exploring the clinical relevance of providing increased removal of large middle molecules. *Clin J Am Soc Nephrol.* 2018;13(5):805–814.
44. Kirsch AH, Lyko R, Nilsson LG, et al. Performance of hemodialysis with novel medium cut-off dialyzers. *Nephrol Dial Transplant.* 2017;32(1):165–172.
45. Lorenzin A, Neri M, Lupi A, et al. Quantification of internal filtration in hollow fiber hemodialyzers with medium cut-off membrane. *Blood Purif.* 2018;46(3):196–204.
46. Ronco C. The rise of expanded hemodialysis. *Blood Purif.* 2017;44(2):I–VIII.
47. Ronco C, Manna GL. Expanded hemodialysis: A new therapy for a new class of membranes. *Contrib Nephrol.* 2017;190:124–133.
48. Azar T, ed. *Modelling and Control of Dialysis Systems.* Berlin, Germany: Springer-Verlag; 2013.

Polimery w Medycynie  
Polymers in Medicine

